An Event Generator for Deep Inelastic Scattering within the POWHEG BOX Framework

Dissertation

der Mathematisch-Naturwissenschaftlichen Fakultät
der Eberhard Karls Universität Tübingen
zur Erlangung des Grades eines
Doktors der Naturwissenschaften
(Dr. rer. nat.)

vorgelegt von
Felix Reichenbach
aus Leipzig

Tübingen
2023

Gedruckt mit Genehmigung der Mathematisch-Naturwissenschaftlichen Fakultät der Eberhard Karls Universität Tübingen.

Tag der mündlichen Qualifikation:	15.03.2024
Dekan:	Prof. Dr. Thilo Stehle
1. Berichterstatterin:	Prof. Dr. Barbara Jäger
2. Berichterstatter:	Prof. Dr. Werner Vogelsang

Abstract

The ultimate goal of the field of particle physics is to find a theory that fully describes nature. The Standard Model (SM) comes closest to achieve this goal. It successfully describes many phenomena, but it fails to explain everything. A lot of resources are spent to expand the SM to a more complete theory. Therefore, the predictions of the SM must be known with very high precision in order to detect its limitations. Experiments with particle accelerators have proven to be promising in the past to detect new physics, such as the latest discovery of the Higgs boson. In the near future, a new particle accelerator, the Electron-Ion Collider (EIC), will be built, requiring theoretical high-precision predictions.

This work presents a new event generator for deep inelastic scattering, the main process at the EIC. With this new tool, events can be generated at next-to leading order in quantum chromodynamics and matched to parton showers. It is an extension to the `POWHEG BOX` framework, and hence uses the positive weight hardest emission generator (POWHEG) method. Initially, the `POWHEG BOX` framework was designed for hadron-hadron collisions. The different kinematics of lepton-hadron collisions require substantial changes to the existing implementations present in the `POWHEG BOX`. Specifically, the momentum mappings in the implementation of the Frixione, Kunszt and Signer (FKS) subtraction mechanism are reworked.

Theory predictions, obtained from the new event generator, are presented and compared to data collected at Hadron-Elektron-Ring-Anlage (HERA). Additionally, a phenomenological study for the experimental setup of the future EIC is shown.

The developed event generator provides a starting point for future studies of other processes observable at the EIC that share similar kinematic features.

Kurzzusammenfassung

Ziel der Teilchenphysik ist es, ein Modell theoretisch zu formulieren und experimentell zu bestätigen, das die Natur erfolgreich beschreibt. Das Standardmodell kommt diesem Ziel bisher am nächsten. Es ist in der Lage, viele Phänomene mit großer Genauigkeit zu beschreiben, lässt aber noch einige Beobachtungen unerklärt. Es wird intensiv daran gearbeitet, das Standardmodell zu erweitern. Dazu muss unteranderem die Präzision theoretischer Vorhersagen immer weiter verbessert werden. Nur dann können Abweichungen zu Experimenten bestimmt werden, um Raum für neue Physik zu finden. Experimente an großen Teilchenbeschleunigern haben sich als effektive Methode erwiesen, um neue physikalische Effekte nachzuweisen. So wurde das Higgs-Teilchen am Large Hadron Collider entdeckt. In naher Zukunft wird ein neuer Teilchenbeschleuniger, der Electron-Ion-Collider (EIC), gebaut werden. Dieser ermöglicht eine genauere Bestimmung von experimentell GröSSen als es zuvor möglich war. Im Gegenzug wird es von der theoretischen Seite erforderlich sein, die Unsicherheiten im gleichen MaSSe zu verringern.

Diese Arbeit präsentiert einen neuen Ereigninsgenerator für die tiefinelastische Streuung, welche der Hauptprozess des neuen EIC sein wird. Mit diesem neuen Werkzeug können Streuereignisse bis zur nächst-führenden Ordnung (NLO) in der Quantenchromodynamik (QCD) erzeugt werden und an einen Parton Shower weitergegeben werden. Dieser Generator wurde als Erweiterung des `POWHEG BOX` Frameworks entwickelt und benutzt folglich die POWHEG Methode. Die Kinematik von Lepton-Hadron-Kollisionen unterscheidet sich grundlegend von Hadron-Hadron-Kollisionen. Dies macht tiefgehende Modifikationen an der Implementation der bestehenden `POWHEG BOX` erforderlich. Betroffen sind insbesondere die Abbildungen der Impulse im Rahmen des Frixione, Kunszt und Signer (FKS) Subtraktionsverfahren.

Die theoretische Vorhersagen, die mit Hilfe des präsentierten Ereignisgenerators erzeugt wurden, werden mit experimentellen Daten verglichen, welche an der Hadron-Elektron-Ring-Anlage (HERA) gesammelt wurden. Darüber

hinaus wird eine phänomenologische Studie zu dem künftigen EIC gezeigt.

Der entwickelte Ereignisgenerator bietet einen Ausgangspunkt für künftige Studien für andere Prozesse am EIC, die eine ähnliche Kinematik besitzen.

Corresponding Publication

[1] A. Banfi, S. Ferrario Ravasio, B. Jäger, A. Karlberg, F. Reichenbach and G. Zanderighi, *A POWHEG generator for deep inelastic scattering*, *JHEP* **02** (2024) 023 [arXiv:2309.02127].

Contents

Acronyms

BNL	Brookhaven National Laboratory
CC	charged current
CKM	Cabibbo-Kobayashi-Maskawa
DESY	Deutsches Elektronen-Synchrotron
DFG	German Research Foundation
DIS	deep inelastic scattering
EIC	Electron-Ion Collider
FKS	Frixione, Kunszt and Signer
FSR	final-state radiation
HERA	Hadron-Elektron-Ring-Anlage
IR	infrared
ISR	initial-state radiation
KLN	Kinoshita-Lee-Nauenberg
LHC	Large Hadron Collider
LL	leading logarithm
LO	leading order
LSZ	Lehmann-Symansik-Zimmermann
$\overline{\textbf{MS}}$	modified minimal subtraction
NC	neutral current
NLL	next-to leading logarithm
NLO	next-to leading order
N^{3}LO	next-to-next-to-next-to leading order
PDF	parton distribution function
POWHEG	Positive Weight Hardest Emission Generator
QCD	quantum chromodynamics
QED	quantum electrodynamics
QFT	quantum field theory
SM	Standard Model
UV	ultraviolet
vev	vacuum expectation value

Chapter 1

Introduction

Humanity has been investigating nature for centuries. One central question has always been: what are the things we see around us made of? The field of particle physics aims to answer not only that question but also what forces exist between the particles that make up our world.

The first discovered elementary particle was the electron in the late 19th century by Joseph John Thomson. His discovery was preceded by decades of cathode rays experiments by other physicists, such as Julius Plücker, William Crookes or Arthur Schuster. Nowadays, the picture of elementary particles is much more refined and experiments are getting more involved and also more accurate.

The current world view of particle physics is condensed in the Standard Model (SM). It describes all known elementary particles and their interactions aside from gravity. The last missing particle, the Higgs boson, was detected 2012 [2, 3] at the Large Hadron Collider (LHC) after being proposed nearly 50 years before [4–9]. Despite its great success, there are still open questions the SM cannot answer. Some of these questions concern the nature of dark matter in the universe or the matter-antimatter asymmetry. This means there has to be physics beyond the SM.

To find this new physics, the accuracy of experimental data and theory predictions is being improved to find small derivations from the SM expectation or constraints that can be imposed on new models. While low energy physics has been explored for centuries, a lot of effort is nowadays put into the search at high energy scales. Collider experiments are a promising way to investigate high energy reactions in a very controlled environment.

The Hadron-Elektron-Ring-Anlage (HERA) is an electron-proton collider built at the Deutsches Elektronen-Synchrotron (DESY). During its operation, electrons (or positrons) with an energy of 27.5 GeV collided with protons with energies of up to 920 GeV. The main process happening during this

collision is deep inelastic scattering (DIS) where the electron (or positron) scatters off of the constituents of the proton, while the energy transfer between the scattering particles is much greater than the proton mass. As the first high energy *ep* collider, HERA cemented the understanding of the inner structure of protons. Data gathered at the detectors H1 and ZEUS led to an accurate determination of parton distribution functions (PDFs) [10–13]. More over, a wide range of quantum chromodynamics (QCD) studies [14–24] resulted from HERA. Although HERA was ultimately shut down in 2007, the collected data is still used in global fits of PDFs [25–28].

Due to technical limitations from roughly 16 years ago, the amount of data collected at HERA cannot compete with the up to date LHC. This is about to change with the future Electron-Ion Collider (EIC) whose construction has been approved in June 2021 by the U.S. Department of Energy[1]. The construction is planned to start in 2024 at Brookhaven National Laboratory (BNL). At the EIC, electrons with an energy range of 5 to 18 GeV will collide with a variety of ion, especially protons in the energy range of 41 to 275 GeV. This leads to a smaller center-of-mass energy compared to HERA, but a peak luminosity of $10^{34}\text{cm}^{-2}\text{s}^{-1}$ with a center-of-mass energy of 105 GeV is aimed at which would be almost three orders of magnitudes larger than the peak luminosity at HERA after the luminosity upgrade [29–32].

The expected increase in experimental accuracy for the DIS process has to be met from the theory side. Since the shutdown of HERA, the calculation of perturbative corrections has been improved considerably [33, 34]. The DIS process has been calculated fully differentially at next-to-next-to-next-to leading order (N^3LO) order in QCD [35, 36]. However, Monte-Carlo event generators have mostly been developed focusing on hadron-hadron collision to suit the needs of physics at the LHC. These generators offer the possibility to match a fixed order calculation to a parton shower, e.g. using the `POWHEG` [37, 38] or `MC@NLO` [39] approach. General purpose event generators, such as `Herwig7` [40, 41], `Sherpa2` [42, 43], and `Pythia8` [44, 45], have been adapted to address *ep* colliders. But there is no dedicated event generator available to interface next-to leading order (NLO) calculations with a parton shower for DIS. This thesis presents a modification to the `POWHEG BOX` framework that represents a dedicated event generator for DIS. The obtained results can be interfaced to a generic parton shower.

This thesis is structured as follows: Chapter 2 shows the theoretical basics that are needed for any NLO calculation in the framework of quantum field theory (QFT) and how to match this calculation to a parton shower.

[1] https://www.energy.gov/science/articles/electron-ion-collider-achieves-critical-decision-1-approval

In chapter 3, the specific modifications to the POWHEG BOX are discussed to accommodate the specifics of DIS. Chapter 4 presents phenomenological studies for HERA and the EIC. In chapter 5 the summary and outlook of this work are displayed.

Chapter 2

Theoretical preliminary

2.1 Quantum field theory

High energy physics is modeled using QFT. QFT combines classical field theory, special relativity and quantum mechanics. QFTs can be build upon fundamental postulates [46–49] and their essence is summarized in the following paragraphs. The goal is to show what the key ingredients of QFT are, and which properties they must have.

Firstly, the states of a system are represented by vectors of a Hilbert space with a positive definite metric. Fields $\Phi(x)$ are defined as linear operators acting on the Hilbert space of states. Poincaré symmetry is one of the most fundamental symmetries in nature and is imposed on QFTs by requiring a unitary representation $U(\Lambda, a)$ of the Poincaré group on the Hilbert space. The field operators $\Phi_\alpha(x)$ shall transform under this Poincaré transformation as $U(\Lambda, a)\Phi_\alpha(x)U^\dagger(\Lambda, a) = M(\Lambda^{-1})_\alpha{}^\beta \Phi_\beta(\Lambda x + a)$. Thereby, $M(\Lambda)_\alpha{}^\beta$ is a representation of the Lorentz group that acts on the the field operators Φ_α.

The infinitesimal generator of the translation operator $U(\mathbb{1}, a)$ is called the momentum operator P^μ, where the component P^0 is also called Hamiltonian. It is postulated that the eigenvalues of the Hamiltonian P^0 shall be non-negative. Further, the Hamiltonian shall have an unique ground state $|\Omega\rangle$ which is invariant under any Poincaré transformation. This ground state is often referred to as vacuum state. Additionally, the existence of 1-particle states $|A, p, s\rangle$ is postulated. A denotes the particle type, p its momentum and s the spin. These states shall form an eigenspace to the operator P^2 and are an irreducible representation of the Poincaré group. This means each state of particle type A can be reached by a Poincaré transformation of any other state with particle type A. Also, an 1-particle state of the particle A does not have any properties other than momentum and spin. Next, it is

imposed that all states of the Hilbert space can be created by the application of the field operators $\Phi(x)$.

Another important feature of special relativity is the result that nothing can travel faster than the speed of light. This means that two events at a space-like distance cannot impact each other. In the context of QFT, this feature is realized by requiring $[\Phi_\alpha(x), \Psi_\beta(y)]_\mp = 0, \forall (x-y)^2 < 0$ for any field operators $\Phi_\alpha(x)$ and $\Psi_\beta(y)$. Here $[\cdot,\cdot]_\mp$ is meant to be the anticommutator $[\cdot,\cdot]_+$, or often $\{\cdot,\cdot\}$, if both fields $\Phi_\alpha(x)$ and $\Psi_\beta(y)$ are fermionic, and the commutator $[\cdot,\cdot]_-$ otherwise. The anticommutator has to be chosen for fermions in order to guarantee a Hamiltonian with eigenvalues that are bounded from below. Since all reasonable observables should consist of an even number of fermionic operators, causality is still conserved.

One common approach to create a QFT is canonical quantization. The starting point of the canonical quantization is the Lorentz invariant Lagrangian density, usually referred to as just Lagrangian, $\mathcal{L}$ of a classical field theory. The occurring classical field functions ϕ_i are promoted to field operators $\hat{\phi}_i$ and are required to fulfill the canonical (anti-)commutation relations $[\hat{\phi}_i(\mathbf{x},t), \hat{\pi}_j(\mathbf{y},t)]_\mp = i\hbar\delta^{(3)}(\mathbf{x}-\mathbf{y})\delta_{ij}$, with $\pi_i = \frac{\partial \mathcal{L}}{\partial \dot{\phi}_i}$.

In the whole work it is assumed that the Lorentz invariant Lagrangian $\mathcal{L}$ can be split into two parts

$$\mathcal{L} = \mathcal{L}_0 + \mathcal{L}_{\text{int}}, \tag{2.1}$$

with

$$\mathcal{L}_0 = \sum_i \frac{1}{k_i} \bar{\phi}_\alpha^{A_i} \Gamma_{A_i}^{\alpha\beta} \phi_\beta^{A_i}, \tag{2.2}$$

$$\mathcal{L}_{\text{int}} = \sum_i -\frac{g_i}{s_i} B^{\alpha_1 \dots \alpha_n} \phi_{\alpha_1}^{A_1} \cdots \phi_{\alpha_n}^{A_n}, \tag{2.3}$$

where $\Gamma_{A_i}^{\alpha\beta}$ is a linear, differential operator acting on $\phi_\beta^{A_i}$. The index A_i labels the different types of fields that can occur in the theory. $\bar{\phi}_\alpha^A$ is a modified adjoint of ϕ_α^A and is defined as $\bar{\phi}_i^A := (\phi_j^A)^\dagger a_{ji}$, such that $\bar{\phi}_i^A \phi_i^A$ transforms as a scalar under Lorentz transformation. k is chosen to be $k_i = 2$ if $\bar{\phi}_\alpha^{A_i} = \phi_\alpha^{A_i}$. s_i is a conventional symmetry factor equal to the number of permutation one can apply to the product $\phi_{\alpha_1}^{A_1} \cdots \phi_{\alpha_n}^{A_n}$ without changing $B^{\alpha_1 \dots \alpha_n} \phi_{\alpha_1}^{A_1} \cdots \phi_{\alpha_n}^{A_n}$. g_i is called a coupling constant.

For free field theories, i.e. theories with $\mathcal{L}_{\text{int}} = 0$, canonical quantization can be done with the creation and annihilation operators $a_A^{s\dagger(\mathbf{p})}$ and $a_A^s(\mathbf{p})$. These operators create or annihilate single particles of type A with momentum $\mathbf{p}$ and spin s and fulfill the (anti-)commutation relation

$$[a_A^s(\mathbf{p}), a_B^{s\dagger}(\mathbf{p}')] = (2\pi)^3 2p^0 \delta^{(3)}(\mathbf{p}-\mathbf{p}')\delta_{ss'}\delta_{AB}, \tag{2.4}$$

where $p^0 \equiv \sqrt{\mathbf{p}^2 + m^2}$. From these operators one can construct the field operators

$$\phi^-_{i,A}(x) = \int \frac{\mathrm{d}^3\mathbf{p}}{(2\pi)^3 2p^0} \sum_s a^s_A(p) u^s_i(p) e^{-ipx},$$
$$\phi^+_{i,A}(x) = \int \frac{\mathrm{d}^3\mathbf{p}}{(2\pi)^3 2p^0} \sum_s a^{s\dagger}_A(p) v^s_i(p) e^{ipx}, \tag{2.5}$$

where $u^s_i(p)e^{-ipx}$ and $v^s_i(p)e^{ipx}$ with $p^0 > 0$ are linear independent solutions to the classical equations of motion. The combination of

$$\phi^A_i := \phi^-_{i,A} + \phi^+_{i,\bar{A}} \tag{2.6}$$

together with $\bar{\phi}^A_i$ will then fulfill the canonical and causal commutation relation. In an example case of a fermion with the Lagrangian

$$\mathcal{L} = \bar{\psi}(i\partial\!\!\!/ - m)\psi, \tag{2.7}$$

one would have the free field

$$\psi_\alpha(x) = \int \frac{\mathrm{d}^3\mathbf{p}}{(2\pi)^3 2p^0} \sum_s \left(a^s_A(p) u^s_\alpha(p) e^{-ipx} + a^{s\dagger}_{\bar{A}}(p) v^s_\alpha(p) e^{ipx} \right) \tag{2.8}$$

that annihilates the fermion and creates the anti-fermion. Here, the Dirac adjoint is

$$\bar{\psi}(x) := \psi^\dagger(x)\gamma^0 = \int \frac{\mathrm{d}^3\mathbf{p}}{(2\pi)^3 2p^0} \sum_s \left(a^{s\dagger}_A(p) \bar{u}^s_i(p) e^{ipx} + a^s_B(p) \bar{v}^s_i(p) e^{-ipx} \right). \tag{2.9}$$

If the classical field ϕ_α is real, then $v^s_\alpha = (u^s_\alpha)^*$ and $A = \bar{A}$. Thereby, particles of type A and $\bar{A}$ are antiparticles to each other, i.e. they have the same mass and opposite charges with respect to a conserved charge that is created by a symmetry other than Poincaré symmetry of the theory.

In order to describe interactions, one common approach is perturbation theory, where the interaction picture proves to be a useful tool. It allows to use the field operators of the free theory and put the interaction terms of the Lagrangian into the time evolution operator that acts on the states.

One of the most important experiments in high energy physics are particle collisions. Therefore, the cross section σ is an important observable that can be measured in actual experiments. The cross section is defined as

$$\sigma = \frac{E}{N_t N_b} A, \tag{2.10}$$

$E \ldots$ number observed events,
$N_t \ldots$ number of target particles,
$N_b \ldots$ number of beam particles,
$A \ldots$ overlapping area of beam and target.

The cross section is tied to the transition amplitude $S_{fi} = {}_{\text{out}}\langle f|i\rangle_{\text{in}}$, where ${}_{\text{out}}\langle f|$ is the final state of the event with the particles being so far away from each other that no interaction is felt between the final state particles to allow the use of the free field operators. $|i\rangle_{\text{in}}$ is the initial state of the particles colliding prepared at a large distance analogous to the out state to justify the use of the free field theory to describe their behavior before the scattering takes place. S_{fi} is called the scattering matrix element or S-matrix element of the scattering process $i \to f$. Often, an additional transition matrix T is defined by $S = \mathbb{1} + iT$. This splits the S-matrix into the part $\mathbb{1}$ which means that the scattering particles do not interact and miss each other, and into the physically more interesting part iT. The transition matrix contains the information about the interactions taking place. The extra prefactor i is convention. The T matrix is split further into

$$T = (2\pi)^4 \delta^{(4)} \left(\sum_i p_i - \sum_f p_f \right) \mathcal{M}, \tag{2.11}$$

where the sum over i runs over all initial state particles and f over final state particles. The delta distribution guarantees the 4-momentum conservation while the newly defined matrix $\mathcal{M}$ carries the physical information of the dynamics of the transitions.

Now, the cross section σ is connected to the amplitude $\mathcal{M}$ by

$$\sigma_{f \leftarrow i} = \int \mathrm{d}\Phi_n \frac{|M_{fi}|^2}{4\sqrt{(p_1 p_2)^2 - m_1^2 m_2^2}}, \tag{2.12}$$

where p_1, p_2 are the 4-momenta of the two incoming particles and $p_i^2 = m_i^2$. The phase space measure $\mathrm{d}\Phi_n$ is

$$\mathrm{d}\Phi_n = \delta^{(4)} \left(p_1 + p_2 - \sum_{i=1}^{n} k_i \right) \prod_{i=1}^{n} \frac{\mathrm{d}^3 k_i}{(2\pi)^3 k^0}, \tag{2.13}$$

and n is the number of final state particles with momentum k_i and $k_i^0 \equiv \sqrt{\mathbf{k}_i^2 + m_i^2}$.

In order to compute a cross section, one needs to calculate the matrix element $\mathcal{M}_{fi}$. A prescribtion to calculate such matrix elements is given by the Lehmann-Symansik-Zimmermann (LSZ) reduction formula [48]. It states

$$\begin{aligned}
&{}_{\text{out}}\langle (B,k,\lambda)_1 \dots (B,k,\lambda)_n | (A,p,s)_1 \dots (A,p,s)_m \rangle_{\text{in}} = \\
&\quad \prod_{i=1}^{m} \left(\sqrt{Z_{A_i}} u_{\alpha_i}^{s_i}(p_i) \right) \prod_{j=1}^{m} \left(\sqrt{Z_{A_j}} \bar{u}_{\beta_j}^{\lambda_j}(k_j) \right) \\
&\quad \times \tilde{G}^{(n+m)}_{\text{amp},\bar{\Phi}_{\alpha_1}^{A_1} \dots \bar{\Phi}_{\alpha_n}^{A_n} \Phi_{\beta_1}^{B_1} \dots \Phi_{\beta_m}^{B_m}}(p_1, \dots, p_m, -k_1, \dots, -k_n).
\end{aligned} \tag{2.14}$$

Thereby $\tilde{G}^{(n+m)}_{\text{amp}}$ is the amputated Green's function, or $n+m$-point function, in momentum space. The Heisenberg fields $\bar{\Phi}_{\alpha_i}^{A_i}$ are the fields that, become the free fields $\bar{\phi}_{\alpha_i}^{A_i}$ in the limit $t \to \pm\infty$. The free fields contain the creation operator $a_{A_i}^{s_i\dagger}(p_i)$ creating a free particle of type A_i, while the fields $\Phi_{\beta_1}^{B_1}$ contain the annihilation operator of particle type B in their free particle limit. The polarization vectors $u_{\alpha_i}^{s_i}(p_i), \bar{u}_{\beta_j}^{\lambda_j}(k_j)$ appear in the respective free field limit of their associated conjugated Heisenberg field together with the annihilation or creation operator of their associated type.

The amputated Green's function is defined as

$$\begin{aligned}
&\tilde{G}^{(n)}_{\text{amp},\Phi_{\alpha_1}^{A_1} \dots \Phi_{\alpha_n}^{A_n}}(p_1, \dots, p_n) \\
&\quad = \left[\tilde{G}^{(2)}_{\Phi_{\alpha_1}^{A_1}}(p_1, -p_1) \right]^{-1} \cdots \left[\tilde{G}^{(2)}_{\Phi_{\alpha_n}^{A_n}}(p_n, -p_n) \right]^{-1} \tilde{G}^{(n)}_{\Phi_{\alpha_1}^{A_1} \dots \Phi_{\alpha_n}^{A_n}}(p_1, \dots, p_n).
\end{aligned} \tag{2.15}$$

$\tilde{G}^{(n)}$ together with $(2\pi)^4 \delta^{(4)}\left(\sum_{i=1}^{m} p_i - \sum_{j=1}^{n} k_j \right)$ is the Fourier transform of the Green's function, or n-point function

$$\begin{aligned}
&G^{(n)}_{\Phi_{\alpha_1}^{A_1} \dots \Phi_{\alpha_n}^{A_n}}(x_1, \dots, x_n) = \\
&\quad \int \frac{\mathrm{d}^4 p_1 \cdots \mathrm{d}^4 p_n}{(2\pi)^{4n}} \tilde{G}^{(n)}_{\Phi_{\alpha_1}^{A_1} \dots \Phi_{\alpha_n}^{A_n}}(p_1, \dots, p_n) (2\pi)^4 \delta^{(4)} \left(\sum_{i=1}^{n} p_i \right) e^{i \sum_{i=1}^{n} p_i x_i},
\end{aligned} \tag{2.16}$$

whereas the n-point function is the vacuum expectation value of the time ordered product of the field operators

$$G^{(n)}_{\Phi_{\alpha_1}^{A_1} \dots \Phi_{\alpha_n}^{A_n}}(x_1, \dots, x_n) = \langle \Omega | \, T\left(\Phi_{\alpha_1}^{A_1}(x_1) \cdots \Phi_{\alpha_n}^{A_n}(x_n) \right) | \Omega \rangle \,. \tag{2.17}$$

These n-point functions can be calculated perturbatively. For that purpose, the Heisenberg fields $\Phi_{\alpha_i}^{A_i}$ are expressed in the interaction picture in order to use the free field operators $\Phi_{\alpha_i}^{A_i}$. One assumes that in the limit of $t \to \pm\infty$ the vacuum of the full interacting theory $|\Omega\rangle$ becomes the vacuum of the free theory $|0\rangle$

$$\begin{aligned} U(t \to -\infty)\,|\Omega\rangle &\to \lambda_-\,|0\rangle\,, \\ \langle\Omega|\,U^\dagger(t \to \infty) &\to \lambda_+\,\langle 0|\,. \end{aligned} \tag{2.18}$$

Then, n-point functions can be calculated using the Gell-Mann and Low theorem [50]

$$\begin{aligned} &\langle\Omega|\,T\big(\Phi_{\alpha_1}^{A_1}(x_1)\cdots\Phi_{\alpha_n}^{A_n}(x_n)\big)\,|\Omega\rangle = \\ &\qquad\frac{\langle 0|\,T\big(\phi_{\alpha_1}^{A_1}(x_1)\cdots\phi_{\alpha_n}^{A_n}(x_n)\exp\big\{i\int \mathrm{d}^4y\mathcal{L}_{\text{int}}(y)\big\}\big)\,|0\rangle}{\langle 0|\,T\exp\big\{i\int \mathrm{d}^4y\mathcal{L}_{\text{int}}(y)\big\}\,|0\rangle}. \end{aligned} \tag{2.19}$$

The exponential of the interaction action can be expanded. The resulting series will be a polynomial in the coupling constants that occur in $\mathcal{L}_{\text{int}}$. If the coupling constants are small, one can evaluate all the terms of the series up to a certain order in the coupling constants.

The free vacuum expectation values of the free fields can be calculated using Wick's theorem [51]. The idea of Wick's theorem is that a vacuum expectation value of free field operators can only be non-zero, if a creation operator is right of an annihilation operator of the same particle. Hence, the vacuum expectation value can be calculated by moving all creation operators to the left such that they act to the left on the vacuum and yield 0. This ordering is called normal order. Wick's Theorem states that each product of commutators can be written as sum of normal ordered products of operators and all full contractions of matching pairs of operators. These full contractions reduce to a c-number. Then, the vacuum expectation value of the normal ordered products of operators gives zero and only the fully contracted terms survive. A contraction $\overbrace{AB}$ of operators A and B is defined as

$$\overbrace{AB} = AB - :AB:, \tag{2.20}$$

where $:AB:$ is the normal order product of A and B. The field operators in the Gell-Mann and Low theorem contain both creation and annihilation operators. Each operator $\phi_{\alpha_n}^{A_n}(x_n)$ has a matching partner in $\bar{\phi}_{\alpha_n}^{A_n}(x_n)$ which contains the appropriate creation and annihilation operator. In case of hermitian fields, they are the same. Then, the contraction of a matching pair

becomes

$$\begin{aligned}\overbrace{\phi^A_\alpha(x)\bar{\phi}^A_\beta}(y) &= \Big(\phi^-_{\alpha,A}(x) + \overline{\phi^+_{\alpha,\bar{A}}(x)}\Big)\Big(\overline{\bar{\phi}^-_{\beta,A}(y)} + \bar{\phi}^+_{\beta,\bar{A}}(y)\Big)\\ &= \overbrace{\phi^-_{\alpha,A}(x)\bar{\phi}^-_{\beta,A}}(y) + \overbrace{\phi^+_{\alpha,\bar{A}}(x)\bar{\phi}^+_{\beta,\bar{A}}}(y)\\ &= \phi^-_{\alpha,A}(x)\bar{\phi}^-_{\beta,A}(y) - :\phi^-_{\alpha,A}(x)\bar{\phi}^-_{\beta,A}(y):\\ &+ \phi^+_{\alpha,\bar{A}}(x)\bar{\phi}^+_{\beta,\bar{A}}(y) - :\phi^+_{\alpha,\bar{A}}(x)\bar{\phi}^+_{\beta,\bar{A}}(y): . \end{aligned} \tag{2.21}$$

Note that in the last line either $\phi^-_{\alpha,A}(x)\bar{\phi}^-_{\alpha,A}(y)$ or $\phi^+_{\alpha,\bar{A}}(x))\bar{\phi}^+_{\alpha,\bar{A}}(y))$ is already normal ordered. If $\phi^A_\alpha(x)$ is defined as in Eq. (2.6) then latter is in normal order. If $\phi^A_\alpha(x)$ is the conjugate version of Eq. (2.6) the former is normal ordered. For now, assume $\phi^A_\alpha(x)$ is defined like in Eq. (2.6), then

$$\begin{aligned}\overbrace{\phi^A_\alpha(x)\bar{\phi}^A_\beta}(y) &= \phi^-_{\alpha,A}(x)\bar{\phi}^-_{\beta,A}(y) - :\phi^-_{\alpha,A}(x)\bar{\phi}^-_{\beta,A}(y)\\ &= \phi^-_{\alpha,A}(x)\bar{\phi}^-_{\beta,A}(y) \mp \bar{\phi}^-_{\beta,A}(y)\phi^-_{\alpha,A}(x) = [\phi^-_{\alpha,A}(x), \bar{\phi}^-_{\beta,A}(y)]_\mp\\ &=: \Delta^{(A)}_{-,\alpha\beta}(x-y). \end{aligned} \tag{2.22}$$

If the particle of type A is a fermion then an additional minus sign in the second line is picked up and yields the anticommutator in the end. The analogous calculation gives

$$\begin{aligned}\overbrace{\bar{\phi}^A_\beta(y)\phi^A_\alpha}(x) &= [\bar{\phi}^+_{\beta,\bar{A}}(y), \phi^+_{\alpha,\bar{A}}(x)]\\ &=: \Delta^{(A)}_{+,\alpha\beta}(x-y). \end{aligned} \tag{2.23}$$

Of particular interest is the time-ordered product, which is

$$T\Big(\overbrace{\phi^A_\alpha(x)\bar{\phi}^A_\beta}(y)\Big) = \Delta^{(A)}_{-,\alpha\beta}(x-y) \mp \Delta^{(A)}_{+,\alpha\beta}(x-y) =: iD^{(A)}_{F,\alpha\beta}(x-y). \tag{2.24}$$

$D^{(A)}_{F,\alpha\beta}(x-y)$ is called the Feynman propagator. The Feynman propagator turns out to be the Green's function of the differential operator $\Gamma_{\alpha\beta}$ that defines the free Lagrangian $\mathcal{L}^{(A)}_0$ associated the the field of particle A and its antiparticle $\bar{A}$

$$\begin{aligned}\Gamma_{\alpha\beta}D^{(A)}_{F,\beta\gamma}(z) &= \delta^{(4)}(z)\delta_{\alpha\gamma},\\ \text{with}\quad \mathcal{L}^{(A)}_0 &= \frac{1}{k}\bar{\phi}^A_\alpha\Gamma_{\alpha\beta}\phi^A_\beta. \end{aligned} \tag{2.25}$$

The symmetry factor k takes the value $k = 2$ for $\phi^A_\alpha = \bar{\phi}^A_\alpha$ and $k = 1$ otherwise. The Feynman propagator is often written as Fourier transform

$$D^{(A)}_{F,\alpha\beta}(z) = \int \frac{\mathrm{d}^4q}{(2\pi)^4} e^{-iqz}\tilde{D}^{(A)}_{F,\alpha\beta}(q). \tag{2.26}$$

Now, remember in order to calculate cross sections one has to evaluate the Fourier transform of Green's functions. This can be done with the Gell-Mann and Low theorem. Therefore, the numerator and denominator of Eq. (2.19) have to be evaluated by finding all possible full contractions. Each contraction gives the Feynman propagator D_F. The exponential can be expanded term by term. Performing the space time integrals coming from expanding the exponential one finds momentum conservation for the momenta that are associated with the propagators that connect to the fields at the space-point that was integrated over. This allows to formulate Feynman rules to visualize and calculate these vacuum expectation values [52]. Since the Green's functions in momentum space occur in the LSZ formula, it is useful to formulate the Feynman rules also in momentum space.

In order to calculate $\tilde{G}^{(n)}_{\Phi^{A_1}_{\alpha_1}\cdots\Phi^{A_n}_{\alpha_n}}(p_1,\ldots,p_n)$:

1. Draw external points for each field $\Phi^{A_i}_{\alpha_i}$.
2. In $\mathcal{O}\big(\mathcal{L}^k_{\text{int}}\big)$ draw k inner points called vertices:
   (a) Each vertex corresponds to a term in $\mathcal{L}_{\text{int}} = \sum_i \mathcal{L}^{(i)}_{\text{int}}$ with $\mathcal{L}^{(i)}_{\text{int}} = -\frac{g_i}{s_i} B_i^{\alpha_1\ldots\alpha_n} \prod_{j=1}^n \Phi^{A_j}_{\alpha_j}$.
   (b) For the sake of the next step, a vertex counts as multiple points, one for each $\Phi^{A_j}_{\alpha_j}$ in $\mathcal{L}^{(i)}_{\text{int}}$.
3. Connect all points such that a point stemming from Φ^A is connected to a point stemming from a $\bar{\Phi}^A$. Now, each vertex must have a number of outgoing lines equal to the number of field in the corresponding $\mathcal{L}^{(i)}_{\text{int}}$ term.
4. If it is impossible to connect all points, the contribution considered is zero. One has to choose different $\mathcal{L}^{(i)}_{\text{int}}$ terms or increase the order k.
5. Label all lines connected to an external point with the incoming momentum p_i that is the associated momentum with the field $\Phi^{A_i}_{\alpha_i}$. They are called them propagators.
6. Label all other lines with a directed momentum k_i, where i is a different index for each inner line. They are called inner propagators.

The resulting diagram can be translated into a mathematical term. Each line represents a contraction and yields the Feynman propagator in momentum space $D^{(A)}_{F,\alpha\beta}(q)$, where A specifies the particle type of the line. Hence, the lines are also called propagators. The momentum q is the directed momentum flowing from the point associated with the $\bar{\Phi}^A_\alpha$ to the point from Φ^A_β.

The indices α and β will either be contracted with a factor stemming from the vertex to which they are connected or left uncontracted if the propagator is connected to an external point. Each vertex yields the factor $-ig_i B_i^{\alpha_1 \cdots \alpha_n}$ where i is the index of $\mathcal{L}_{\text{int}}^{(i)}$ that created the vertex. The field operators in $\mathcal{L}_{\text{int}}^{(i)}$ are contracted, and the factor $1/s_i$ is assumed to cancel due to the multiple permutations of the fields that lead to the same contractions. For the case the factor $1/s_i$ is not canceled, an additional symmetry factor $1/m$ is applied. The inverse symmetry factor m is equal to the number of all possible ways to connect the inner points and get the same Feynman diagram. This usually happens for diagrams with closed loop that identical particle propagators in the loop. The factor $1/k!$ coming from the expansion of the exponential cancels with the $k!$ permutations of the $\mathcal{L}_{\text{int}}^{(i)}$ terms. Next, one has to integrate over all momenta of inner propagators $\int \prod \mathrm{d}^4 k_i$. Each vertex yields a delta distribution $(2\pi)^4 \delta^{(4)}(\sum q_i)$ stemming from the space-time integral over $\mathcal{L}$ in the exponential. Thereby, q_i are the momenta flowing into the vertex. If a momentum is drawn with the direction going away from the vertex a minus sign must be added for that momentum. These delta distribution ensure momentum conservation at every vertex. After carrying out all integrals over $\mathrm{d}^4 k_i$ until no k_i remains in a delta distribution, only delta distributions containing external momenta p_i remain. The number of remaining delta distributions is equal to the number of connected subdiagrams in the Feynman diagram. The delta distributions are $(2\pi)^4 \delta(\sum_i p_i)$, where the p_i in the sum are the momenta of the external legs of the connected subdiagram.

This procedure has to be done for every possible way to connect the k vertices for every selection of k $\mathcal{L}_{\text{int}}^{(i)}$ terms, in all orders of k. In practice, one cannot evaluate an infinite amount of Feynman diagrams, therefore one can sort the Feynman diagrams by their orders in g_i and stop the evaluation after a selected order of g_i.

With the use of Feynman rules, the Gell-Mann and Low theorem Eq. (2.19) can be evaluated in the momentum space. The denominator has the structure of

$$\langle 0 | \, T \exp\left\{ i \int \mathrm{d}^4 y \mathcal{L}_{\text{int}}(y) \right\} | 0 \rangle = 1 + \sum_{v \in V} v, \tag{2.27}$$

where V is the set of all diagrams without any external points, i.e. vacuum diagrams. Meanwhile, the nominator is

$$\langle 0 | \, T \left(\phi_{\alpha_1}^{A_1}(x_1) \cdots \phi_{\alpha_n}^{A_n}(x_n) \exp\left\{ i \int \mathrm{d}^4 y \mathcal{L}_{\text{int}}(y) \right\} \right) | 0 \rangle = \sum_{c \in C} c + \sum_{\tilde{v} \in \tilde{V}} \tilde{v}. \tag{2.28}$$

Here, C is the set of all the diagrams where every internal vertex is connected to at least one external point and $\tilde{V}$ is the set containing all the other diagrams. Hence, all diagrams in $\tilde{V}$ are not connected Feynman diagrams and can be written as product of connected Feynman diagrams. In particular the diagrams in $\tilde{V}$ contain vacuum diagrams as a disconnected part. Consequently, one can write

$$\forall \tilde{v} \in \tilde{V} \exists! c_{\tilde{v}} \in C, v_{\tilde{v}} \in V : \tilde{v} = c_{\tilde{v}} v_{\tilde{v}}. \tag{2.29}$$

Now, the sum of the diagrams can be reordered

$$\begin{aligned}
&\langle 0| T\left(\phi_{\alpha_1}^{A_1}(x_1)\cdots\phi_{\alpha_n}^{A_n}(x_n)\exp\left\{i\int \mathrm{d}^4y \mathcal{L}_{\mathrm{int}}(y)\right\}\right)|0\rangle \\
&\qquad = \sum_{c\in C} c + \sum_{\tilde{v}\in\tilde{V}} \tilde{v} \\
&\qquad = \sum_{c\in C} c + \sum_{\tilde{v}\in\tilde{V}} c_{\tilde{v}} v_{\tilde{v}} \\
&\qquad = \sum_{c_{\tilde{v}}\in C} c_{\tilde{v}} + \sum_{v_{\tilde{v}}\in V} c_{\tilde{v}} v_{\tilde{v}} \\
&\qquad = \sum_{c_{\tilde{v}}\in C} c_{\tilde{v}}\left(1 + \sum_{v_{\tilde{v}}\in V} v_{\tilde{v}}\right).
\end{aligned} \tag{2.30}$$

In the end, one obtains

$$\begin{aligned}
&\langle \Omega| T\big(\Phi_{\alpha_1}^{A_1}(x_1)\cdots\Phi_{\alpha_n}^{A_n}(x_n)\big)|\Omega\rangle \\
&\qquad = \frac{\langle 0| T\big(\phi_{\alpha_1}^{A_1}(x_1)\cdots\phi_{\alpha_n}^{A_n}(x_n)\exp\big\{i\int \mathrm{d}^4y \mathcal{L}_{\mathrm{int}}(y)\big\}\big)|0\rangle}{\langle 0| T\exp\big\{i\int \mathrm{d}^4y \mathcal{L}_{\mathrm{int}}(y)\big\}|0\rangle} \\
&\qquad = \frac{\sum_{c_{\tilde{v}}\in C} c_{\tilde{v}}\big(1+\sum_{v_{\tilde{v}}\in V} v_{\tilde{v}}\big)}{1+\sum_{v\in V} v} \\
&\qquad = \sum_{c\in C} c.
\end{aligned} \tag{2.31}$$

Hence, in order to calculate a Green's function one only needs to calculate all the Feynman diagrams without vacuum diagrams as subdiagrams.

For the LSZ theorem, only the amputated Green's function is needed. Diagrammatically, one can understand the amputated Green's function as all the Feynman diagrams, where all the external legs are cut off. On can find that Feynman diagrams, in which two external points are connected to each other but not to any other external points, yield 0 in the context of

the S-matrix element. Furthermore, for processes with two particles in the initial state, the only possible non-connected Feynman diagrams, excluding the vacuum diagram and diagrams where the initial and final state particles are not connected, are the diagrams in which both initial states decay into the final state particles independently from one another. If these decays are not possible for any reason, like it is the case for processes considered in this work, then only connected Feynman diagrams can contribute to the S-matrix elements. If all diagrams are connected, then each of them has only one connected subdiagram, namely the diagram itself. This leads to only one remaining delta distribution $(2\pi)^4\delta^{(4)}(\sum p_i - \sum p_f)$ in the Fourier transformed Green's function, which can be factored out

$$\tilde{G}^{(n+m)}_{\text{amp},\bar{\Phi}^{A_1}_{\alpha_1}\dots\bar{\Phi}^{A_n}_{\alpha_n}\Phi^{B_1}_{\beta_1}\dots\Phi^{B_m}_{\beta_m}}(p_1,\dots,p_m,-k_1,\dots,-k_n) = (2\pi)^4\delta^{(4)}(\sum p_i - \sum k_f) M_{\text{amp},\bar{\Phi}^{A_1}_{\alpha_1}\dots\bar{\Phi}^{A_n}_{\alpha_n}\Phi^{B_1}_{\beta_1}\dots\Phi^{B_m}_{\beta_m}}(p_1,\dots,p_m,-k_1,\dots,-k_n). \tag{2.32}$$

Then, the matrix element $\mathcal{M}_{f\leftarrow i}$, needed for the cross section, is

$$\mathcal{M}_{f\leftarrow i} = \prod_{i=1}^{m}\left(\sqrt{Z_{A_i}}u^{s_i}_{\alpha_i}(p_i)\right)\prod_{j=1}^{m}\left(\sqrt{Z_{A_j}}\bar{u}^{\lambda_j}_{\beta_j}(k_j)\right) \times M_{\text{amp},\bar{\Phi}^{A_1}_{\alpha_1}\dots\bar{\Phi}^{A_n}_{\alpha_n}\Phi^{B_1}_{\beta_1}\dots\Phi^{B_m}_{\beta_m}}(p_1,\dots,p_m,-k_1,\dots,-k_n). \tag{2.33}$$

In other words, the amplitude $\mathcal{M}_{f\leftarrow i}$ is the sum of all amputated and connected Feynman diagrams multiplied with a polarization factor for every external field and the square root of the residue of the two point function of each field.

2.2 Standard Model

2.2.1 Gauge theory

The concept of gauge theories was first discussed by Weyl in Ref. [53]. Here, it is shown for the simplest theory that describes relativistic fields, the Dirac Lagrangian [54]

$$\mathcal{L}_{\text{Dirac}} = \bar{\psi}(i\partial\!\!\!/ - m)\psi. \tag{2.34}$$

The Dirac slash is used $a\!\!\!/ = \gamma^\mu a_\mu$ as well as the bar notation $\bar{\psi} = \psi^\dagger\gamma^0$. Thereby, γ^μ are referred to as gamma matrices and their defining property is fulfilling the Clifford algebra

$$\{\gamma^\mu,\gamma^\nu\} = \gamma^\mu\gamma^\nu + \gamma^\nu\gamma^\mu = 2g^{\mu\nu}. \tag{2.35}$$

By looking at the Lagrangian $\mathcal{L}_{\text{Dirac}}$, one can quickly see that it is invariant under the transformation

$$\psi \longrightarrow U\psi = e^{i\theta}\psi, \tag{2.36}$$

if θ is a constant real number. One can promote this global transformation to a local one by modifying θ to a function $\theta(x)$ and observe the impact of the transformation on the Lagrangian

$$\begin{aligned}\mathcal{L}_{\text{Dirac}} &\longrightarrow \bar{\psi}U^\dagger(i\partial\!\!\!/ - m)U\psi \\ &= \bar{\psi}(iU^\dagger\partial\!\!\!/ U - m)\psi = \bar{\psi}(i\partial\!\!\!/ - (\partial\!\!\!/\theta) - m)\psi.\end{aligned} \tag{2.37}$$

One can alter the Lagrangian to make it invariant under this transformation. In order to do this, one has to include a new term that transforms such that the extra term $-\bar{\psi}(\partial\!\!\!/\theta)\psi$ is canceled. Or equivilantly, replace $\partial\!\!\!/ \rightarrow D\!\!\!/ = \partial\!\!\!/ + i\tilde{Q}A\!\!\!/$ such that $D\!\!\!/$ transforms as $D\!\!\!/ \rightarrow UD\!\!\!/U^\dagger$. Thereby, A^μ is a newly introduced field. The transformation properties of A^μ can be seen by evaluating

$$\begin{aligned}UD\!\!\!/U^\dagger &= e^{i\theta}(\partial\!\!\!/ + i\tilde{Q}A\!\!\!/)e^{-i\theta} \\ &= \partial\!\!\!/ - i(\partial\!\!\!/\theta) + i\tilde{Q}A\!\!\!/.\end{aligned} \tag{2.38}$$

Then, A^μ has to transform as

$$\begin{aligned}A^\mu &\longrightarrow A^\mu - \frac{1}{\tilde{Q}}\partial^\mu\theta \\ &=: A^\mu + \partial^\mu\chi.\end{aligned} \tag{2.39}$$

In the last line χ is defined as $\chi = -\theta/\tilde{Q}$. This transformation is the same as the gauge transformation for the electromagnetic vector field in the Maxwell theory. Hence, this transformation will also be called gauge transformation from now on. Now, one can write down the modified Dirac Lagrangian

$$\begin{aligned}\mathcal{L}_{\text{Dirac, mod.}} &= \bar{\psi}(iD\!\!\!/ - m)\psi, \\ D^\mu &= \partial^\mu + i\tilde{Q}A^\mu.\end{aligned} \tag{2.40}$$

So far, the newly defined field A^μ does not contain any physical degrees of freedom, because there are no kinetic terms in the Lagrangian. The goal is to interpret A^μ as the electromagnetic vector potential. Consequently, the kinetic term of the Maxwell Lagrangian is a natural choice, since it is Lorentz

invariant and also invariant under the gauge transformation. This leads to the Lagrangian for electrodynamics

$$\begin{aligned}\mathcal{L}_{\mathrm{ED}} &= -\frac{1}{4}F^{\mu\nu}F_{\mu\nu} + \bar{\psi}(i\not{D} - m)\psi,\\ D^{\mu} &= \partial^{\mu} + ieQA^{\mu},\\ F^{\mu\nu} &= \frac{1}{ieQ}[D^{\mu}, D^{\nu}] = \partial^{\mu}A^{\nu} - \partial^{\nu}A^{\mu}.\end{aligned} \tag{2.41}$$

Here, $\tilde{Q} = eQ$ is rescaled to the elementary charge e to match common notation.

So far, no quantization has taken place. Everything was classical field theory. Now, one can try to quantize $\mathcal{L}_{\mathrm{ED}}$ using canonical quantization. One would find that it is impossible. The gauge freedom prevents quantization. By looking at the momentum conjugate π^0 of A^0 one finds

$$\pi^0 = \frac{\partial \mathcal{L}_{\mathrm{ED}}}{\partial \dot{A}_0} = 0. \tag{2.42}$$

In canonical quantization it is required that

$$[\hat{A}^0(\mathbf{x}, t), \hat{\pi}^0(\mathbf{y}, t)]_{\mp} = i\hbar\delta^{(3)}(\mathbf{x} - \mathbf{y}), \tag{2.43}$$

which is impossible if $\pi^0 = 0$. In order to solve this problem, one can introduce a gauge fixing term in the Lagrangian $\mathcal{L}_{\mathrm{QED}} = \mathcal{L}_{\mathrm{ED}} + \mathcal{L}_{\mathrm{fix}}$ [55]. This term has to break gauge symmetry and represents choosing a gauge. One common choice is [56]

$$\mathcal{L}_{\mathrm{fix}} = \frac{1}{2\xi}(\partial^{\mu}A_{\mu})^2. \tag{2.44}$$

In this gauge fixing term, the freedom of choosing the gauge it embodied by the gauge parameter ξ. Every physical observable has to be independent of ξ. Therefore, one can choose a value of ξ arbitrarily. A common choice is the Feynman gauge $\xi = 1$. In the Feynman gauge the propagator of the photon is particularly compact.

All gauge transformations U form the group of one dimensional unitary matrices U(1). One can generalize the above procedure to other gauge groups. Especially interesting are the special unitary groups of rank n, SU(n). These are complex $n \times n$ matrices with determinant 1. In general, two different gauge transformations $U_1, U_2 \in SU(n)$ do not commute. Those gauge theories are therefore referred to as non-Abelian gauge theories or Yang-Mills theories [57]. Since matrices $U \in SU(n)$ are unitary, one can write them as

$$U = \exp\{-i\theta_a T^a\}, \tag{2.45}$$

where T^a are $n^2 - 1$ traceless, hermitian matrices and θ_a are real functions $\theta = \theta(x)$. T^a are called the generators of the Lie group. They define the Lie algebra

$$[T^a, T^b] = i f^{ab}{}_c T^c, \tag{2.46}$$

and are conventionally normed to

$$\mathrm{tr}\left[T^a T^b\right] = \frac{\delta^{ab}}{2}. \tag{2.47}$$

$f^{ab}{}_c$ are the totally antisymmetric structure constants. Every set of operators t^a that fulfills Eq. (2.46) is a representation of the gauge transformation. In particle physics, three representations are especially important. Firstly, the fundamental representation $t^a_{\text{fund}} := T^a$ that generates the transformation from Eq. (2.45). Next, there is the trivial representation $t^a_{\text{trivial}} := 0$, which obviously fulfills Eq. (2.46). Lastly, the adjoint representation $\left(t^a_{\text{adj}}\right)_{bc} = -i f^a{}_{bc}$ defines the transformation of gauge bosons.

One can repeat the same process for this new gauge transformation. Now, the field ψ has n components ψ_i in the space the gauge transformation takes place

$$\begin{aligned}
\mathcal{L}_{\text{Dirac, mod2}} &= \bar{\psi}(i\not{D} - m)\psi, \\
U D^\mu U^\dagger &= U(\partial^\mu + igA^\mu)U^\dagger \\
&= \partial^\mu + iT^a(\partial^\mu \theta_a) + igUA^\mu U^\dagger. \\
\Longrightarrow A^\mu &\longrightarrow UA^\mu U^\dagger + \frac{1}{g} T^a(\partial^\mu \theta_a).
\end{aligned} \tag{2.48}$$

The last line shows that A^μ cannot be a scalar in the space of the $SU(n)$ matrices, but it rather is a matrix $(A^\mu)_i{}^j$ acting on the vector ψ_j. In fact, A^μ can be understood as the connection field that transports $\psi_i(x)$ parallel to an infinitesimal adjacent space-time point $\psi_{\|i}(x + \mathrm{d}x)$. One can expand A^μ by the generators T^a and define

$$(A^\mu)_i{}^j =: A^\mu_a (T^a)_i{}^j. \tag{2.49}$$

This means one gets one gauge field for each generator T^a.

Now, only the kinetic terms of the gauge fields A^μ_a are missing for the Lagrangian. To this end,a field strength tensor $A^{\mu\nu}$ is defined in the same manner as in the Abelian case

$$A^{\mu\nu} := \frac{1}{ig}[D^\mu, D^\nu] = \partial^\mu A^\nu - \partial^\nu A^\mu + ig[A^\mu, A^\nu]. \tag{2.50}$$

Since D^μ was constructed to transform as $D^\mu \longrightarrow U D^\mu U^\dagger$, $A^{\mu\nu}$ has the same gauge transformation law $A^{\mu\nu} \longrightarrow U A^{\mu\nu} U^\dagger$. Due to the cyclic property of the trace, the expression

$$\mathrm{tr}\,[A^{\mu\nu} A_{\mu\nu}] \tag{2.51}$$

is locally gauge invariant. The field strength tensor can be expanded in the same way as the gauge field

$$(A^{\mu\nu})_i{}^j = A_a^{\mu\nu} (T^a)_i{}^j. \tag{2.52}$$

Then, one can write

$$\mathrm{tr}\,[A^{\mu\nu} A_{\mu\nu}] = A_a^{\mu\nu} A_{\mu\nu b}\,\mathrm{tr}\left[T^a T^b\right] = \frac{1}{2} A_a^{\mu\nu} A^a_{\mu\nu}, \tag{2.53}$$

where the normalization of the generators T^a was used. The field strength tensor can be rewritten as

$$\begin{aligned} A^{\mu\nu} &= \partial^\mu A^\nu - \partial^\nu A^\mu + ig[A^\mu, A^\nu] \\ &= \partial^\mu A^\nu - \partial^\nu A^\mu + ig A_a^\mu A_b^\nu [T^a, T^b] \\ &= \partial^\mu A^\nu - \partial^\nu A^\mu - g A_a^\mu A_b^\nu f^{ab}{}_c T^c, \\ \Rightarrow A_a^{\mu\nu} &= \partial^\mu A_a^\nu - \partial^\nu A_a^\mu - g A_b^\mu A_c^\nu f_a{}^{bc}. \end{aligned} \tag{2.54}$$

This allows to formulate a Yang-Mills Lagrangian that is gauge invariant,

$$\begin{aligned} \mathcal{L}_{\mathrm{YM}} &= -\frac{1}{4} A_a^{\mu\nu} A^a_{\mu\nu} + \bar{\psi}(i\not{D} - m)\psi, \\ D^\mu &= \partial^\mu + igT^a A_a^\mu, \\ A_a^{\mu\nu} &= \partial^\mu A_a^\nu - \partial^\nu A_a^\mu - g A_b^\mu A_c^\nu f_a{}^{bc}. \end{aligned} \tag{2.55}$$

One major feature of this theory that is absent in the Abelian gauge theory is the self-interaction of the gauge fields A_a^μ. Due to the fact that $[A^\mu, A^\nu] \neq 0$, one gets cubic and quartic terms in A^μ in the Lagrangian.

In order to quantize the Lagrangian in Eq. (2.55), a gauge fixing term has to be added. However, this is not possible in the same straight forward manner as in the Abelian case. The procedure uses a trick reported first by Faddeev and Popov in Ref. [56]

2.2.2 Lagrangian of the Standard Model

In the second half of the 20th century the Standard Model of particle physics was developed [4–6,9,57–60]. This section gives a brief overview of its content.

Table 2.1: Particles of the Standard Model together and their respective representation under the gauge transformations.

Particle	Field operator	$SU(3)_c$	$SU(2)_L$	$U(1)_Y$
Higgs doublet	$\Phi = \begin{pmatrix} G^+ \\ \frac{v+H+iG}{\sqrt{2}} \end{pmatrix}$	$T_s^a \Phi = 0$	$T_w^a \Phi = \frac{\sigma^a}{2} \Phi$	$Y\Phi = \frac{1}{2}\Phi$
Quark doublet	$Q_L = P_L Q_L = \begin{pmatrix} u_L \\ d_L \end{pmatrix}$	$T_s^a Q_L = \frac{\lambda^a}{2} Q_L$	$T_w^a Q_L = \frac{\sigma^a}{2} Q_L$	$YQ_L = \frac{1}{6} Q_L$
Up-type-singlet	$u_R = P_R u_R$	$T_s^a u_R = \frac{\lambda^a}{2} u_R$	$T_w^a u_R = 0$	$Y u_R = \frac{2}{3} u_R$
Down-type-singlet	$d_R = P_R d_R$	$T_s^a d_R = \frac{\lambda^a}{2} d_R$	$T_w^a d_R = 0$	$Y d_R = -\frac{1}{3} d_R$
Lepton doublet	$L_L = P_L L_L = \begin{pmatrix} \nu_L \\ e_L \end{pmatrix}$	$T_s^a L_L = 0$	$T_w^a L_L = \frac{\sigma^a}{2} L_L$	$Y L_L = -\frac{1}{2} L_L$
Electron-singlet	$e_R = P_R e_R$	$T_s^a e_R = 0$	$T_w^a e_R = 0$	$Y e_R = -1 e_R$

The Standard Model is a gauge theory with a $U(1)_Y \times SU(2)_L \times SU(3)_c$ gauge group. The gauge symmetry of $U(1)_Y \times SU(2)_L$ is spontaneously broken to a $U(1)_Q$ gauge symmetry by a scalar doublet field Φ. The matter content and their representations under the various gauge transformations can be seen in Table 2.1. In the Standard Model, fermion spinors are seperated into their two irreducible representations of the Lorentz group, a right-handed and left-handed chirality spinor, $\psi = \psi_L + \psi_R$. Projection operators are defined as $P_L := (1 - \gamma^5)/2$ and $P_R := (1 + \gamma^5)/2$, with $\gamma^5 = i\gamma^0\gamma^1\gamma^2\gamma^3$, that fulfill the properties

$$\begin{aligned} &P_L^2 = P_L, && P_R^2 = P_R, && P_R + P_L = \mathbb{1}, \\ &P_R P_L = 0, && \psi_L = P_L \psi, && \psi_R = P_R \psi. \end{aligned} \tag{2.56}$$

The Lagrangian is

$$\begin{aligned} \mathcal{L}_{\text{SM}} &= \mathcal{L}_{\text{matter}} + \mathcal{L}_{\text{gauge}} + \mathcal{L}_{\text{Yukawa}} + \mathcal{L}_{\text{H-potential}} + \mathcal{L}_{\text{gauge fix}} + \mathcal{L}_{\text{ghost}}, \\ \mathcal{L}_{\text{matter}} &= (D^\mu \Phi)^\dagger D_\mu \Phi + \bar{Q}_L i \not{D} Q_L + \bar{u}_R i \not{D} u_R \\ &\quad + \bar{d}_R i \not{D} d_R + \bar{L}_L i \not{D} L_L + \bar{e}_R i \not{D} e_R, \\ \mathcal{L}_{\text{gauge}} &= -\frac{1}{4} G_a^{\mu\nu} G^a_{\mu\nu} - \frac{1}{4} W_a^{\mu\nu} W^a_{\mu\nu} - \frac{1}{4} B^{\mu\nu} B_{\mu\nu}, \\ \mathcal{L}_{\text{Yukawa}} &= -y_e \bar{L}_L \Phi e_R - y_d \bar{Q}_L \Phi d_R - y_u \tilde{\Phi} \bar{Q}_L u_R + h.c., \\ \mathcal{L}_{\text{H-potential}} &= -\mu^2 \Phi^\dagger \Phi - \lambda \big(\Phi^\dagger \Phi\big)^2, \end{aligned} \tag{2.57}$$

with

$$\begin{aligned} D^\mu &= \partial^\mu + ig_s T_s^a G_a^\mu + ig_W T_W^a W_a^\mu + ig_Y Y B^\mu, \\ G^{\mu\nu} &= \frac{1}{ig_s}[\partial^\mu + ig_s G^\mu, \partial^\nu + ig_s G^\nu], \\ W^{\mu\nu} &= \frac{1}{ig_W}[\partial^\mu + ig_W W^\mu, \partial^\nu + ig_W W^\nu], \\ B^{\mu\nu} &= \frac{1}{ig_Y Y}[\partial^\mu + ig_Y Y B^\mu, \partial^\nu + ig_Y Y B^\nu]. \end{aligned} \tag{2.58}$$

The explicit forms of $\mathcal{L}_{\text{gauge fix}}$ and $\mathcal{L}_{\text{ghost}}$ are not relevant in this work, they introduce non-physical ghost fields that interact with non-Abelian gauge fields and the massive Higgs field. They can be reviewed in Refs. [61–65]

Thereby, the generators T_s^a, T_W^a and the so called hyper charge Y can be understood as operators acting on the various field operators. The parameter μ^2 in the Higgs boson potential is set to be $\mu^2 < 0$. This leads to spontaneous symmetry breaking of the $U(1)_Y \times SU(2)_L$ symmetry. The classical minimum of the Higgs potential is at $|\Phi_{\text{min}}|^2 = -\frac{\mu^2}{2\lambda}$. The idea is to study small excitations around this minimum $\Phi = \Phi_{\text{min}} + \Phi_{\text{excitation}}$, with $\Phi_{\text{excitation}}$ containing the field operators and the physical degrees of freedom. The electric charge operator Q can be defined as

$$Q := T^3 + Y. \tag{2.59}$$

Motivated by observation, the electric charge is forced to be conserved and shall generate the $U(1)_Q$ symmetry. This fixes Φ_{min}

$$\begin{aligned} Q\Phi_{\text{min}} &= \begin{pmatrix} 1 & 0 \\ 0 & 0 \end{pmatrix} \Phi_{\text{min}} \stackrel{!}{=} 0 \\ \Rightarrow \Phi_{\text{min}} &= \begin{pmatrix} 0 \\ \sqrt{-\frac{\mu^2}{2\lambda}} \end{pmatrix}. \end{aligned} \tag{2.60}$$

Therefore, one parametrizes the Higgs boson field as shown in table 2.1 by defining the new parameter

$$v^2 = -\frac{\mu^2}{\lambda} > 0. \tag{2.61}$$

Due to the non-vanishing vacuum expectation value (vev) of the Higgs boson, the term $(D^\mu \Phi)^\dagger D_\mu \Phi$ contains bilinear terms in the gauge bosons W_a^μ and B_a^μ. By appropriate redefinitions, one can diagonalize these terms and

obtain proper mass terms. These redefinitions are

$$W^{\pm\mu} := \frac{1}{\sqrt{2}}(W_1^\mu \mp W_2^\mu),$$
$$\begin{pmatrix} A^\mu \\ Z^\mu \end{pmatrix} := \begin{pmatrix} \cos\theta & \sin\theta \\ -\sin\theta & \cos\theta \end{pmatrix} \begin{pmatrix} B^\mu \\ W_3^\mu \end{pmatrix}. \tag{2.62}$$

The new defined gauge boson A^μ represents the photon and thus the gauge boson the the electromagnetic force. It shall not interact with the neutrino ν. By plugging the redefinitions into the covariant derivative D^μ and investigating the action of D^μ on the lepton doublet L, the condition

$$\tan\theta = \frac{g_Y}{g_W} \Leftrightarrow \sin\theta = \frac{g_Y}{\sqrt{g_Y^2 + g_W^2}} \tag{2.63}$$

ensures no interaction between a photon and a neutrino. Further, the electron shall have the electric charge $-e$, i.e. the interaction term between the photon A^μ and electron e_L shall be $-ieA^\mu e_L$. This is achieved by identifying

$$e := \frac{g_Y g_W}{\sqrt{g_Y^2 + g_W^2}}. \tag{2.64}$$

The covariant derivative becomes

$$D^\mu = \partial^\mu + ieQA^\mu + i\frac{e}{\sin\theta\cos\theta}\big(T^3 - Q\sin^2\theta\big)Z^\mu$$
$$+i\frac{e}{\sqrt{2}\sin\theta}\big[(T^1 + iT^2)W^{+\mu} + (T^1 - iT^2)W^{-\mu}\big]. \tag{2.65}$$

The last piece missing to complete the Standard Model are the three fermion generations that have been observed. In order to account for this, all fermion operators get an additional generation index $I \in 1, 2, 3$, e.g. e_R^I. A priori, all Yukawa couplings y now become matrices in the generation space

$$\mathcal{L}_{\text{Yukawa}} = -y_{eIJ}\bar{L}_L^I \Phi e_R^J - y_{dIJ}\bar{Q}_L^I \Phi d_R^J - y_{uIJ}\tilde{\Phi}\bar{Q}_L^I u_R^J + h.c.. \tag{2.66}$$

By appropriate redefinitions of the mass eigenstate fields $e_L, e_R, \nu_L, u_L, u_R, d_L$ and d_R, y_e and y_u can be transformed into diagonal matrices of positive entries, without changing any other term in the Lagrangian. However, this is not possible at the same time for y_d. Consequently, the mass eigenstate fields of the down-type quarks are not the same as the interaction eigenstate fields. By diagonalizing the y_d, the replacement $d \to V^{IJ}d_J$ takes place everywhere in the Lagrangian. The matrix V^{IJ} is called Cabibbo-Kobayashi-Maskawa (CKM) matrix. The CKM matrix is unitary, therefore it cancels in every term of the form of $\sim \bar{d}d$ and it can only occur in interaction terms that involve an up-type quark together with a down-type quark.

2.2.3 Feynman rules of the Standard Model

From the Lagrangian of the previous section one can derive Feynman rules. The following rules are used to calculate the amplitudes of the deep inelestic scattering process.

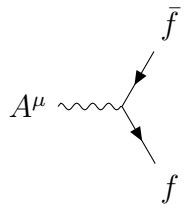

$$= -iQ_f e\gamma^\mu$$

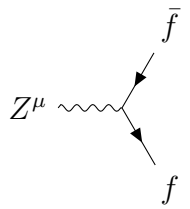

$$= -\frac{ie}{2\sin\theta\cos\theta}\gamma^\mu\Big(I_3^f P_L - 2Q_f \sin^2\theta\Big)$$

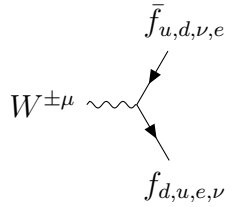

$$= -\frac{ie}{\sqrt{2}\sin\theta}\gamma^\mu P_L$$

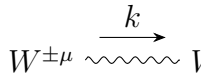

$$= \frac{-ig_{\mu\nu}}{k^2 - M_W^2 + i\varepsilon}$$

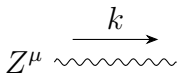

$$= \frac{-ig_{\mu\nu}}{k^2 - M_Z^2 + i\varepsilon}$$

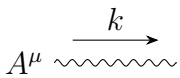

$$= \frac{-ig_{\mu\nu}}{k^2 - M_Z^2 + i\varepsilon} \tag{2.67}$$

2.2.4 Calculation method in the Standard Model

One important feature of any non-Abelian gauge theory, as QCD, is the increasing gauge coupling for low energy scales. Physically this means, forces between strongly interacting particles increase with longer distances. Hence, perturbation theory is not applicable for describing long distance or equivalently low energy effects. Consequently, strongly interacting elementary

particles cannot exist as isolated single particles. They clump up to form hadrons. This breaks assumptions that were put in the formalism discussed thus far. However, inside of these compound particle states, where distances become very short, the strong interaction becomes weak and the quarks forming the hadron can be considered free.

The general strategy to deal with strongly interacting particles in initial and final state is to split the scattering process in different time steps [66]. The first time step describes the incoming scattering hadrons before they interact with each other. Therefore, they are described as a bundle of partons, where each parton carries a fraction x of the hadron momentum P. To this end, PDFs $f(x)$ are defined for each parton. At leading order (LO) they describe the probability density of finding the parton with momentum fraction x in the hadron. These PDFs can not be calculated within perturbation theory and are determined by experimental data.

The next step, the actual collision takes place. If the incoming scattering particles have a large energy, this collision takes place in a very short time frame, such that it can be described perturbatively. Thereby, cross sections $\hat{\sigma}_q(x)$ for each parton q with momentum fraction x are calculated and convoluted with the PDFs $f_q(x)$ to yield the total hadronic cross section σ

$$\sigma = \sum_q \int \mathrm{d}x f_q(x) \hat{\sigma}_q(x). \tag{2.68}$$

After the hard collision, final state particles can radiate more particles with increasing time scale. Parton shower algorithms are used to describe this behavior until the time scale of this radiation is too large to justify perturbation theory. The last step is hadronization in which strongly interacting final state elementary particles form bound states.

2.3 Next-to-leading order calculation

In order to evaluate Green's functions, one has to expand the exponential in Eq. (2.19) in all orders. In practice this is impossible. Therefore, one stops the series at a particular order in the coupling constants. The lowest order in the coupling constants that contributes to the process at hand is called the LO. For simple processes, the LO consists only of Feynman diagrams that do not contain any closed loops. These Feynman diagrams are referred to as tree-level diagrams. The next terms in higher order of the coupling constants are called NLO contributions. These diagrams contain closed loops, leading to momenta that are not constrained by momentum conservation, and therefore have to be integrated over. They are called n-loop diagrams, with n being the

number of unconstrained momenta that need to be integrated. Physically, loop diagrams contain the quantum effects of the theory, while tree-level diagrams represent the classical effects, which are possible to obtain without QFT.

The calculation of 1-loop diagrams is conceptually solved if the process is not too complicated. By applying the Feynman rules of the theory, one will find divergent loop diagrams. The divergences are classified as a infrared (IR) or ultraviolet (UV) divergence. A divergence is called a UV divergence if it originates from the loop momentum $k \to \pm\infty$. All other divergences are infrared divergences. This section will only focus on UV divergences.

2.3.1 Dimensional regularization

Divergences in QFTs can be be brought under control via regularization. The most popular regularization is the dimensional regularization [67]. In dimensional regularization, the space-time dimension D is continued into the complex place $\mathbb{C}$. Thereby, time is assigned to the 0th dimension and the remaining $D-1$ dimensions describe the space. A detailed description can be found in Ref. [68].

The main feature of dimensional regularization is the use of D dimensional integrals. They are defined to have the properties:

- Linearity:

$$\int \mathrm{d}^D k(af_1(k) + f_2(k)) = a\int \mathrm{d}^D k f_1(k) + \int \mathrm{d}^D k f_2(k). \tag{2.69}$$

- Translation invariance:

$$\int \mathrm{d}^D k f(k+p) = \int \mathrm{d}^D k f(k). \tag{2.70}$$

- Scaling:

$$\int \mathrm{d}^D k f(sk) = s^{-D}\int \mathrm{d}^D k f(k), \qquad \forall s \in \mathbb{C}. \tag{2.71}$$

- If $D \in \mathbb{N}$ and the integral is convergent, then the dimensional integral coincides with the usual integral.

By doing this continuation, the mass dimension $[\mathcal{L}]$ of the Lagrangian is altered. The Lagrangian is an energy density and, therefore, has units of

energy raised to the power of the number of dimensions $[\mathcal{L}] = [E]^D$. Parameters in the Lagrangian, like the coupling constants g_i, have their dimension altered such that the overall dimension is correct. The part carrying the altered dimension of parameters is factored out by $g \to \mu^a g$, with $[\mu] = [E]$ and a being chosen such that the term in the Lagrangian, in which g appears, has the correct dimension. In practice, all loop momentum integrals are replaced

$$\int \frac{\mathrm{d}^4 k}{(2\pi)^4} \to \mu^{4-D} \int \frac{\mathrm{d}^D k}{(2\pi)^D}. \tag{2.72}$$

This leaves the dimension of the integral invariant. The newly defined parameter μ is called renormalization scale.

1-loop integrals of the form

$$\mu^{4-D} \int \frac{\mathrm{d}^D k}{(2\pi)^D} \frac{1}{D_1(k) \cdots D_n(k)}, \tag{2.73}$$

where $D_n(k)$ is the nominator of the Feynman propagator, can be reduced to a master integral

$$I_n := \mu^{4-D} \int \frac{\mathrm{d}^D k}{(2\pi)^D} \frac{(-1)^n (n-1)!}{\left[k^2 - Q^2 + i\varepsilon\right]^n}. \tag{2.74}$$

This can be done by a technique called Feynman parametrization [69]. Thereby, $n-1$ Feynman parameter integrals $\int \mathrm{d}z_i$ are introduced. These newly introduced integrals have to be carried out later, which can be a difficult task on its own, depending on the number of parameters the loop integral depends on.

In Eq. (2.74), Q^2 is a quantity that does not depend on k but depends in general on the Feynman parameters and carries a mass dimension. This master integral can be calculated analytically using a Wick rotation [70]. The result is

$$I_n = \frac{i}{16\pi^2} Q^{4-2n} \left(\frac{4\pi\mu^2}{Q^2} \right)^{\epsilon} \Gamma(n - 2 + \epsilon). \tag{2.75}$$

Γ is the gamma function and the dimension D was substituted by $D =: 4-2\epsilon$. Hence, the four dimensional limit is retrieved by $\epsilon \to 0$. To get the final result the integral over any Feynman parameters has to be evaluated.

In general, 1-loop integrals may contain a polynomial in the loop momentum k^μ in the numerator of the integrand. By the Passarino-Veltman reduction, they can be reduced to integrals of the form of Eq. (2.73) [71, 72]. The concept of Passarino-Veltman is to make the ansatz that the integral has

to be a linear combination of all tensorial quantities appearing in the integral. By contracting with these tensorial quantities, one obtains a linear system of equations that can be solved for the components of the tensors. These components turn out to be a linear combination itself of scalar integrals of the form of Eq. (2.73)

The Gamma function in Eq. (2.75) is carrying the UV divergence. It has a pole for $n = 1, 2$ for $\epsilon \to 0$. Usually, the final result, after integrating the loop integrals, is expanded in ϵ around 0. The expansion of the Gamma function will then lead to $\frac{1}{\epsilon}$-poles for the UV divergent integrals.

2.3.2 Renormalization

UV divergent Green's functions are a problem for a theory, since they lead to divergent physical observables. On the other hand, measured observables in the real world are finite. The solution is called renormalization. The concept of renormalization is to find a Lagrangian $\mathcal{L}^{(\epsilon)}$, such that the observables and Green's functions of the theory are finite in the limit $\epsilon \to 0$. Therefore, the UV divergencies are shifted into the Lagrangian itself. A UV divergent Lagrangian is not problematic, since it is not an observable. Here, only renormalization at 1-loop level is considered. The procedure is described for example in Ref. [73] or various QFT textbooks [74, 75].

The most common approach to renormalize a theory with Lagrangian $\mathcal{L}$ is multiplicative renormalization. To this end, the Lagrangian is transformed into the bare Lagrangian $\mathcal{L} \to \mathcal{L}_b$ by replacing all fields Φ_α and parameters g_i of the theory into their bare versions $\Phi_\alpha \to \Phi_{b\,\alpha}$, $g_i \to g_{b\,i}$. Then, one defines

$$\begin{aligned} \Phi_{b\,\alpha} &=: \sqrt{Z_\Phi}\Phi_\alpha =: \sqrt{(1+\delta Z_\Phi)}\Phi_\alpha, \\ g_{b\,i} &=: (1+\delta Z_{g_i})g_i =: g_i + \delta g_i, \\ \Rightarrow \mathcal{L}_b &= \mathcal{L}_{\text{ren}} + \mathcal{L}_{\text{ct}}. \end{aligned} \tag{2.76}$$

All δZ and δg_i are called renormalization constants. The bare Lagrangian $\mathcal{L}_b$ can be expanded in the renormalization constants and all terms without renormalization constants are collected in the renormalized Lagrangian $\mathcal{L}_{\text{ren}}$. As a result, $\mathcal{L}_{\text{ren}}$ looks identical to the starting Lagrangian. $\mathcal{L}_{\text{ct}}$ contains all terms involving renormalization constants and is called the counter term Lagrangian. Each renormalization constant is treated formally as a 1-loop quantity, hence quadratic terms, or higher, in the renormalization constants, in $\mathcal{L}_{\text{ct}}$, are omitted. $\mathcal{L}_{\text{ct}}$ leads to a set of new counter term Feynman rules.

In the next step of renormalization, all UV divergent Green's functions are calculated at 1-loop level. Then, renormalization constraints are imposed, in general one constraint for each renormalization constant. The choice of these

constraints defines the renormalization scheme. The constraints have to be chosen such that the Green's function become finite. Two popular choices for renormalization schemes are the on-shell scheme and the modified minimal subtraction ($\overline{\text{MS}}$) scheme.

In the on-shell scheme, it is required that all mass parameters m_Φ of a particle field Φ in the Lagrangian $\mathcal{L}_{\text{ren}}$ are equal to the pole of the two-point function $\tilde{G}^{(2)}_{\Phi\Phi}(p_1, -p_1)$ of the respective field Φ. In this way, the mass parameter coincides with the physical, observable mass. Further, the residues of all two-point functions are set to 1. Lastly, the coupling renormalization constants have to be fixed. This can be done by setting a specific S-matrix element to a certain value.

In the $\overline{\text{MS}}$ scheme, a different set of constraints is chosen. Here, the renormalization constants are chosen such that they cancel exactly the $\frac{1}{\bar{\epsilon}}$ poles, where $\bar{\epsilon}$ is defined as

$$\frac{1}{\bar{\epsilon}} := \frac{1}{\epsilon} + \log 4\pi - \gamma_E, \tag{2.77}$$

where $\gamma_E \approx 0.577$ is the Euler-Mascheroni constant.

2.3.3 Infrared divergences

As mentioned in the previous sections, NLO calculations can give rise to two different types of divergences. Technically, UV divergences originate from the Gamma function in Eq. (2.75), while IR divergences may occur from divergent Feynman parameter integrals. However, both kinds of divergences can be regularized by dimensional regularization. Unlike UV divergences, IR divergences cannot be removed by the means of renormalization. This can be seen by studying the prefactors of the $\frac{1}{\epsilon}$-poles. In the case of a renormalizable theory, UV poles have only a polynomial in momenta as a prefactor. Since the Fourier transform of a polynomial gives delta distributions and their derivatives, these divergences can be interpreted as local interactions. Therefore, they can be compensated by adding local interaction terms to the Lagrangian. On the other hand, IR divergences come with logarithms of momenta as prefactors, and hence cannot be compensated by local interactions. This means IR divergences are a physical feature of the theory.

The phenomenon of IR divergence was first discussed in dept in Ref. [76]. Every theory containing massless gauge bosons will give rise to IR divergences. In the SM, those bosons are the photon and the gluons. The IR divergences originate from the fact that charged particles in quantum electrodynamics (QED) or QCD cannot be isolated at asymptotic times, due to the long range of electromagnetic and strong interactions. A charged particle

can emit or absorb a massless gauge boson of vanishing energy, without a detector being able to tell if this emission or absorption has happened. In other words, a final state of a charged particle is indistinguishable from the state in which the particle emitted a soft gauge boson. The LSZ reduction formula does not hold if it is impossible to isolate the initial or final state particles. In practice, this detail is ignored in calculations. The calculation of the S matrix elements is performed as if the LSZ formula holds [77]. The Kinoshita-Lee-Nauenberg (KLN) theorem [78, 79] states that these radiative contributions are canceled by loop contributions. This means, in order to obtain a finite NLO correction to a process involving charged particles in the initial or final state, one has to not only include the according 1-loop Feynman diagrams but also the radiative correction arising from a process with an additional gauge boson in the final state. This procedure has proven very successful and is hence widely used.

For now, it is assumed that the initial state particles will not produce IR divergences. These divergences will be discussed later. The NLO cross section σ of a $2 \to n$ scattering process can be separated into a LO part which is also called Born contribution σ_{Born}, the virtual contribution σ_{virt} which is the loop correction, and the real correction σ_{real} with the radiative corrections

$$\sigma = \sigma_{\text{Born}} + \sigma_{\text{virt}} + \sigma_{\text{real}}. \tag{2.78}$$

Each individual contribution can be calculated in dimensional regularization and the sum will be finite for $\epsilon \to 0$. The cross sections are integrals over the n particle phase space for the Born and virtual contribution and over the $n+1$ particle phase space for the real contribution

$$\sigma = \int \mathrm{d}\Phi_n \frac{\mathrm{d}\sigma_{\text{Born}}}{\mathrm{d}\Phi_n} + \int \mathrm{d}\Phi_n \frac{\mathrm{d}\sigma_{\text{virt}}}{\mathrm{d}\Phi_n} + \int \mathrm{d}\Phi_{n+1} \frac{\mathrm{d}\sigma_{\text{real}}}{\mathrm{d}\Phi_{n+1}}. \tag{2.79}$$

The individual virtual and real integrals are only finite in D dimensions. This raises the problem that performing a numerical calculation in D dimensions is impossible. Analytical calculations are also not feasible in general. A solution is to add and subtract a counter term. In order to do so, the $n+1$ particle phase space measure has to be factorized into the n particle phase space measure and the integration over the momentum of the additional radiation

$$\mathrm{d}\Phi_{n+1} = \mathrm{d}\Phi_n \mathrm{d}\Phi_{\text{rad}}. \tag{2.80}$$

Here, $\mathrm{d}\Phi_{\text{rad}}$ is the integration over the 3 degrees of freedom of the radiation times an appropriate Jacobian factor. Then, a counter term $\mathcal{C}(\Phi_{n+1})$ has to

be constructed such that is has the same divergence as $\frac{\mathrm{d}\sigma_{\mathrm{real}}}{\mathrm{d}\Phi_{n+1}}$. One possibility is to take $\frac{\mathrm{d}\sigma_{\mathrm{real}}}{\mathrm{d}\Phi_{n+1}}$ in the kinematic limits that cause the IR divergences and sum over these limits. Furthermore, the counter term should be analytically integrable over $\mathrm{d}\Phi_{\mathrm{rad}}$. Then, one can write

$$\sigma = \int \mathrm{d}\Phi_n \frac{\mathrm{d}\sigma_{\mathrm{Born}}}{\mathrm{d}\Phi_n} + \int \mathrm{d}\Phi_n \left(\frac{\mathrm{d}\sigma_{\mathrm{virt}}}{\mathrm{d}\Phi_n} + \int \mathrm{d}\Phi_{\mathrm{rad}} \mathcal{C}(\Phi_{n+1}) \right) + \int \mathrm{d}\Phi_{n+1} \left(\frac{\mathrm{d}\sigma_{\mathrm{real}}}{\mathrm{d}\Phi_{n+1}} - \mathcal{C}(\Phi_{n+1}) \right). \tag{2.81}$$

This ensures that all terms are individually finite, and the phase space integrals can be numerically computed. Still, the IR divergence in the virtual correction has to be calculated analytically and canceled by hand with the divergence from the counter term. Luckily, the IR divergence in QED and QCD factorizes into a part that is proportional to the Born process, which is finite, and a second part that is the same for all processes [80, 81]. Hence, the IR divergence can be evaluated at NLO order once and for all, allowing to be reused for other processes.

The canceling of IR divergences between virtual and real contributions is guaranteed as long as IR safe observables are calculated. An observable is considered IR safe, if it is insensitive to low energy effects that create these divergences. An example for an IR safe observable is the sum of all final state transverse momenta, since the sum does not change if extra soft massless vector bosons are emitted.

2.3.4 Frixione, Kunszt and Signer subtraction

A method to deal with IR divergences in numerical calculations is the Frixione, Kunszt and Signer (FKS) subtraction method proposed in Refs. [82,83]. A detailed review can also be found in Ref. [38]. For the sake of brevity, one can define

$$\mathcal{B}(\Phi_n) = \frac{\mathrm{d}\hat{\sigma}_{\mathrm{Born}}}{\mathrm{d}\Phi_n}, \qquad \mathcal{V}(\Phi_n) = \frac{\mathrm{d}\hat{\sigma}_{\mathrm{virt}}}{\mathrm{d}\Phi_n}, \qquad \mathcal{R}(\Phi_{n+1}) = \frac{\mathrm{d}\hat{\sigma}_{\mathrm{real}}}{\mathrm{d}\Phi_{n+1}}. \tag{2.82}$$

In the FKS subtraction the phase space integral over the real contribution R is split into multiple integrals. Each integral contains at most the IR divergence corresponding to one final state particle becoming soft and the same particle becoming collinear to another massless particle. Originally, this was achieved by theta functions cutting the phase space into disjoint parts that add up to the whole phase space. For numerical integrations it

is advantageous to avoid non-continuous behavior in the integrand. Hence, these theta functions were replaced by continuous functions.

First, one defines the singular regions. IR divergences coming from the final state particle i being soft or collinear to one of the initial state particles are labeled i. The IR divergences originating from the particle i being softly emitted from the final state particle j or collinear to the final state particle j are labeled ij. For each singular region, the functions $S_i(\Phi_{n+1})$ and $S_{ij}(\Phi_{n+1})$ are introduced with the properties

$$\sum_i S_i + \sum_{ij} S_{ij} = 1. \tag{2.83}$$

Thereby, the second sum contains both S_{ij} and S_{ji} only if both final state particles i, j give rise to soft singularities. Otherwise, only one of the two terms is included in the sum, where the first index represents the particle that leads to soft divergences, if any.

In order to single out the divergent regions, the newly introduced functions S_i and S_{ij} have to fulfill the properties

$$\begin{aligned}
\lim_{k_m^0 \to 0} \left(S_i + \sum_j S_{ij} \right) &= \delta_{im}, \\
\lim_{\vec{k}_m \| k_\pm} S_i &= \delta_{im}, \\
\lim_{\vec{k}_m \| k_l} (S_{ij} + S_{ji}) &= \delta_{im}\delta_{jl} + \delta_{il}\delta jm, \\
\lim_{\vec{k}_m \| k_\pm} S_{ij} &= 0, \\
\lim_{\vec{k}_m \| k_l} S_i &= 0.
\end{aligned} \tag{2.84}$$

Then, the real cross section contribution can be split like

$$\mathcal{R} = \mathcal{R}\left(\sum_i S_i + \sum_{ij} S_{ij} \right) =: \sum_i \mathcal{R}_i + \sum_{ij} \mathcal{R}_{ij}. \tag{2.85}$$

Each individual R_i and R_{ij} has at most a IR divergence for a single particle becoming soft or collinear to another particle. Thus, one can construct counter terms easily for each individual R_i and R_{ij}. It proves useful to use a specific parametrization in the phase space integral. The unique particle giving rise to the IR divergence in R_i or R_{ij} is called the FKS particle. Its momentum is k_i. Then, the phase space integral is over the FKS particle is factored

$$\mathrm{d}\Phi_{n+1} = \mathrm{d}\Phi_n \mathrm{d}^3 k_i J. \tag{2.86}$$

Now the FKS momentum gets parametrized further in two different ways. For initial-state radiation (ISR), i.e. the phase space integral over R_i, it is parametrized as

$$k_i = \xi k_+^0 \Big(1, \sqrt{1-y^2}\cos\phi, \sqrt{1-y^2}\sin\phi, y\Big). \tag{2.87}$$

In the case of final-state radiation (FSR), i.e. phase space integrals over any of the R_{ij}, it is parametrized such that

$$\xi = \frac{k_i^0}{k_+^0}, \quad y = \frac{\vec{k}_i \cdot \vec{k}_j}{\left|\vec{k}_{n+1}\right|\left|\vec{k}_j\right|}, \quad \phi \ = \angle\Big(\vec{\eta} \times \Big(\vec{k}_i + \vec{k}_j\Big), \vec{k}_i \times \Big(\vec{k}_i + \vec{k}_j\Big)\Big). \tag{2.88}$$

Thereby, k_j is the momentum of the particle that the FKS particle becomes collinear to in the collinear IR divergence of R_{ij}. This means, ξ is the energy of the FKS particle normalized to half of the center-of-mass energy, y is the cosine of the angle between the FKS particle and its emitter, and ϕ is the azimuthal angle around the sum of the momenta $\vec{k}_i$ and $\vec{k}_j$, where the arbitrary unit vector $\vec{\eta}$ defines a direction for which $\phi = 0$. In this thesis and also in the implementation in the `POWHEG BOX`, $\vec{\eta}$ is set to $\vec{\eta} = \vec{e}_z$.

In this parametrization, the IR counter terms can be constructed from R_i and R_{ij} in the infrared limits, i.e. $\xi \to 0$ and $y \to 1$. If the particle i generates an IR divergence when it is collinear to the incoming particle that is along the negative z axis, then one has to consider R_i in the limit $y \to -1$ as well. The phase space integral over these limits take a generic form that is proportional to the process without the additional radiation. The integral over the FKS variables ξ, y and ϕ can be performed analytically in D dimensions, to get the expression that has to be subtracted from the virtual contribution V.

2.3.5 QCD factorization

This section explains how the initial state IR divergences can be handled. A detailed explanation of the subject can be found in Ref. [84]. A cross section $\hat{\sigma}_{\mathrm{NLO}}$ with strongly interacting particles in the initial and final state consists of the LO cross section $\hat{\sigma}_{\mathrm{LO}}$ and virtual and real corrections

$$\hat{\sigma}_{\mathrm{NLO}} = \hat{\sigma}_{\mathrm{LO}} + \hat{\sigma}_{\mathrm{virt}} + \hat{\sigma}_{\mathrm{real}}. \tag{2.89}$$

Performing this calculation will raise the problem, that not all IR divergences cancel. In particular, IR divergences originating from collinear radiation of an initial parton cannot be canceled by virtual corrections. Figure 2.1

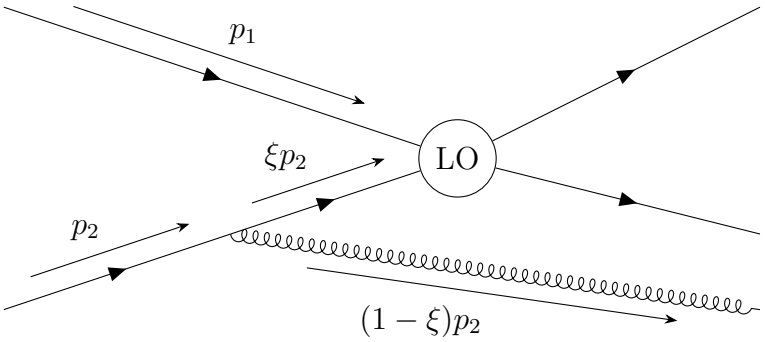

Figure 2.1: Sketch for initial state collinear radiation, where an incoming gluon splits into a collinear quark-anti-quark pair. The blob represents a LO diagram of the process.

shows an example diagram that leads to collinear initial state radiation. The collinear radiation leads to a particle entering the leading order subdiagram with an energy ξp_2^0, with $\xi < 1$. Therefore, the IR divergence will be proportional to $\hat{\sigma}_{\mathrm{LO}}(\xi p_2^0)$. All IR divergences coming from virtual corrections are proportional to $\hat{\sigma}_{\mathrm{LO}}(p_2^0)$, since no energy can be lost due to radiation. Hence, there cannot be any cancellation of these initial state collinear divergences.

Initial state collinear IR divergences only occur for strongly interacting initial state particles. Due to confinement, they cannot exist as isolated particles but only in bound states, called hadrons. Hence, cross sections $\hat{\sigma}_a$ with initial state quarks or gluons do not represent real world observables, but rather cross sections σ involving colliding hadrons such as protons. In the following, the discussion is reduced to the case with only one initial hadron to allow for a shorter notation. The extension to two initial state hadrons is straight forward. These hadronic cross sections are the convolution of the partonic cross sections with PDFs $f_a(x)$ [66]

$$\begin{aligned}\sigma &= \sum_a \int \mathrm{d}x f_a(x) \hat{\sigma}_{a,\mathrm{NLO}}(x) \\ &= \sum_a \int \mathrm{d}x f_a(x) (\hat{\sigma}_{a,\mathrm{LO}}(x) + \hat{\sigma}_{a,\mathrm{virt}}(x) + \hat{\sigma}_{a,\mathrm{real}}(x)).\end{aligned} \tag{2.90}$$

The sum over a runs over all partons for which the PDF is non-zero. Note that it is possible that $\hat{\sigma}_{a,\mathrm{LO}}(x) \equiv \hat{\sigma}_{a,\mathrm{virt}}(x) \equiv 0$ for some parton a, if there does not exist any LO diagram with a in the initial state, but $\hat{\sigma}_{a,\mathrm{real}}(x)) \neq 0$ for the same a.

In theory, each individual partonic cross section can be calculated separately in dimensional regularization to handle the IR divergences. Now,

the real correction cross section leads to multiple divergences coming from collinear and soft configurations in the initial state as well as in the final state. Let $\hat{\sigma}_{a,\text{real,IC}}(x)$ contain only terms with an initial state collinear divergence, $\hat{\sigma}_{a,\text{real,FC+S}}(x)$ all other IR divergences, and all finite terms are collected in $\hat{\sigma}_{a,\text{real,fin}}(x)$. Note that this also includes divergences originating from configurations where a parton becomes simultaneously soft and collinear to an initial state. Then, one can split off all IR divergences from the partonic cross sections

$$\begin{aligned}\sigma = \sum_a \int \mathrm{d}x f_a(x) \big[&\hat{\sigma}_{a,\text{LO}}(x) + \hat{\sigma}_{a,\text{virt,fin}}(x) + \hat{\sigma}_{a,\text{virt,ir}}(x) \\ &+ \hat{\sigma}_{a,\text{real,fin}}(x) + \hat{\sigma}_{a,\text{real,IC}}(x) + \hat{\sigma}_{a,\text{real,FC+S}}(x)\big].\end{aligned} \tag{2.91}$$

Now, the cancellation works out as

$$\hat{\sigma}_{a,\text{virt,ir}}(x) + \hat{\sigma}_{a,\text{real,FC+S}}(x) = 0, \tag{2.92}$$

leaving $\hat{\sigma}_{a,\text{real,IC}}(x)$ without a counter part within the perturbative cross sections

$$\sigma = \sum_a \int \mathrm{d}x f_a(x) \big[\hat{\sigma}_{a,\text{LO}}(x) + \hat{\sigma}_{a,\text{virt,fin}}(x) + \hat{\sigma}_{a,\text{real,fin}}(x) + \hat{\sigma}_{a,\text{real,IC}}(x)\big]. \tag{2.93}$$

As it turns out, the initial state collinear divergence of the real contribution can be factorized into the LO contribution $\hat{\sigma}_{a,\text{LO}}(x)$ times a universal IR divergent factor $\mathcal{P}_{ab}(\xi)$ that only depends on the initial parton a and the parton b entering the LO sub diagram with the momentum fraction ξ of the incoming parton (see Fig. 2.1) [80]

$$\hat{\sigma}_{a,\text{real,IC}}(x) = \sum_b \int_0^1 \mathrm{d}\xi \mathcal{P}_{ab}(\xi) \hat{\sigma}_{b,\text{LO}}(\xi x). \tag{2.94}$$

With this factorization one can write

$$\begin{aligned}&\int_0^1 \mathrm{d}x \sum_a f_a(x)(\hat{\sigma}_{a,\text{LO}}(x) + \hat{\sigma}_{a,\text{real,IC}}(x)) \\ &= \int_0^1 \mathrm{d}x \left(\sum_a f_a(x) \hat{\sigma}_{a,\text{LO}}(x) + \int_0^1 \mathrm{d}\xi \sum_{ab} f_a(x) \mathcal{P}_{ab}(\xi) \hat{\sigma}_{b,\text{LO}}(\xi x) \right) \\ &= \int_0^1 \mathrm{d}x \left(\sum_a f_a(x) \hat{\sigma}_{a,\text{LO}}(x) + \int_0^1 \mathrm{d}\xi \sum_{ab} f_b(x) \mathcal{P}_{ba}(\xi) \hat{\sigma}_{a,\text{LO}}(\xi x) \right).\end{aligned} \tag{2.95}$$

In the last line the summation indices a and b have been renamed such that the LO partonic cross section carries the same index. The second term can be written as

$$\begin{aligned}
&\int_0^1 \mathrm{d}x \int_0^1 \mathrm{d}\xi \sum_{ab} f_b(x)\mathcal{P}_{ba}(\xi)\hat{\sigma}_{a,\mathrm{LO}}(\xi x)) \\
&= \int_0^1 \mathrm{d}x \int_0^1 \mathrm{d}\xi \int_0^1 \mathrm{d}\chi \delta(\chi - \xi x) \sum_{ab} f_b(x)\mathcal{P}_{ba}(\xi)\hat{\sigma}_{a,\mathrm{LO}}(\xi x) \\
&= \int_0^1 \mathrm{d}\chi \int_\chi^1 \frac{\mathrm{d}x}{x} \sum_{ab} f_b(x)\mathcal{P}_{ba}\left(\frac{\chi}{x}\right)\hat{\sigma}_{a,\mathrm{LO}}(\chi) \\
&= \int_0^1 \mathrm{d}x \int_x^1 \frac{\mathrm{d}\chi}{\chi} \sum_{ab} f_b(\chi)\mathcal{P}_{ba}\left(\frac{x}{\chi}\right)\hat{\sigma}_{a,\mathrm{LO}}(x). \qquad (2.96)
\end{aligned}$$

In the last line the integration variables were renamed. With this the LO contribution plus the initial collinear contribution becomes

$$\begin{aligned}
&\int_0^1 \mathrm{d}x \sum_a f_a(x)(\hat{\sigma}_{a,\mathrm{LO}}(x) + \hat{\sigma}_{a,\mathrm{real,IC}}(x)) \\
&= \sum_a \int_0^1 \mathrm{d}x \left(f_a(x) + \int_x^1 \frac{\mathrm{d}\chi}{\chi} \sum_b f_b(\chi)\mathcal{P}_{ba}\left(\frac{x}{\chi}\right)\right)\hat{\sigma}_{a,\mathrm{LO}}(x) \\
&= \sum_a \int_0^1 \mathrm{d}x f_a^{\mathrm{NLO}}(x)\hat{\sigma}_{a,\mathrm{LO}}(x) \qquad (2.97)
\end{aligned}$$

With this manipulation the problematic initial state collinear divergence is absorbed into the PDF to define a new renormalized PDF

$$f_a^{\mathrm{NLO}}(x) = \sum_b \int_x^1 \frac{\mathrm{d}\chi}{\chi} f_b(\chi)\left(\chi\delta_{ab}\delta(x-\chi) + \mathcal{P}_{ba}\left(\frac{x}{\chi}\right)\right). \qquad (2.98)$$

Thereby, the renormalization is process independent since it only depends on the universal factors $\mathcal{P}_{ab}$.

Similar to renormalization of UV divergences, the PDFs $f_a(x)$ have to be regarded as unmeasurable bare distributions, which can only be determined after absorbing the collinear singularity. Further, one can add additional finite terms $\mathcal{K}_{ba}$ as long as they are in the same order in coupling constants as $\mathcal{P}_{ab}$

$$f_a^{\mathrm{NLO}}(x) = \sum_b \int_x^1 \frac{\mathrm{d}\chi}{\chi} f_b(\chi)\left(\chi\delta_{ab}\delta(x-\chi) + \mathcal{P}_{ba}\left(\frac{x}{\chi}\right) + \mathcal{K}_{ba}\left(\frac{x}{\chi}\right)\right). \quad (2.99)$$

The choice of the finite term $\mathcal{K}$ fixes the choice of the factorization scheme.

The renormalized PDFs can be plugged into Eq. (2.91) while using the fact that $\mathcal{P}_{ba} + \mathcal{K}_{ba}$ multiplied by either the real or virtual correction gives terms of higher order and can be neglected in a NLO calculation. The renormalized PDFs will by definition cancel the initial state collinear divergence to leave

$$\begin{aligned}\sigma = &\sum_a \int \mathrm{d}x \left[\sum_b \int_x^1 \frac{\mathrm{d}\chi}{\chi} f_b^{\mathrm{NLO}}(\chi) \left(\chi \delta_{ab} \delta(x-\chi) - \mathcal{P}_{ba}\left(\frac{x}{\chi}\right) - \mathcal{K}_{ba}\left(\frac{x}{\chi}\right)\right)\right] \\ &\times \left[\hat{\sigma}_{a,\mathrm{LO}}(x) + \hat{\sigma}_{a,\mathrm{virt,fin}}(x) + \hat{\sigma}_{a,\mathrm{real,fin}}(x) + \hat{\sigma}_{a,\mathrm{real,IC}}(x)\right] \\ = &\sum_a \int \mathrm{d}x f_a^{\mathrm{NLO}}(x) \Big[\hat{\sigma}_{a,\mathrm{LO}}(x) + \hat{\sigma}_{a,\mathrm{virt,fin}}(x) + \hat{\sigma}_{a,\mathrm{real,fin}}(x) \\ &- \sum_b \int_0^1 \mathrm{d}\xi \mathcal{K}_{ab}(\xi) \hat{\sigma}_{b,\mathrm{LO}}(\xi x) \Big] \end{aligned} \tag{2.100}$$

f_q^{NLO} represents a quantity that cannot be calculated perturbatively by its very nature. In fact, there does not exist an accepted method, thus far, to calculate it from first principles. In practice, one has to choose a scheme and use experimental data to match the renormalized PDFs. Then, one can use the experimentally determined PDFs to calculate other processes to make predictions. This procedure only works because the divergent terms $\mathcal{P}_{ab}$ are universal and do not depend on the specific process at hand. In dimensional regularization, they take the form

$$\mathcal{P}_{ab}(\xi) = -\frac{\alpha_s}{2\pi}\frac{1}{\epsilon} P_{ab}(\xi), \tag{2.101}$$

where P_{ab} are the Altarelli-Parisi splitting functions [80]. A common factorization scheme is the $\overline{\mathrm{MS}}$ scheme in which

$$\mathcal{K}_{ab}(\xi) = \frac{\alpha_s}{2\pi}(\gamma_E - \log 4\pi) P_{ab}(\xi). \tag{2.102}$$

In numerical calculations, it is not practical to split $\hat{\sigma}_{a,\mathrm{real}}(x)$ into its finite and individual divergent parts. In the previous sections 2.3.3 and 2.3.4, the addition of counter terms to handle the IR cancellation between virtual and real corrections was discussed. The cancellation between initial state collinear

divergences and PDF IR divergences can be handled in a similar way

$$
\begin{aligned}
\sigma &= \sum_a \int \mathrm{d}x f_a(x) \Bigg[\int \mathrm{d}\Phi_{n+1} \left(\frac{\mathrm{d}\sigma_{a,\mathrm{real}}}{\mathrm{d}\Phi_{n+1}}(x) - \mathcal{C}_a(\Phi_{n+1}, x) \right) \\
&+ \int \mathrm{d}\Phi_n \left(\frac{\mathrm{d}\sigma_{a,\mathrm{Born}}}{\mathrm{d}\Phi_n}(x) + \frac{\mathrm{d}\sigma_{a,\mathrm{virt}}}{\mathrm{d}\Phi_n}(x) + \int \mathrm{d}\Phi_{\mathrm{rad}} \mathcal{C}_a(\Phi_{n+1}, x) \right) \Bigg] \\
&= \sum_a \int \mathrm{d}x \left[f_a^{\mathrm{NLO}}(x) - \sum_b \int_x^1 \frac{\mathrm{d}\chi}{\chi} f_b^{\mathrm{NLO}}(\chi) \left(\mathcal{P}_{ba}\left(\frac{x}{\chi}\right) + \mathcal{K}_{ba}\left(\frac{x}{\chi}\right) \right) \right] \\
&\Bigg[\int \mathrm{d}\Phi_n \left(\frac{\mathrm{d}\sigma_{a,\mathrm{Born}}}{\mathrm{d}\Phi_n}(x) + \frac{\mathrm{d}\sigma_{a,\mathrm{virt}}}{\mathrm{d}\Phi_n}(x) + \int \mathrm{d}\Phi_{\mathrm{rad}} \mathcal{C}_a(\Phi_{n+1}, x) \right) \\
&+ \int \mathrm{d}\Phi_{n+1} \left(\frac{\mathrm{d}\sigma_{a,\mathrm{real}}}{\mathrm{d}\Phi_{n+1}}(x) - \mathcal{C}_a(\Phi_{n+1}, x) \right) \Bigg] \\
&= \sum_a \int \mathrm{d}x f_a^{\mathrm{NLO}}(x) \Bigg[\int \mathrm{d}\Phi_{n+1} \left(\frac{\mathrm{d}\sigma_{a,\mathrm{real}}}{\mathrm{d}\Phi_{n+1}}(x) - \mathcal{C}_a(\Phi_{n+1}, x) \right) \\
&+ \int \mathrm{d}\Phi_n \left(\frac{\mathrm{d}\sigma_{a,\mathrm{Born}}}{\mathrm{d}\Phi_n}(x) + \frac{\mathrm{d}\sigma_{a,\mathrm{virt}}}{\mathrm{d}\Phi_n}(x) + \int \mathrm{d}\Phi_{\mathrm{rad}} \mathcal{C}_a(\Phi_{n+1}, x) \right) \\
&- \int \mathrm{d}\Phi_n \mathrm{d}\xi (\mathcal{P}_{ab}(\xi) + \mathcal{K}_{ab}(\xi)) \frac{\mathrm{d}\sigma_{b,\mathrm{Born}}}{\mathrm{d}\Phi_n}(\xi x) \Bigg] \\
&= \sum_a \int \mathrm{d}x f_a^{\mathrm{NLO}}(x) \Bigg[\int \mathrm{d}\Phi_n \frac{\mathrm{d}\sigma_{a,\mathrm{Born}}}{\mathrm{d}\Phi_n}(x) \\
&+ \int \mathrm{d}\Phi_{n+1} \left(\frac{\mathrm{d}\sigma_{a,\mathrm{real}}}{\mathrm{d}\Phi_{n+1}}(x) - \mathcal{C}_a(\Phi_{n+1}, x) \right) \\
&+ \int \mathrm{d}\Phi_n \left(\frac{\mathrm{d}\sigma_{a,\mathrm{virt}}}{\mathrm{d}\Phi_n}(x) + \int \mathrm{d}\Phi_{\mathrm{rad}} \mathcal{C}_a(\Phi_{n+1}, x) + \int \mathrm{d}\xi \mathcal{G}_a(\xi, x) \right) \Bigg]. \qquad (2.103)
\end{aligned}
$$

Each individual line in the last step is finite on its own. Note that $C_a(\Phi_{n+1}, x)$ is to be understood as a sum of counter terms that cancel each IR divergence, including divergences coming from initial state collinear configurations. The newly introduced term $\mathcal{G}_a(\xi, x)$ is usually referred to as collinear counter term. It consists of the terms that are absorbed into the bare PDF and is dependent on the factorization scheme.

If both incoming particles give rise to IR collinear divergences, the procedure is analogous. In that case, one has two sets of PDFs, one for each incoming hadron, and one needs two collinear counter terms.

2.3.6 Observables at next-to-leading order

When calculating observables, it proves useful to reorganize Eq. (2.103). Since all strongly charged particles are experimentally indistinguishable, one has to include all processes where partons in initial or final state are replaced by other partons. Here, only processes with one strongly charged parton in the initial state will be considered. The `POWHEG BOX`organizes the calculation in a particular way as described in Ref. [38]. This section briefly reviews the calculation organization adjusted to a single hadron in initial state.

Let f_b be all flavor structures that lead to non-zero amplitudes at LO. Thereby, a flavor structure is a partly ordered list of particle flavor, where the first two particles are the flavors of the initial state particles and the other entries are the final state particles. Furthermore, two flavor structures are considered identical if they only differ by a permutation of the initial or final state particles. All virtual corrections must have a flavor structure equal to one f_b, since at NLO, only the interference terms with LO diagrams contribute.

In section 2.3.4, it was discussed how one can split the real correction R_{f_r} into individual contributions with isolated IR divergences $R_{f_r,i}$ and $R_{f_r,ij}$. This can be done for each possible flavor structure f_r of the real correction

$$\mathcal{R} = \sum_{f_r} \mathcal{R}_{f_r} = \sum_{f_r} \left(\sum_i \mathcal{R}_{f_r,i} + \sum_{ij} \mathcal{R}_{f_r,ij} \right) =: \sum_{\alpha_r} \mathcal{R}_{\alpha_r}. \tag{2.104}$$

Here, the IR divergent regions α_r are introduced. Each specific α_r corresponds to a real flavor structure f_r and a parton becoming soft or collinear. Additionally, each α_r can be assigned to a LO flavor structure that the soft or collinear limit of R_{α_r} is proportional to. This LO flavor structure is called the underlying Born flavor structure. It is also useful to introduce the notation of an underlying Born phase space point $\bar{\Phi}_n^{\alpha_r}$. For ease of notation, one can also define $\mathbf{\Phi}_n := \{x, \Phi_n\}$. Then, let M^{α_r} be a mapping that maps $\mathbf{\Phi}_{n+1}$ to the IR divergent phase space point α_r is referring to

$$\tilde{\mathbf{\Phi}}_{n+1}^{\alpha_r} = M^{\alpha_r} \mathbf{\Phi}_{n+1}. \tag{2.105}$$

Now, the underlying Born phase space point $\bar{\mathbf{\Phi}}_n^{\alpha_r}$ is defined as the phase space point $\tilde{\mathbf{\Phi}}_{n+1}^{\alpha_r}$ where:

- the soft vector is removed if α_r specifies a soft divergent region,
- the two collinear momenta are replaced by their sum if α_r specifies a final state collinear divergent region and

- the radiated parton is removed and the momentum fraction x is replaced by the momentum fraction after the radiation.

The same idea can be applied to the phase space point of the collinear counter term which has an initial state collinear origin. One defines

$$\bar{\mathbf{\Phi}}_n = \{\bar{x}, \Phi_n\} := \{\xi x, \Phi_n\}. \tag{2.106}$$

With this notation one can calculate the expectation value of an observable O as

$$\begin{aligned}\langle O\rangle = \sum_{f_b} \int \mathrm{d}x \Bigg[& \int \mathrm{d}\Phi_n f_{f_b}^{\mathrm{NLO}}(x) O(\mathbf{\Phi}_n)(\mathcal{B}_{f_b}(\mathbf{\Phi}_n) + \mathcal{V}_{f_b}(\mathbf{\Phi}_n)) \\ & + \int \mathrm{d}\Phi_{n+1} \sum_{\alpha_r \in \{\alpha_r | f_b\}} f_{\alpha_r}^{\mathrm{NLO}}(x) \big(O(\mathbf{\Phi}_{n+1}) \mathcal{R}_{\alpha_r}(\mathbf{\Phi}_{n+1}) - O(\bar{\mathbf{\Phi}}_n^{\alpha_r}) \mathcal{C}_{\alpha_r}(\mathbf{\Phi}_{n+1}) \big) \\ & + \int \mathrm{d}\Phi_n \sum_{\alpha_r \in \{\alpha_r | f_b\}} \int \mathrm{d}\Phi_{\mathrm{rad}} f_{\alpha_r}^{\mathrm{NLO}}(x) O(\bar{\mathbf{\Phi}}_n^{\alpha_r}) \mathcal{C}_{\alpha_r}(\mathbf{\Phi}_{n+1}) \\ & + \int \mathrm{d}\Phi_n \sum_{\alpha_g \in \{\alpha_g | f_b\}} \int \mathrm{d}\xi f_{\alpha_r}^{\mathrm{NLO}}(x) O(\bar{\mathbf{\Phi}}_n) \mathcal{G}_{\alpha_g}(\xi, \bar{\mathbf{\Phi}}_n) \Bigg]. \end{aligned} \tag{2.107}$$

Thereby, $\{\alpha_r | f_b\}$ is the set that contains all α_r that are assigned with the underlying Born flavor structure f_b, and α_g describes all initial state collinear regions that the collinear counter terms have to cancel. Often, the observable O is a product of Theta-functions that determine a bin in a histogram.

2.4 Parton shower

Feynman diagrams can be split into subdiagrams to be evaluated individually and afterwards combined again. This offers the possibility to evaluate common subdiagrams and reuse them in all kinds of processes. As discussed in the previous sections, the branching of an off-shell quark into the same quark with an additional gluon, $q^* \to qg$, gives rise to large amplitudes for a soft or collinear gluon. This subdiagram is part of any real correction of a process with a quark in the final state. The correction to the next order contains a subdiagram where the quark undergoes the same branching again. This correction would contain the subdiagram $q^* \to qg$ twice, meaning it is a product of two large quantities. The full calculation would consist of an infinite series of nested $q^* \to qg$ subdiagrams, which cannot be expected to

be small. Another effect enhancing these large corrections is the proportionality of the subdiagram $q^* \to qg$ to the strong coupling g_s. Since the QCD is a non-Abalian gauge theory, g_s increases with decreasing energy scale and each branching introduces new smaller energy scale compared to the ones involved before the branching. This behavior is shared with all subdiagrams that contain IR divergences and also applies with lesser degree to IR divergences coming from QED processes. Since the QED is an Abelian gauge theory its coupling e decreases with lower energy scale.

In order to make sensible theoretical predictions for scattering processes with strongly interacting particles in the final state, one has to take these large corrections into account. Obviously, one cannot perform a straightforward complete calculation because it involves an infinite amount of Feynman diagrams with an increasing number of final state particles. However, one can use a procedure called the parton shower to simulate the endless branching using reasonable approximations [85–87]. A review of the field of parton showers can be found in Refs. [88, 89]. Parton showers are implemented as event generators. Prominent examples are `Pythia8` [44, 45], `Herwig7` [40, 41] and `Sherpa2` [42, 43].

The parton shower is largely independent of the actual process at hand and only depends on the number of strongly interacting final state particles. In practice, a parton shower is used in Monte Carlo generators. The work flow then consists first of calculating the hard process, meaning calculating the cross section for the partonic process at leading order. Then, an event is generated. This event consists of the momenta of all final state particles. The precise momenta are generated randomly according to a probability density. This probability density is given by the differential cross section normed to the total cross section. Now, the parton shower is applied to the final state momenta. Thereby, the branching of final state particles into more final state particles is done iteratively to build a complex final state of many particles to simulate actual observations in scattering experiments. At each iteration in the parton shower a final state particle is replaced by two branching products. The momenta of the branching products are once again chosen randomly according to a probability density, which is a product of an approximate amplitude of the branching and a Sudakov factor. The Sudakov factor takes the virtual contribution into account which was not discussed thus far.

After generating momenta according to the cross section of the hard process at leading order, all final state momenta are on-shell as required from the LSZ reduction formula. However, in order to enable branching the final state particle i needs to have a virtuality $Q_i^2 = p_i^2 - m_i^2$, otherwise the branching is kinematically impossible. In fact, only particles in the final state after

the showering process have to be on-shell since the hard process happens at very small time scales, the uncertainty theorem allows for virtualities $Q_i \neq 0$. Therefore, the momenta of the final state particles of the hard process are reshuffled before the parton shower to give them a virtuality. One has to ensure that the virtualities Q_i^2 are much smaller than the scale of the hard process Q^2_{hard}. Otherwise, the matrix element for the hard process, in which $Q_i^2 = 0$, would not be a good approximation anymore. Then, the showering process can be done iteratively, where after each step the virtualities are decreased until they fall under a cutoff threshold. Below the threshold, non-perturbative effects of QCD take over.

The differential probability $\mathrm{d}\mathcal{P}$ for a branching $a \to bc$ to happen is given by

$$\mathrm{d}\mathcal{P}_{a\to bc} = \frac{\mathrm{d}\sigma_{\text{real},a\to bc}}{\sigma_{\text{LO}}}. \tag{2.108}$$

Thereby, $\mathrm{d}\sigma_{\text{real},a\to bc}$ is the differential cross section for the process in which the final state particle a is replaced by its branching products b and c and σ_{LO} is the LO cross section. In the collinear or soft limit, one can neglect all Feynman diagrams in $\sigma_{\text{real},a\to bc}$ except the one which contains the branching as subdiagram, because this is the diagram that diverges in this limit. Hence, all interference terms can be neglected. In this limit, $\sigma_{\text{real},a\to bc}$ factorizes into

$$\sigma_{\text{real},a\to bc} = \sigma_{\text{LO}} \frac{\alpha_s}{2\pi} \frac{\mathrm{d}Q_a^2}{Q_a^2} P_{a\to bc}(z)\mathrm{d}z, \tag{2.109}$$

where $Q_a^2 = (p_b + p_c)^2$, $z = E_b/(E_b + E_c)$ and $P_{a\to bc}(z)$ are splitting functions that only depend on the particle type of the particles involved in the splitting. Hence, the probability is independent of the hard process σ_{LO}.

This differential probability diverges for $Q_a^2 \to 0$, which makes it impossible to interpret it as a proper probability. At each iteration step of the parton shower the virtuality Q_a that is given to the branching particle a has to decrease. The momenta of the branching products b and c have to be generated according to the probability density $\mathrm{d}\mathcal{P}_{\text{first}}$ that some branching happens with Q_a^2 but not with any other virtuality $Q^2 > Q_a^2$

$$\mathrm{d}\mathcal{P}_{\text{first}}(Q_a^2) = \mathrm{d}\mathcal{P}_{\text{bran}}(Q_a^2)\mathcal{P}_{\text{no bran}}(Q^2_{\text{max}} > Q^2 > Q_a^2). \tag{2.110}$$

Here, Q^2_{max} is a maximal virtuality that has to be much smaller than the hard scale of the process. Probabilities for any further branching with a scale below Q_a^2 do not enter at this point, because they are considered in later iteration steps.

The probabilities of a particle branching and not branching have to add up to one, since there is no other possibility

$$\mathcal{P}_{\text{bran}}(Q_1^2 > Q^2 > Q_2^2) + \mathcal{P}_{\text{no bran}}(Q_1^2 > Q^2 > Q_2^2) = 1. \tag{2.111}$$

Further, the probability of no branching is multiplicative

$$\mathcal{P}_{\text{no bran}}(Q_1^2 > Q^2 > Q_2^2)\mathcal{P}_{\text{no bran}}(Q_2^2 > Q^2 > Q_3^2) = \mathcal{P}_{\text{no bran}}(Q_1^2 > Q^2 > Q_3^2). \tag{2.112}$$

These properties allow to reformulate the no branching probability by subdividing the energy scale as

$$Q_i^2 = (i/n)(Q_{\text{max}}^2 - Q_a^2) + Q_a^2, \tag{2.113}$$

then

$$\begin{aligned}\mathcal{P}_{\text{no bran}}(Q_{\text{max}}^2 > Q^2 > Q_a^2) &= \lim_{n\to\infty} \prod_{i=0}^{n-1} \mathcal{P}_{\text{no bran}}(Q_i^2 > Q^2 > Q_{i+1}^2) \\ &= \lim_{n\to\infty} \prod_{i=0}^{n-1} \big(1 - \mathcal{P}_{\text{bran}}(Q_i^2 > Q^2 > Q_{i+1}^2)\big).\end{aligned} \tag{2.114}$$

For a continuous probability function, $\mathcal{P}_{\text{bran}}(Q_i^2 > Q^2 > Q_{i+1}^2)$ becomes very small in the limit $n \to \infty$ and one can write it as exponential

$$\lim_{n\to\infty} \big(1 - \mathcal{P}_{\text{bran}}(Q_i^2 > Q^2 > Q_{i+1}^2)\big) = \exp\Big[\lim_{n\to\infty} \big(-\mathcal{P}_{\text{bran}}(Q_i^2 > Q^2 > Q_{i+1}^2)\big)\Big]. \tag{2.115}$$

This transforms the product into a sum in the exponent, which can be written as an integral together with the limit

$$\mathcal{P}_{\text{no bran}}(Q_{\text{max}}^2 > Q^2 > Q_a^2) = \exp\left[-\int_{Q_a^2}^{Q_{\text{max}}^2} \frac{\mathrm{d}\mathcal{P}_{\text{bran}}(Q^2)}{\mathrm{d}Q^2}\mathrm{d}Q^2\right]. \tag{2.116}$$

This is called the Sudakov form factor. Then, the probability density for a branching $a \to bc$ is

$$\begin{aligned}\mathrm{d}\mathcal{P}_{\text{first},a\to bc} &= \mathrm{d}\mathcal{P}_{a\to bc} \exp\left[-\sum_{a,b}\int_{Q_a^2}^{Q_{\text{max}}^2} \frac{\mathrm{d}\mathcal{P}_{a\to bc}(Q^2)}{\mathrm{d}Q^2}\mathrm{d}Q^2\right] \\ &= \frac{\alpha_s}{2\pi}\frac{\mathrm{d}Q_a^2}{Q_a^2} P_{a\to bc}(z)\mathrm{d}z \exp\left[-\frac{\alpha_s}{2\pi}\sum_{a,b}\int_{Q_a^2}^{Q_{\text{max}}^2} \frac{\mathrm{d}Q^2}{Q^2}\int P_{a\to bc}(z')\mathrm{d}z'\right].\end{aligned} \tag{2.117}$$

Now, one can generate additional radiated partons according to this probability density. After the first iteration, $Q^2_{\max}$ has to be set to the randomly selected Q^2_a of the previous iteration. If the generated Q^2_a falls below a threshold $Q^2_{\min}$, one aborts the algorithm. Note that in practice Q^2_a is often changed to different order variables by a variable transformation.

2.5 POWHEG method

The previous section demonstrated how one can enhance a LO calculation with a parton shower. Each order in the couplings is a polynomial in logarithms of physical quantities, where the polynomial order increases with each order in the coupling. The parton shower provides a method to resum the leading logarithms of the higher orders. But one can do better. The next step is to include all the terms in the NLO. This has to be done carefully, since the NLO corrections will contain real corrections. These real corrections are processes with an additional parton in the final state. Adding a parton to the final state corresponds to the first step of the shower algorithm which raises the problem of double counting. Therefore, events of a NLO event generator have to be correctly interfaced with a shower algorithm. One possible method is the Positive Weight Hardest Emission Generator (POWHEG) method [37,38]. The main features of this method are the independence of the specific shower algorithm, which has to be slightly adapted, and the mostly avoidance of events with negative weights, which would have no physical interpretation.

The strategy of the POWHEG method is to generate the first radiation with full NLO precision. As a reminder, a normal shower would use the soft and collinear limits of the NLO contribution in order to obtain the leading logarithms for the first radiation. In this context, first radiation means hardest radiation in the sense that the first radiated parton has the largest transverse momentum p_T with respect to the direction of the splitting parton. Each subsequent radiation is required to have a smaller transverse momentum. For transverse momentum ordered shower algorithms this requirement is easy to fulfill by setting the hard scale Q_{Hard} to the transverse momentum p_T of that first NLO radiation. Angular ordered shower algorithms on the other hand have to be adopted slightly. With these showers, the first radiation does not have to be the hardest with the largest p_T. One proposed solution is to slightly modify the shower algorithm by implementing a veto that prohibits the generation of radiations harder than the first with NLO accuracy.

For the description of the POWHEG method, it is helpful to introduce

the notation of absorbed the PDFs into the individual contributions they are convoluted with

$$\begin{aligned} B_{f_b}(\mathbf{\Phi}_n) &= f_{f_b}^{\mathrm{NLO}}(x)\mathcal{B}_{f_b}(\mathbf{\Phi}_n), & V_{f_b}(\mathbf{\Phi}_n) &= f_{f_b}^{\mathrm{NLO}}(x)\mathcal{V}_{f_b}(\mathbf{\Phi}_n), \\ R_{\alpha_r}(\mathbf{\Phi}_{n+1}) &= f_{\alpha_r}^{\mathrm{NLO}}(x)\mathcal{R}_{\alpha_r}(\mathbf{\Phi}_{n+1}), & C_{\alpha_r}(\mathbf{\Phi}_{n+1}) &= f_{\alpha_r}^{\mathrm{NLO}}(x)\mathcal{C}_{\alpha_r}(\mathbf{\Phi}_{n+1}), \\ G_{\alpha_g}(\mathbf{\Phi}_n,\xi) &= f_{\alpha_g}^{\mathrm{NLO}}(x)\mathcal{G}_{\alpha_g}(\mathbf{\Phi}_n,\xi). \end{aligned} \tag{2.118}$$

For the POWHEG method the NLO formula for the expectation value of an observable O Eq. (2.107) is rewritten to

$$\begin{aligned} \langle O\rangle &= \sum_{f_b}\langle O\rangle_{f_b}\,, \\ \langle O\rangle_{f_b} &= \int \mathrm{d}\mathbf{\Phi}_n O_n(\mathbf{\Phi}_n)\bar{B}_{f_b}(\mathbf{\Phi}_n) \\ &\quad + \sum_{\alpha_r\in\{\alpha_r|f_b\}}\int \mathrm{d}\bar{\mathbf{\Phi}}_n^{\alpha_r}\mathrm{d}\Phi_{\mathrm{rad}}^{\alpha_r} R_{\alpha_r}(\mathbf{\Phi}_{n+1})\big[O_{n+1}(\mathbf{\Phi}_{n+1}) - O_n(\bar{\mathbf{\Phi}}_n^{\alpha_r})\big], \end{aligned} \tag{2.119}$$

$$\begin{aligned} \bar{B}_{f_b}(\mathbf{\Phi}_n) &= B_{f_b}(\mathbf{\Phi}_n) + V_{f_b}(\mathbf{\Phi}_n) + \sum_{\alpha_r\in\{\alpha_r|f_b\}}\int [\mathrm{d}\Phi_{\mathrm{rad}}^{\alpha_r} C_{\alpha_r}(\mathbf{\Phi}_{n+1})]^{\bar{\mathbf{\Phi}}_n^{\alpha_r}=\mathbf{\Phi}_n} \\ &\quad + \sum_{\alpha_r\in\{\alpha_r|f_b\}}\int [\mathrm{d}\Phi_{\mathrm{rad}}^{\alpha_r}\{R_{\alpha_r}(\mathbf{\Phi}_{n+1}) - C_{\alpha_r}(\mathbf{\Phi}_{n+1})\}]^{\bar{\mathbf{\Phi}}_n^{\alpha_r}=\mathbf{\Phi}_n} \\ &\quad + \sum_{\alpha_g\in\{\alpha_g|f_b\}}\int \left[\frac{\mathrm{d}\xi}{\xi} G_{\alpha_g}(\mathbf{\Phi}_n,\xi)\right]^{\bar{\mathbf{\Phi}}_n=\mathbf{\Phi}_n}. \end{aligned} \tag{2.120}$$

Thereby, the notation $[\cdots]^{\bar{\mathbf{\Phi}}_n^{\alpha_r}=\mathbf{\Phi}_n}$ is to be understood that such the phase space point $\mathbf{\Phi}_{n+1}$ inside the square bracket is factorized into $(\bar{\mathbf{\Phi}}_n^{\alpha_r}, \Phi_{\mathrm{rad}}^{\alpha_r})$ and $\bar{\mathbf{\Phi}}_n^{\alpha_r}$ is evaluated at $\mathbf{\Phi}_n$. The measure $\mathrm{d}\Phi_{\mathrm{rad}}^{\alpha_r}$ contains the appropriate Jacobian factor such that

$$\mathrm{d}\mathbf{\Phi}_{n+1} = \mathrm{d}\bar{\mathbf{\Phi}}_n^{\alpha_r}\mathrm{d}\Phi_{\mathrm{rad}}^{\alpha_r}. \tag{2.121}$$

Similarly, the notation $[\cdots]^{\bar{\mathbf{\Phi}}_n=\mathbf{\Phi}_n}$ for the collinear counter term means that the phase space point inside the squared bracket is transformed as

$$\mathbf{\Phi}_n \to \bar{\mathbf{\Phi}}_n = (\bar{x}, \Phi_n) = (\xi x, \Phi_n), \tag{2.122}$$

and the transformed phase space point $\bar{\mathbf{\Phi}}_n$ is evaluated at $\mathbf{\Phi}_n$.

Now, the POWHEG-Sudakov factor can be introduced, which is the NLO accurate version of Eq. (2.116)

$$\Delta_{f_b}(\mathbf{\Phi}_n, p_T) = \exp\left\{ - \sum_{\alpha_r \in \{\alpha_r | f_b\}} \int \left[\mathrm{d}\Phi_{\mathrm{rad}}^{\alpha_r} \frac{R_{\alpha_r}(\mathbf{\Phi}_{n+1})}{B_{f_b}(\mathbf{\Phi}_n)} \theta(k_T^{\alpha_r}(\mathbf{\Phi}_{n+1}) - p_T) \right]^{\bar{\mathbf{\Phi}}_n^{\alpha_r} = \mathbf{\Phi}_n} \right\}. \tag{2.123}$$

Here, $k_T^{\alpha_r}(\mathbf{\Phi}_{n+1})$ is a function of the phase space point $\mathbf{\Phi}_{n+1}$ and depends on the divergent region α_r. It is the ordering variable and should be proportional to the transverse component of the radiation momentum with respect to:

- the beam axis if the emitter is an initial state particle, or
- the 3-momentum sum of emitter and radiation if the emitter is a final state particle.

It can be shown that Eq. (2.119) is equivalent to

$$\langle O \rangle = \sum_{f_b} \int \mathrm{d}\mathbf{\Phi}_n \bar{B}_{f_b}(\mathbf{\Phi}_n) \left\{ O_n(\mathbf{\Phi}_n) \Delta_{f_b}(\mathbf{\Phi}_n, p_T^{\min}) + \right. \\ \left. + \sum_{\alpha_r \in \{\alpha_r | f_b\}} \int \mathrm{d}\Phi_{\mathrm{rad}} O_{n+1}(\mathbf{\Phi}_{n+1}) \frac{R_{\alpha_r}(\mathbf{\Phi}_{n+1})}{B_{f_b}(\mathbf{\Phi}_n)} \Delta_{f_b}(\mathbf{\Phi}_n, k_T^{\alpha_r}) \theta(k_T^{\alpha_r} - p_T^{\min}) \right\} \tag{2.124}$$

up to terms that are in higher order than NLO. The first term in Eq. (2.124) corresponds to all n-particle contributions to the observable since $\Delta_{f_b}(\mathbf{\Phi}_n, p_T^{\min})$ is the probability of no radiation being produced above the cutoff $p_T^{\min}$. The second term contains the contribution of the first radiation because

$$\sum_{\alpha_r \in \{\alpha_r | f_b\}} \int \mathrm{d}\Phi_{\mathrm{rad}} O_{n+1}(\mathbf{\Phi}_{n+1}) \frac{R_{\alpha_r}(\mathbf{\Phi}_{n+1})}{B_{f_b}(\mathbf{\Phi}_n)} \Delta_{f_b}(\mathbf{\Phi}_n, k_T^{\alpha_r}) \theta(k_T^{\alpha_r} - p_T^{\min}) \tag{2.125}$$

is the NLO accurate version of the probability density Eq. (2.117) with which a radiation in a shower algorithm is generated.

In order to implement Eq. (2.124), one generates an n-particle phase space point $\mathbf{\Phi}_n$ and flavor structure index f_b with a probability proportional to $\mathrm{d}\mathbf{\Phi}_n \bar{B}_{f_b}(\mathbf{\Phi}_n)$. In practice, this is done using the hit and miss technique. If the n-particle phase space point is generated, the first emission can be added.

Therefore, one has to generate the hardest radiation variables a $\alpha_r \in \{\alpha_r | f_b\}$ with a probability proportional to

$$\mathrm{d}\Phi_{\mathrm{rad}} \frac{R_{\alpha_r}(\mathbf{\Phi}_{n+1})}{B_{f_b}(\mathbf{\Phi}_n)} \Delta_{f_b}^{\alpha_r}(\mathbf{\Phi}_n, k_T^{\alpha_r}) \theta(k_T^{\alpha_r} - p_T^{\min}). \tag{2.126}$$

In this context hardest radiation means the configuration with the greatest $k_T^{\alpha_r}(\mathbf{\Phi}_{n+1})$. Ultimately, this problem can be reduced to generate a value $p_T^{\alpha_r}$ for each $\alpha_r \in \{\alpha_r | f_b\}$ proportional to

$$\Delta_{f_b}^{\alpha_r}(\mathbf{\Phi}_n, p_T) = \exp\left\{ - \int \left[\mathrm{d}\Phi_{\mathrm{rad}}^{\alpha_r} \frac{R_{\alpha_r}(\mathbf{\Phi}_{n+1})}{B_{f_b}(\mathbf{\Phi}_n)} \theta(k_T^{\alpha_r}(\mathbf{\Phi}_{n+1}) - p_T) \right]^{\bar{\mathbf{\Phi}}_n^{\alpha_r} = \mathbf{\Phi}_n} \right\}. \tag{2.127}$$

Then the pair $(p_T^{\alpha_r}, \alpha_r)$ with the highest value for $p_T^{\alpha_r}$ is accepted for the event and the radiation variables are built to yield $k_T^{\alpha_r} = p_T^{\alpha_r}$. In order to generate the value for $p_T^{\alpha_r}$, one has to generate a random number $0 < r < 1$ and solve the equation

$$r = \Delta_{f_b}^{\alpha_r}(\mathbf{\Phi}_n, p_T) \tag{2.128}$$

for p_T.

Solving Eq. (2.128) is in general a time consuming task. To handle this technical problem one can define an upper bounding function $U(\Phi_{\mathrm{rad}})$ such that

$$U(\Phi_{\mathrm{rad}}^{\alpha_r}) \geq \left[\frac{R_{\alpha_r}(\mathbf{\Phi}_{n+1})}{B_{f_b}(\mathbf{\Phi}_n)} \right]^{\bar{\mathbf{\Phi}}_n^{\alpha_r} = \mathbf{\Phi}_n}, \tag{2.129}$$

and that the equation

$$r = \Delta_{f_b}^{\alpha_r, U}(\mathbf{\Phi}_n, p_T) := \exp\left\{ - \int \left[\mathrm{d}\Phi_{\mathrm{rad}}^{\alpha_r} U(\Phi_{\mathrm{rad}}^{\alpha_r}) \theta(k_T^{\alpha_r}(\mathbf{\Phi}_{n+1}) - p_T) \right]^{\bar{\mathbf{\Phi}}_n^{\alpha_r} = \mathbf{\Phi}_n} \right\} \tag{2.130}$$

is solvable in a more timely manner. By using the veto method, one can generate a p_T with the probability density $\Delta_{f_b}^{\alpha_r}$ using $\Delta_{f_b}^{\alpha_r, U}$. Consequently, one has to find the $p_{T,\max}$ with $\Delta_{f_b}^{\alpha_r, U}(p_{T,\max}) = 1$. Then, one generates a uniform random number $0 < r < 1$ and solves

$$r = \frac{\Delta_{f_b}^{\alpha_r, U}(p_T)}{\Delta_{f_b}^{\alpha_r, U}(p_{T,\max})} \tag{2.131}$$

for p_T. From this p_T the radiation variables $\Phi_{\text{rad}}^{\alpha_r}$ are built proportional to the density

$$U(\Phi_{\text{rad}}^{\alpha_r})\delta(k_T^{\alpha_r}(\Phi_{\text{rad}}^{\alpha_r}) - p_T). \tag{2.132}$$

Now, a second random number $0 < r' < 1$ is generated, and if

$$r' > \left[\frac{R_{\alpha_r}(\mathbf{\Phi}_{n+1})}{B_{f_b}(\mathbf{\Phi}_n)}\right]^{\bar{\mathbf{\Phi}}_n^{\alpha_r}=\mathbf{\Phi}_n} U(\Phi_{\text{rad}}^{\alpha_r})^{-1}, \tag{2.133}$$

the event is vetoed. In case of a vetoed event $p_{T,\max}$ is set to $p_{T,\max} = p_T$ and the procedure is started again from Eq. (2.131) with new random numbers r, r'. Eventually, one either finds an accepted event, or the generated p_T falls below the cutoff $p_{T,\min}$. In any case, the veto procedure stops and one gets the radiation variables $\Phi_{\text{rad}}^{\alpha_r}$ or a rejected radiation for that α_r.

After this is done for each $\alpha_r \in \{\alpha_r | f_b\}$, the IR divergent region with the highest $k_T^{\alpha_r}(\Phi_{\text{rad}}^{\alpha_r})$ is accepted. If all radiations are rejected because each region generated a $p_T < p_{T,\min}$, then the event is an n-particle event.

2.6 Deep inelastic scattering

This work focuses on the process referred to as DIS, which is traditionally the scattering of an electron and a proton. The focus of DIS is probing the inner structure of a hadron or nuclei with a high energy lepton. In DIS, the incoming lepton interacts with a constituent of the proton via an exchange boson of momentum q (see Fig. 2.2). One selects the scattering events where the exchanging boson has a high virtuality $-q^2 \gg M_P^2$. This ensures the validity of the perturbative QFT methods described in the previous sections to obtain accurate predictions.

Throughout this work, momenta will be numbered as indicated in Fig. 2.2, i.e. the incoming lepton will be called p_1, the incoming parton p_2, the outgoing lepton p_3 and all outgoing partons are numbered from 4 onwards. The momentum of the incoming proton is denoted with P. In the context of DIS, kinematic variables are often defined as [90]

$$\begin{aligned} Q^2 &:= -q^2 = -(p_1 - p_3)^2 > 0, & y_{\text{DIS}} &:= \frac{p_2 q}{p_1 p_2}, \\ x_B &:= \frac{Q^2}{2Pq}, & \lambda &:= \frac{Q^2}{2p_2 q}. \end{aligned} \tag{2.134}$$

Let x be the momentum fraction of the incoming proton that is carried by the incoming parton $p_2 = xP$. Then, it follows

$$\lambda = \frac{x_B}{x}. \tag{2.135}$$

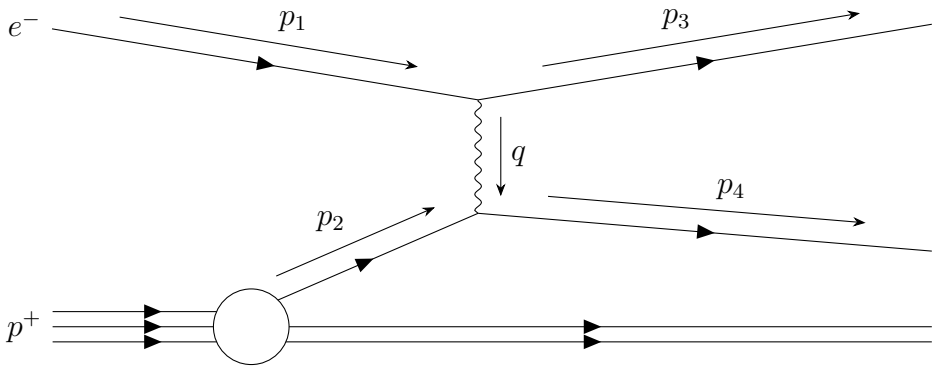

Figure 2.2: Example of a Feynman diagram for electron-proton scattering.

At LO the partonic process will only have two particles in the final state. From momentum conservation follows $q = p_4 - p_2$, and hence $\lambda = 1$, or $x_B = x$. If a radiated parton is added, one obtains in general $\lambda < 1$, or $x_B < x$.

The averaged spin and color summed squared matrix element at LO consists only of the Feynman diagram depicted in Fig. 2.2, where the exchange boson is a photon or a Z-boson. The contributions from Z-boson exchange are suppressed by a factor $1/M_Z^2$ for small $Q^2 \ll M_Z^2$. Hence, the first approximation can be given by neglecting the Z-boson contribution, leaving only one Feynman diagram to calculate. With the `Mathematica` tools `FeynArts` [91] and `FeynCalc` [92–94] one obtains

$$\overline{|\mathcal{M}_q|^2} = 32\pi^2\alpha^2 Q_q^2 \frac{Q^4 - 2Q^2 s + 2s^2}{Q^4}, \tag{2.136}$$

where Q_q is the electric charge of the quark flavor q. One can easily see that the squared matrix element diverges for $Q^2 \to 0$. For small energy transfers Q^2, the assumption that the electron scatters off of the constituents of the proton does not hold up, and the idea to factor out a hard scattering process breaks down. At small Q^2 the electron would interact with the proton as a whole rather than the partons. This emphasizes the importance to impose a lower cut $Q^2_{\text{cut}} < Q^2$ on the events that are to be described by this prediction.

2.6.1 Breit frame

When describing DIS, a popular reference frame is the Breit frame. It is defined by the condition

$$2x_B\mathbf{P} + \mathbf{q} = 0. \tag{2.137}$$

It is practical to choose a direction for the vector q. This work uses

$$p_{2,\text{Breit}} = E_{2,\text{Breit}}(1,0,0,-1), \qquad q_{\text{Breit}} = Q(0,0,0,1). \tag{2.138}$$

Any momentum p_{breit} with $p_{\text{breit}} q_{\text{Breit}} > 0$ is labeled to be in the current hemisphere, while momenta not fulfilling this condition make up the remnant hemisphere. By defining observables using only the particles in the current hemisphere, one can easily single out effects from the scattering process from effects that occur due to the proton remnant. The proton remnant is nearly collinear to the incoming proton and hence in the remnant hemisphere. With all momenta being transformed into the Breit frame, commonly studied observable is the jet broadening

$$B_{z,E} := \frac{\sum_h |\mathbf{p}_{T,h}|}{2\sum_h |\mathbf{p}_h|}. \tag{2.139}$$

The notation $\sum_h$ means the sum over all particles in the current hemisphere and $\mathbf{p}_{T,h}$ is the transverse momentum of $\mathbf{p}_h$ with respect to $\mathbf{q}$. Some more common observables are the thrust variable with respect to the boson axis τ, the jet mass ρ and the C-parameter. They are defined as

$$\begin{aligned} \tau_{z,E} &:= 1 - \frac{\sum_h |\mathbf{p}_h^3|}{\sum_h |\mathbf{p}_h|}, \\ \rho &:= \frac{\left(\sum_h E_h\right)^2 - \left(\sum_h \mathbf{p}_h\right)^2}{\left(2\sum_h |\mathbf{p}_h|\right)^2}, \\ C &:= \frac{3\sum_{h,h'} |\mathbf{p}_h||\mathbf{p}_{h'}| \cos^2\theta_{hh'}}{2\left(\sum_h |\mathbf{p}_h|\right)^2}. \end{aligned} \tag{2.140}$$

If the incoming lepton is along the positive z-axis and the incoming proton along the negative z-axis, one can write the transformation matrix Λ_{Breit} as

$$\Lambda_{\text{Breit}} = \begin{pmatrix} \frac{Q}{q^0+q^3} + \frac{q^0}{Q} & -\frac{q^1}{Q} & -\frac{q^2}{Q} & \frac{Q}{q^0+q^3} - \frac{q^3}{Q} \\ -\frac{q^1}{q^0+q^3} & 1 & 0 & -\frac{q^1}{q^0+q^3} \\ -\frac{q^2}{q^0+q^3} & 0 & 1 & -\frac{q^2}{q^0+q^3} \\ -\frac{q^0}{Q} & \frac{q^1}{Q} & \frac{q^2}{Q} & \frac{q^3}{Q} \end{pmatrix}, \tag{2.141}$$

where q is the boson momentum in the original frame. This transformation matrix is a modified version of the one reported in Appendix 7.11 of Ref. [90]. The modifications take into account the different sign for q_{Breit} and an arbitrary rotation around the beam axis. This transformation will transform the

momenta

$$\Lambda_{\text{Breit}} \begin{pmatrix} q^0 \\ q^1 \\ q^2 \\ q^3 \end{pmatrix} = \begin{pmatrix} 0 \\ 0 \\ 0 \\ Q \end{pmatrix},$$
$$\Lambda_{\text{Breit}} \begin{pmatrix} 1 \\ 0 \\ 0 \\ -1 \end{pmatrix} = \frac{q^0 + q^3}{Q} \begin{pmatrix} 1 \\ 0 \\ 0 \\ -1 \end{pmatrix}. \tag{2.142}$$

When doing a phase space integral in the Breit frame, one has to include a Jacobian factor for the transformation, despite Λ_{Breit} being a Lorentz transformation. Because Λ_{Breit} depends on the momentum of the out going lepton, its Jacobian determinant $|\Lambda_{\text{Breit}}| \neq 1$. Instead, one finds

$$\mathrm{d}\Phi_n = 2y_{\text{DIS}}\mathrm{d}\Phi_{n,\text{Breit}}, \tag{2.143}$$

with $p^3_{3,\text{breit}} < 0$, i.e. the outgoing lepton is restricted to the remnant hemisphere.

2.6.2 2-particle Phase space

In this section, the phase space measure $\mathrm{d}\mathbf{\Phi}_2$ is calculated. It will be referred to as Born kinematics. All Born momenta and kinematic variables will be denoted with barred variables to distinguish them from momenta associated to the real correction. The starting point is

$$\mathrm{d}\mathbf{\Phi}_2 = \mathrm{d}\bar{x}\frac{\mathrm{d}^3\bar{\mathbf{p}}_3}{2(2\pi)^3\bar{E}_3}\frac{\mathrm{d}^3\bar{\mathbf{p}}_4}{2(2\pi)^3\bar{E}_4}(2\pi)^4\delta^{(4)}(\bar{p}_1 + \bar{p}_2 - \bar{p}_3 - \bar{p}_4), \tag{2.144}$$

with $\bar{E}_n := |\mathbf{p}_n|$ and $\bar{p}_2 = \bar{x}P$, where P is the incoming proton momentum. Now, $\mathrm{d}^3\bar{\mathbf{p}}_4$ can be eliminated with the delta distribution, and the DIS variables defined in Eq. (2.134) can be introduced. This can be easily done in the center-of-mass frame in which

$$\bar{p}_1 = \frac{\sqrt{\bar{s}}}{2}(1,0,0,1),$$
$$\bar{p}_2 = \frac{\sqrt{\bar{s}}}{2}(1,0,0,-1). \tag{2.145}$$

Then, one gets

$$\mathrm{d}\mathbf{\Phi}_2 = \frac{1}{16\pi^2}\mathrm{d}x_B\mathrm{d}\bar{E}_3\mathrm{d}\bar{c}_3\mathrm{d}\bar{\phi}_3\delta\big(\sqrt{\bar{s}} - 2\bar{E}_3\big), \tag{2.146}$$

with

$$\begin{aligned} \bar{p}_3 &= E_3(1, \cos\bar{\phi}_3\sqrt{1-\bar{c}_3^2}, \sin\bar{\phi}_3\sqrt{1-\bar{c}_3^2}, \bar{c}_3), \\ \Rightarrow y_{\mathrm{DIS}} &= \frac{1-\bar{c}_3}{2}, \qquad Q^2 = \frac{\bar{s}}{2}(1-\bar{c}_3). \end{aligned} \tag{2.147}$$

Hence, the phase space measure becomes

$$\mathrm{d}\mathbf{\Phi}_2 = \frac{\mathrm{d}x_B \mathrm{d}y_{\mathrm{DIS}} \mathrm{d}\bar{\phi}_3}{16\pi^2}. \tag{2.148}$$

Since the setup of two incoming particles along the z-axis is symmetric under rotations around the z-axis, the differential cross section cannot depend on $\mathrm{d}\bar{\phi}_3$. Hence, one can perform the integration over $\mathrm{d}\bar{\phi}_3$ to get an extra factor 2π.

Chapter 3

Software implementation

This chapter describes the changes to the POWHEG BOX that had to be made to generate DIS events. The POWHEG BOX is set up to handle hadron-hadron collisions as they happen in the large hadron collider. The obvious difference between DIS and hadron-hadron collisions is a lepton in the initial state instead of the second hadron. The POWHEG method relies on the mapping of the $n+1$ particle phase space $\mathbf{\Phi}_{n+1}$ of the real correction to the underlying Born phase space $\bar{\mathbf{\Phi}}_n$. This mapping is done for each IR divergent region in a generic way. In the implementation of the POWHEG BOX, this mapping is inverted and the phase space point $\mathbf{\Phi}_{n+1}$ is built for a given n particle phase space point $\bar{\mathbf{\Phi}}_n$. This mapping is not unique. A specific mapping suited for proton-proton collisions was chosen and impelented in the POWHEG BOX. In particular, this mapping includes a mapping of the momentum fractions $\bar{x}_\pm \to x_\pm$ of the incoming partons, where in general $\bar{x}_\pm \neq x_\pm$. However, if one of the incoming particles is a lepton, then this lepton has to carry the whole momentum of the beam, i.e. $\bar{x}_{\text{lepton}} = x_{\text{lepton}} = 1$. Another feature of DIS is the divergent behavior for $Q^2 \to 0$. Hence, experimental data will incorporate a lower cut on the momentum transfer Q^2 that must be respected in theoretical simulations. Since the POWHEG BOX generates the phase space for the radiation based on the underlying Born phase space, it would be efficient if the mapping would fulfill $\bar{Q}^2 = Q^2$. If this condition is fulfilled, one will not encounter the problem of needing to generate n-particle events outside of the Q^2 boundaries in order to ensure that all $n+1$-particle events inside the boundaries can be generated or vice versa. The mapping between underlying Born configurations and the real correction configurations do not respect these conditions and have to be modified. This chapter shows how the mapping can be modified to fulfill these conditions and which subsequent modifications must be made to obtain a functioning event generator that can be interfaced to a shower algorithm to obtain showered events at NLO

accuracy.

3.1 POWHEG BOX

This section is a brief description of the functionality of the POWHEG BOX. The detailed describtion can be found in Ref. [95]. The POWHEG BOX is split into four stages. The first two stages are fixed order phases. In those stages the phase space integral for the cross section is evaluated using Monte Carlo integration. For this purpose, random variables, one for each unrestricted dimension in the phase space integral, are generated. Then, these random variables are mapped onto the n-particle phase space, for which the LO and IR subtracted virtual corrections are evaluated. Three more random variables are used to build the $n+1$-particle phase space on top of the n-particle phase space to evaluate the real corrections together with their counter terms. The first stage of the POWHEG BOX serves the purpose to optimize the importance sampling of the random variables for the Monte Carlo integration. At the second stage, the fixed order calculation is performed using the optimized importance sampling. This calculation yields fixed order histograms and the total cross section, that is used for the normalization of the later stages.

In the third stage, the upper bounding normalization constant $N^r_{f_b}$ is estimated for each radiation region r and Born flavor structure f_b. This is done by evaluating the phase space integral at random points according to the optimized importance sampling of the prior stages, such that

$$\frac{J^r R^r(\mathbf{\Phi}_{n+1})}{B_{f_b}(\bar{\mathbf{\Phi}}_n)} < N^r_{f_b}\, U^r(\mathbf{\Phi}_{n+1}). \tag{3.1}$$

The radiation region r is defined as $r = 1$ if the emitter of the radiation is an initial state particle and $r = n_{\text{emitter}} - n_{\text{lightparton}} + 2$ otherwise. Thereby, n_{emitter} is the particle number of the emitter and $n_{\text{lightparton}}$ is the particle number of the first light parton. The particle numbering is with respect to the defined flavor structures in the implementation. They use the convention that the first two particles in the flavor structure are the initial state particles, the next particles are QCD singlets, then heavy quarks, and lastly massless quarks where the radiation is the very last entry. Further, R^r and J^r are defined as

$$R^r(\mathbf{\Phi}_{n+1}) := \sum_{\alpha_r \in \{\alpha_r | f_b, r\}} R_{\alpha_r}(\mathbf{\Phi}_{n+1}), \tag{3.2}$$

where the phase space point $\mathbf{\Phi}_{n+1}$ is given by

$$\mathbf{\Phi}_{n+1} := J^r \bar{\mathbf{\Phi}}_n \mathrm{d}\xi \mathrm{d}y \mathrm{d}\phi. \tag{3.3}$$

ξ, y and ϕ are the FKS variables and will be discussed in detail in the next section.

In the last stage of the POWHEG BOX, the final events are generated as described in section 2.5. The generated events can then be used as input for a Monte Carlo shower program to produce histograms using the showered events.

3.2 Phase space generation

The phase space generation for the Born kinematics required by the POWHEG BOX can be done manually by the user or automatically. Its generation is straight forward and does not cause any complications. The advantage of manually building the phase space by hand, as opposed to using a generic method, is the ability to incorporate kinematic cuts already at this level. In that way, the generation of unnecessary events that will not be considered in the analysis is avoided. For DIS this is especially helpful since the matrix element diverges for $Q^2 \to 0$. If no cuts are applied in the phase space generation, then the optimization for Monte Carlo integration of the phase space will increase the amount of points for low Q^2 values that would ultimately be cut in the analysis.

The 2-particle phase space is already discussed in section 2.6.2. The phase space point $\mathbf{\Phi}_2$ has the three unrestricted parameters x_B, y_{DIS} and $\bar{\phi}_3$. This means, three random variables X_i are mapped onto these kinematic variables with the restrictions

$$x_B^{\text{low}} < x_B < x_B^{\text{up}}, \qquad y_{\text{DIS}}^{\text{low}} < y_{\text{DIS}} < y_{\text{DIS}}^{\text{up}}, \qquad Q^2_{\text{low}} < Q^2 < Q^2_{\text{up}}. \tag{3.4}$$

$x_B^{\text{low}}, x_B^{\text{up}}, y_{\text{DIS}}^{\text{low}}, y_{\text{DIS}}^{\text{up}}, Q^2_{\text{low}}, Q^2_{\text{up}}$ are input values that can be set for a specific run. Note that

$$Q^2 = y_{\text{DIS}} x_B S_{\text{beams}}, \tag{3.5}$$

where $S_{\text{beams}} = 4E_{\text{beam},1}E_{\text{beam},2}$, with $E_{\text{beam},i}$ being the energies of the two beams. Then, the Born momenta in the partonic center-of-mass frame are

$$\begin{aligned}
\bar{p}_1 &= \frac{\sqrt{x_B S_{\text{beams}}}}{2}(1,0,0,1),\\
\bar{p}_2 &= \frac{\sqrt{x_B S_{\text{beams}}}}{2}(1,0,0,-1),\\
\bar{p}_3 &= \frac{\sqrt{x_B S_{\text{beams}}}}{2}(1,\sqrt{2y_{\text{DIS}}}\cos\bar{\phi}_3,\sqrt{2y_{\text{DIS}}}\sin\bar{\phi}_3,1-2y_{\text{DIS}}),\\
\bar{p}_4 &= \frac{\sqrt{x_B S_{\text{beams}}}}{2}(1,-\sqrt{2y_{\text{DIS}}}\cos\bar{\phi}_3,-\sqrt{2y_{\text{DIS}}}\sin\bar{\phi}_3,-1+2y_{\text{DIS}}).
\end{aligned} \tag{3.6}$$

With three additional random variables $\{X_1^{\text{rad}}, X_2^{\text{rad}}, X_3^{\text{rad}}\}$ the real correction phase space point $\mathbf{\Phi}_3$ has to be built. The mapping

$$\mathbf{\Phi}_3 \to \left(\bar{\mathbf{\Phi}}_2, X_1^{\text{rad}}, X_2^{\text{rad}}, X_3^{\text{rad}}\right) \tag{3.7}$$

is dependent on the IR divergent region α_r. The FKS framework for the subtraction of the IR divergences is implemented in the `POWHEG BOX`. This method uses the three variables ξ, y and ϕ to describe the momentum of the radiation. Their meaning is different for ISR and FSR. Hence, one needs two different mappings. In both cases, the goal is to express the measure

$$\mathrm{d}\mathbf{\Phi}_3 = \mathrm{d}x \frac{\mathrm{d}^3\mathbf{p}_3}{2E_3(2\pi)^3} \frac{\mathrm{d}^3\mathbf{p}_4}{2E_4(2\pi)^3} \frac{\mathrm{d}^3\mathbf{p}_5}{2E_5(2\pi)^3} (2\pi)^4 \delta^{(4)}(p_1 + p_2 - p_3 - p_4 - p_5) \tag{3.8}$$

in terms of $\mathrm{d}\mathbf{\Phi}_2$ and the three FKS variables. Without loss of generality, it is assumed that p_5 is the momentum of the radiation, while p_4 is the momentum of the emitter.

The FKS subtraction terms are dependent on the exact definition of the FKS variables. In order to allow minimal modifications to the code, it useful to use the exact same definitions. In particular, this means to perform the phase space parametrization in the partonic center-of-mass frame.

3.2.1 Phase space for initial-state radiation

Firstly, the FKS variables for ISR are defined such that

$$p_5 = \xi \frac{\sqrt{s}}{2} \Big(1, \sqrt{1-y^2}\cos\phi, \sqrt{1-y^2}\sin\phi, y\Big), \tag{3.9}$$

where $s = xS_{\text{beams}}$ is the partonic center-of-mass energy squared of the real correction process. Further, the incoming momenta in the center-of-mass frame are

$$\begin{aligned} p_1 &= \frac{\sqrt{s}}{2}(1,0,0,1), \\ p_2 &= \frac{\sqrt{s}}{2}(1,0,0,-1). \end{aligned} \tag{3.10}$$

Starting from Eq. (3.8), the integral over $\mathrm{d}^3\mathbf{p}_4$ can be performed using the delta distribution to yield

$$\mathbf{p}_4 = -\mathbf{p}_3 - \mathbf{p}_5. \tag{3.11}$$

The mapping to the underlying Born configuration should fulfill $p_{1,3} = \bar{p}_{1,3}$. It is important to note that the center-of-mass frames for the two configurations are different since $x \neq x_B$. The outgoing lepton momentum can be parametrized in spherical coordinates

$$\begin{aligned} \mathbf{p}_3 &= E_3\left(1, \sqrt{1-c_3^2}\cos\phi_3, \sqrt{1-c_3^2}\sin\phi_3, c_3\right), \\ \mathrm{d}^3\mathbf{p}_3 &= \mathrm{d}E_3\mathrm{d}c_3\mathrm{d}\phi_3 E_3^2. \end{aligned} \tag{3.12}$$

Then, the phase space measure becomes

$$\begin{aligned} \mathrm{d}\mathbf{\Phi}_3 &= \frac{1}{8(2\pi)^5}\mathrm{d}x\,\mathrm{d}E_3\,\mathrm{d}c_3\,\mathrm{d}\phi_3\,\mathrm{d}\xi\,\mathrm{d}y\,\mathrm{d}\phi\,\frac{\sqrt{s}}{2}\frac{E_3E_5}{E_4}\delta(E_1+E_2-E_3-E_4-E_5), \\ E_1 &= E_2 = \frac{\sqrt{s}}{2}, \qquad E_4 = \sqrt{(\mathbf{p}_3+\mathbf{p}_5)^2}, \qquad E_5 = \xi\frac{\sqrt{s}}{2}. \end{aligned} \tag{3.13}$$

Using the definitions of the DIS variables in Eq. (2.134) and the given parametrization one obtains

$$\begin{aligned} q &= \left(\frac{\sqrt{s}}{2} - E_3, -E_3\sqrt{1-c_3^2}\cos\phi_k, -E_3\sqrt{1-c_3^2}\sin\phi_k, \frac{\sqrt{s}}{2} - E_3c_3\right), \\ Q^2 &= E_3\sqrt{s}(1-c_3), \\ y_{\mathrm{DIS}} &= 1 - \frac{E_3(1+c_3)}{\sqrt{s}}, \\ \mathrm{d}E_3\,\mathrm{d}c_3 &= \mathrm{d}y_{\mathrm{DIS}}\,\mathrm{d}Q^2\frac{1}{2E_3} = \mathrm{d}y_{\mathrm{DIS}}\,\mathrm{d}Q^2\frac{\sqrt{s}}{s(1-y_{\mathrm{DIS}})+Q^2}. \end{aligned} \tag{3.14}$$

By substituting E_3 and c_3 with the DIS variables y_{DIS} and Q^2, one obtains

$$\mathrm{d}\mathbf{\Phi}_3 = \frac{\sqrt{s}}{32(2\pi)^5}\mathrm{d}x\,\mathrm{d}y_{\mathrm{DIS}}\,\mathrm{d}Q^2\,\mathrm{d}\phi_3\,\mathrm{d}\xi\,\mathrm{d}y\,\mathrm{d}\phi\,\frac{E_5}{E_4}\delta\Big(\tilde{f}(s,Q^2,y_{\mathrm{DIS}},\Delta\phi,\xi,y)\Big), \tag{3.15}$$

with $\Delta\phi = \phi - \phi_3$. In order to factorize $\mathrm{d}\mathbf{\Phi}_2$, one has to eliminate either $\mathrm{d}y_{\mathrm{DIS}}$ or $\mathrm{d}Q^2$. However, the equation $\tilde{f}(Q^2, y_{\mathrm{DIS}}, \Delta\phi, \xi, y) = 0$ would have two solutions for Q^2 or y_{DIS}. This would make it impossible to perform the factorization of

$$\mathrm{d}\mathbf{\Phi}_3 = \mathrm{d}\mathbf{\Phi}_2\,\mathrm{d}\xi\,\mathrm{d}y\,\mathrm{d}\phi\,J. \tag{3.16}$$

A solution is to introduce the DIS variable λ and use the identity

$$1 = \int \mathrm{d}\lambda\delta\left(\lambda - \frac{Q^2}{2p_2q}\right). \tag{3.17}$$

As discussed in section 2.6, this also ensures $\lambda = x_B/x$. By plugging in the parametrization, one finds

$$2p_2q = sy_{\mathrm{DIS}}. \tag{3.18}$$

Hence, one can write

$$\begin{aligned} \mathrm{d}\mathbf{\Phi}_3 = \frac{\sqrt{s}}{32(2\pi)^5}\mathrm{d}x\,\mathrm{d}y_{\mathrm{DIS}}\,\mathrm{d}Q^2\,\mathrm{d}\phi_3\,\mathrm{d}\xi\,\mathrm{d}y\,\mathrm{d}\phi\,\frac{E_5}{E_4} \\ \times\,\delta\Big(\tilde{f}(s,Q^2,y_{\mathrm{DIS}},\Delta\phi,\xi,y)\Big)\mathrm{d}\lambda\delta\bigg(\lambda-\frac{Q^2}{sy_{\mathrm{DIS}}}\bigg). \end{aligned} \tag{3.19}$$

By integrating over $\mathrm{d}Q^2$ using the newly introduced delta distribution and afterwards over $\mathrm{d}\lambda$ using the delta distribution with the function $\tilde{f}$ as an argument, the two branches are moved onto the λ integration. Ultimately, one obtains

$$\mathrm{d}\mathbf{\Phi}_3 = \frac{s^{\frac{3}{2}}y_{\mathrm{DIS}}}{32(2\pi)^5}\mathrm{d}x\,\mathrm{d}y_{\mathrm{DIS}}\,\mathrm{d}\lambda\,\mathrm{d}\phi_3\,\mathrm{d}\xi\,\mathrm{d}y\,\mathrm{d}\phi\,\frac{E_5}{E_4}\delta(f(s,\lambda,y_{\mathrm{DIS}},\Delta\phi,\xi,y)). \tag{3.20}$$

The next step is to integrate over $\mathrm{d}\lambda$ to eliminate the delta distribution. The argument of the delta distribution is

$$\begin{aligned} f(s,\lambda,y_{\mathrm{DIS}},\Delta\phi,\xi,y) = \frac{\sqrt{s}}{2}\Bigg[&(y_{\mathrm{DIS}}(1-\lambda)+1-\xi) \\ &-\Big(4\xi\sqrt{\lambda(1-y^2)(1-y_{\mathrm{DIS}})y_{\mathrm{DIS}}}\cos\Delta\phi \\ &-2\xi y(y_{\mathrm{DIS}}(1+\lambda)-1)+((\lambda-1)y_{\mathrm{DIS}}+1)^{\,2}+\xi^2\Big)^{1/2}\Bigg]. \end{aligned} \tag{3.21}$$

Solving for the zeros in λ gives two solutions

$$\begin{aligned} \lambda_\pm = \frac{1}{y_{\mathrm{DIS}}(\xi(1+y)-2)^2}\Bigg[&(\pm 2\xi\cos\Delta\phi\sqrt{A}+2(1-\xi)(2y_{\mathrm{DIS}}-\xi(1+y)) \\ &+\xi^2\left(1-y^2\right)(1-y_{\mathrm{DIS}})\cos\left(2\Delta\phi\right)\Bigg], \end{aligned} \tag{3.22}$$

with

$$\begin{aligned} A = &\left(1-y^2\right)^2(1-y_{\mathrm{DIS}})^2 \\ &\times\left[\xi^2\cos^2\Delta\phi+\frac{(2-\xi(1+y))(2y_{\mathrm{DIS}}-\xi((1-y)y_{\mathrm{DIS}}+y+1))}{(1-y^2)(1-y_{\mathrm{DIS}})}\right]. \end{aligned} \tag{3.23}$$

In order to obtain these solutions, one has to square the equation $f(s, \lambda, y_{\mathrm{DIS}}, \Delta\phi, \xi, y) = 0$ twice. Hence, it is necessary to verify the solutions, as signs may be lost in the process of squaring. The verification will be done later. For now, one can proceed with the factorization of the Born phase space. Therefore, one can reformulate the phase space measure using

$$\mathrm{d}\lambda f(s, \lambda, y_{\mathrm{DIS}}, \Delta\phi, \xi, y) = \frac{\mathrm{d}\lambda}{|D|}[\delta(\lambda - \lambda_-) - \delta(\lambda - \lambda_+)], \tag{3.24}$$

with

$$\begin{aligned} D &= \frac{\partial f(s, \lambda, y_{\mathrm{DIS}}, \Delta\phi, \xi, y)}{\partial\lambda} \\ &= -\frac{s\left(\xi\cos\Delta\phi\sqrt{\lambda\left(1-y^2\right)\left(y_{\mathrm{DIS}}-y_{\mathrm{DIS}}^2\right)} + \lambda y_{\mathrm{DIS}}(1-\xi y-(1-\lambda)y_{\mathrm{DIS}})\right)}{4E_4\lambda} \\ &\quad - \frac{\sqrt{s}y_{\mathrm{DIS}}}{2}. \end{aligned} \tag{3.25}$$

The solutions $\lambda_\pm$ ensure that

$$E_1 + E_2 = E_3 + E_4 + E_5. \tag{3.26}$$

This allows to find a shorter expression for E_4, rather than plugging in the parametrization in Eq. (3.13). One finds

$$E_4 = \frac{\sqrt{s}}{2}(1 + y_{\mathrm{DIS}}(1 - \lambda_\pm) - \xi). \tag{3.27}$$

The last step before factorizing the Born phase space is the transformation

$$x = \frac{x_B}{\lambda} \Rightarrow \mathrm{d}x = \frac{\mathrm{d}x_B}{\lambda}. \tag{3.28}$$

Thereby, one has to carefully handle the integration limits. Since the x integration goes from 0 to 1, the x_B integration will be going from 0 to λ after the variable transformation. However, in the Born phase space the integration of x_B goes from 0 to 1. Since $\lambda < 1$, one can extend the x_B integration by supplying an according theta function

$$\mathrm{d}x = \frac{\mathrm{d}x_B}{\lambda}\Theta(\lambda - x_B). \tag{3.29}$$

Since the integration over λ is still present, one can adjust the lower integration limit of λ to x_B to eliminate the extra theta function.

If everything is put together, the phase space can be simplified to

$$\begin{aligned}
\mathrm{d}\mathbf{\Phi}_3 = &\frac{1}{16(2\pi)^5}\mathrm{d}x_B\ \mathrm{d}y_{\mathrm{DIS}}\ \mathrm{d}\phi_3\ \mathrm{d}\lambda\ \mathrm{d}\xi\ \mathrm{d}\phi\ \mathrm{d}y\ [\delta(\lambda-\lambda_+)+\delta(\lambda-\lambda_-)] \\
&\times \frac{\bar{s}y_{\mathrm{DIS}}\xi}{\lambda\left|\lambda y_{\mathrm{DIS}}(\xi(1+y)-2)-\xi\cos\Delta\phi\sqrt{\lambda\,(1-y^2)\,(1-y_{\mathrm{DIS}})y_{\mathrm{DIS}}}\right|} \\
= &\frac{1}{32\pi^3}\mathrm{d}\mathbf{\Phi}_2\ \mathrm{d}\lambda\ \mathrm{d}\xi\ \mathrm{d}\phi\ \mathrm{d}y\ (\delta(\lambda-\lambda_+)+\delta(\lambda-\lambda_-)) \\
&\times \frac{\bar{s}y_{\mathrm{DIS}}\xi}{\lambda\left|\lambda y_{\mathrm{DIS}}(\xi(1+y)-2)-\xi\cos\Delta\phi\sqrt{\lambda\,(1-y^2)\,(1-y_{\mathrm{DIS}})y_{\mathrm{DIS}}}\right|},
\end{aligned} \tag{3.30}$$

where $\bar{s} = x_B S_{\mathrm{beams}} = \lambda s$ is the squared partonic center-of-mass energy of the underlying Born kinematics.

3.2.1.1 Validation of the solutions $\lambda_\pm$

It was already hinted that the solving process for $\lambda_\pm$ involves squaring of roots. Hence, one has to investigate in detail the signs of both sides of the equation. First, it is helpful to remember the physical limits of the integration variables $\xi, y, y_{\mathrm{DIS}}, \lambda, x_B$, which are

$$\xi, y_{\mathrm{DIS}}, x_B \in [0,1], \quad y \in [-1,1], \quad \lambda \in [x_B, 1]. \tag{3.31}$$

The solving for $\lambda_\pm$ starts with setting Eq. (3.21) to zero, which is equivalent to

$$(1-\lambda)y_{\mathrm{DIS}} + 1 - \xi = \sqrt{B + 4\xi\sqrt{\lambda\,(1-y^2)\,(1-y_{\mathrm{DIS}})\,y_{\mathrm{DIS}}}\cos\Delta\phi}, \tag{3.32}$$

with

$$B = -2\xi y\,(\lambda y_{\mathrm{DIS}} + y_{\mathrm{DIS}} - 1) + ((\lambda-1)y_{\mathrm{DIS}} + 1)^{\,2} + \xi^2. \tag{3.33}$$

The right-hand side of Eq. (3.32) is always positive as long as it is real, which it has to be to satisfy the equation. With the restrictions on the integration variables, it is easy to see that also the left-hand side is always positive. Hence, squaring both sides will lead to an equivalent equation. After squaring Eq. (3.32) and isolating the remaining square root one finds the equation

$$\begin{aligned}
&\xi y_{\mathrm{DIS}}(\lambda + \lambda y + y - 1) + 2(1-\lambda)y_{\mathrm{DIS}} - \xi(y+1) \\
&\qquad = 2\xi\sqrt{\lambda\,(1-y^2)\,(1-y_{\mathrm{DIS}})\,y_{\mathrm{DIS}}}\cos\Delta\phi.
\end{aligned} \tag{3.34}$$

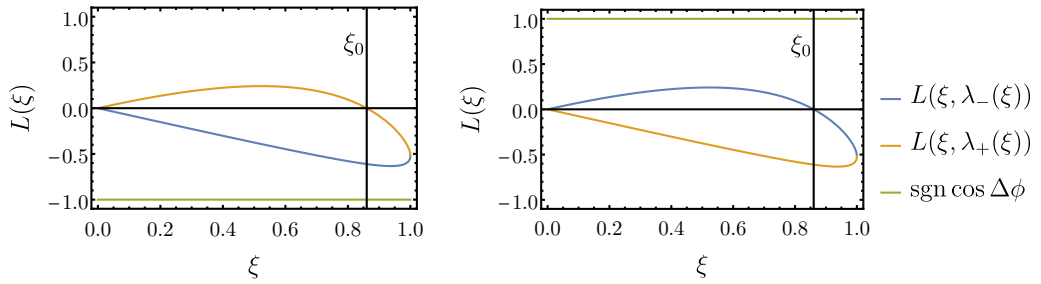

Figure 3.1: Plot of $L(\xi, y, y_{\mathrm{DIS}}, \lambda)$ in two different scenarios with partly fixed variables. The fixed variables are: $y = 0.3$, $y_{\mathrm{DIS}} = 0.8$ and $\cos\Delta\phi = -1$ on the left-hand side and $\cos\Delta\phi = 1$ on the right-hand side. The vertical black line shows the zero of $L(\xi, y, y_{\mathrm{DIS}}, \lambda)$.

Now, the right-hand side of Eq. (3.34) has the same sign as $\cos\Delta\phi$, which can be both positive or negative. The left-hand side can be positive or negative as well. In order for $\lambda_\pm$ to be a solution to Eq. (3.34), it has to give the left-hand side of Eq. (3.34) the same sign as $\cos\Delta\phi$. One can quickly see that the dependence of the solutions $\lambda_\pm$ (see Eq. (3.22)) on the sign of $\cos\Delta\phi$ turns out as

$$\lambda_+(\cos\Delta\phi) = \lambda_-(-\cos\Delta\phi). \tag{3.35}$$

For the sake of brevity, it is useful to define

$$L(\xi, y, y_{\mathrm{DIS}}, \lambda) := \xi y_{\mathrm{DIS}}(\lambda + \lambda y + y - 1) + 2(1-\lambda)y_{\mathrm{DIS}} - \xi(y+1). \tag{3.36}$$

Further, let ξ_0 be defined as

$$\xi_0 = \frac{2y_{\mathrm{DIS}}}{1 - yy_{\mathrm{DIS}} + y_{\mathrm{DIS}} + y}, \tag{3.37}$$

which is a zero in ξ of $L(\xi, y, y_{\mathrm{DIS}}, \lambda_\pm)$. In fact, it is the only zero in ξ that is greater than 0 and less than 1, and it fulfills

$$\begin{aligned} L(\xi_0, y, y_{\mathrm{DIS}}, \lambda_-) &= 0, \quad \text{if } \cos\Delta\phi > 0, \\ L(\xi_0, y, y_{\mathrm{DIS}}, \lambda_+) &= 0, \quad \text{if } \cos\Delta\phi < 0. \end{aligned} \tag{3.38}$$

In the case of $\cos\Delta\phi > 0$, one finds that

$$L(\xi, y, y_{\mathrm{DIS}}, \lambda_-) \begin{cases} > 0, & \text{if } \xi < \xi_0, \\ < 0, & \text{if } \xi > \xi_0, \end{cases} \tag{3.39}$$

while

$$L(\xi, y, y_{\mathrm{DIS}}, \lambda_+) < 0 \qquad \forall \xi \in (0,1). \tag{3.40}$$

This means that λ_- is the only zero of Eq. (3.21) if $\cos\Delta\phi > 0$ (see Fig. 3.1 on the right). In the other case of $\cos\Delta\phi < 0$, one finds (see Fig. 3.1 on the left)

$$\begin{aligned} &L(\xi, y, y_{\mathrm{DIS}}, \lambda_-) < 0 \qquad \forall \xi \in (0,1), \\ &L(\xi, y, y_{\mathrm{DIS}}, \lambda_+) \begin{cases} > 0, & \text{if } \xi < \xi_0, \\ < 0, & \text{if } \xi > \xi_0. \end{cases} \end{aligned} \tag{3.41}$$

In other words, λ_- is a correct solution for the whole range in ξ, while λ_+ is only the correct zero if $\xi > \xi_0$. Since λ_+ can only be a valid solution of Eq. (3.34) when $\xi > \xi_0$, in the soft limit of $\xi \to 0$, λ_- is the only possibility. The same holds for the collinear limit of $y \to -1$. Hence, all IR divergent kinematics can only be on the negative branch λ_-.

3.2.1.2 Integration limits of ξ

As already discussed before, the λ integration is restricted to the interval $[x_B, 1]$. This restriction can be shifted onto the ξ integration. Therefore, the dependence of the solutions $\lambda_\pm$ on ξ has to be analyzed. The general dependence $\lambda_\pm(\xi)$ is shown in Fig. 3.2. The graphs $\lambda_-(\xi)$ and $\lambda_+(\xi)$ form a closed loop, since $\lambda_-(\xi = 0) = \lambda_+(\xi = 0) = 1$ and $\lambda_-(\xi_{\max}) = \lambda_+(\xi_{\max})$. $\xi_{\max}$ is the value for which the root of $\lambda_\pm$ becomes zero, hence both solutions must be identical at this point. Either $\lambda_-(\xi)$ or $\lambda_+(\xi)$ has a zero at ξ_0. The closed loop formed by $\lambda_\pm(\xi)$ is intersected by the horizontal line at x_B exactly two times at ξ_{low} and ξ_{up}, with $\xi_{\mathrm{low}} < \xi_{\mathrm{up}}$. They are

$$\begin{aligned} \xi_{\mathrm{low}} &= \frac{2\,(x_B - 1)\, y_{\mathrm{DIS}}\,(2\sqrt{c}\,|\cos(\Delta\phi)| + y_{\mathrm{DIS}}\,(x_B(y+1) + y - 1) - y - 1)}{d}, \\ \xi_{\mathrm{up}} &= \frac{2\,(x_B - 1)\, y_{\mathrm{DIS}}\,(-2\sqrt{c}\,|\cos(\Delta\phi)| + y_{\mathrm{DIS}}\,(x_B(y+1) + y - 1) - y - 1)}{d}, \\ d &= -2(y+1) y_{\mathrm{DIS}}\,(2x_B + y - 1) + {y_{\mathrm{DIS}}}^2\left((y+1)^2 x_B^2 + (y-1)^2\right) \\ &\quad - 2c\cos(2\Delta\phi) + (y+1)^2, \\ c &= (1 - y^2) x_B (1 - y_{\mathrm{DIS}}) y_{\mathrm{DIS}}. \end{aligned} \tag{3.42}$$

The maximum value of ξ can be calculated by setting the argument of the root in $\lambda_\pm$ to zero. This yields

$$\begin{aligned} \xi_{\max} &= \frac{4 y_{\mathrm{DIS}}}{R + 2y_{\mathrm{DIS}} + y + 1}, \\ R &= \sqrt{(1 + y(1 - 2y_{\mathrm{DIS}}))^{\,2} - 4\,(1 - y^2)\,(1 - y_{\mathrm{DIS}})\, y_{\mathrm{DIS}} \cos^2(\Delta\phi)}. \end{aligned} \tag{3.43}$$

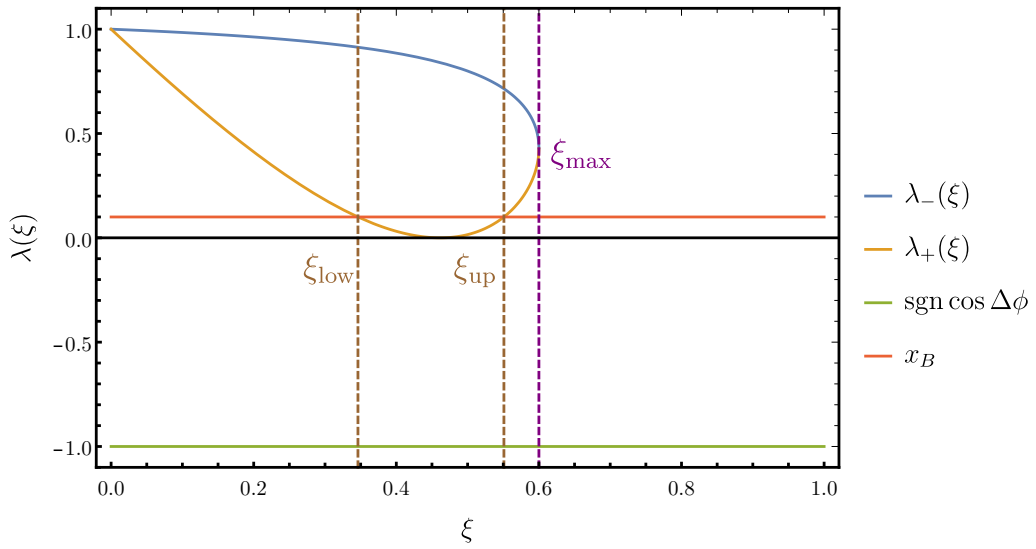

Figure 3.2: Dependence of the solutions $\lambda_\pm$ on ξ. In the depicted scenario the sign of $\cos\Delta\Phi$ is negative. If the sign is positive, λ_+ and λ_- are interchanged.

One can picture the ξ integration by following the closed loop formed by $\lambda_\pm$ from Fig. 3.2. The integration starts at $\xi = 0$ along the negative branch λ_-, and one follows the loop until it intersects the horizontal line of x_B. To sketch the integration, one can write

$$I_\xi := \int_0^1 \mathrm{d}\xi \int_{x_B}^1 \mathrm{d}\lambda f(\mathbf{\Phi}_3)[\delta(\lambda - \lambda_-) + \delta(\lambda - \lambda_+)]. \tag{3.44}$$

Here, $f(\mathbf{\Phi}_3)$ is meant to be the whole integrand for the real correction to the cross section including the matrix element and Jacobian factors. With the definitions

$$f_\pm(\mathbf{\Phi}_3) = \int_{x_B}^1 \mathrm{d}\lambda f(\mathbf{\Phi}_3)\delta(\lambda - \lambda_\pm) \tag{3.45}$$

the ξ integral becomes

$$I_\xi = \int_0^{\xi_{\max,-}} \mathrm{d}\xi f_-(\mathbf{\Phi}_3) + \int_{\xi_{\min,+}}^{\xi_{\max,+}} \mathrm{d}\xi f_+(\mathbf{\Phi}_3), \tag{3.46}$$

where the integral limits $\xi_{\max,-}, \xi_{\min,+}$ and $\xi_{\max,+}$ depend on the other inte-

gration variables

$$\xi_{\max,-} = \begin{cases} \xi_{\text{low}}, & \text{if } \cos\Delta\phi > 0, \\ \xi_{\text{up}}, & \text{if } \cos\Delta\phi < 0 \wedge \lambda_-(\xi_{\max}) < x_B, \\ \xi_{\max}, & \text{otherwise,} \end{cases}$$
$$\xi_{\min,+} = \begin{cases} \xi_{\text{up}}, & \text{if } \cos\Delta\phi < 0 \wedge \lambda_-(\xi_{\max}) > x_B, \\ \xi_{\max}, & \text{otherwise,} \end{cases}$$
$$\xi_{\max,+} = \xi_{\max}. \tag{3.47}$$

Note that if $\cos\Delta\phi > 0 \vee \lambda_-(\xi_{\max}) < x_B$, then $\xi_{\min,+} = \xi_{\max,+}$, since λ_+ is not a valid solution in that case.

In the POWHEG BOX the ξ integration is set up as an integration over a $\tilde{\xi}$ from 0 to 1, where $\tilde{\xi}$ is mapped to the actual ξ. Thereby, the soft IR limit is at $\tilde{\xi} \to 0$. In the case where one the negative branch is possible, this is straight forward by implementing the mapping $\xi = \xi_{\max,-}\tilde{\xi}$. If both λ branches are possible, this map is not sufficient. Since the positive branch does not contain any IR divergent kinematics, it can be attached at the end of the negative branch. In case of both branches being possible, one has $\xi_{\max,-} = \xi_{\max,+} = \xi_{\max}$. With the definition of $\Delta\xi := \xi_{\max} - \xi_{\text{up}}$, the integration over ξ becomes

$$\begin{aligned} I_\xi &= \int_0^{\xi_{\max}} \mathrm{d}\xi f_-(\xi) + \int_{\xi_{\text{up}}}^{\xi_{\max}} \mathrm{d}\xi f_+(\xi) \\ &= \int_0^{\xi_{\max}+\Delta\xi} \mathrm{d}\xi f_-(\xi)\Theta(\xi_{\max} - \xi) + \int_0^{\xi_{\max}+\Delta\xi} \mathrm{d}\xi f_+(2\xi_{\max} - \xi)\Theta(\xi - \xi_{\max}). \end{aligned} \tag{3.48}$$

Now, the two integrals can be combined into one. With the variable transformation $\tilde{\xi} = \xi/\tilde{\xi}_{\max}$, where $\tilde{\xi}_{\max} = \xi_{\max} + \Delta\xi$, one obtains

$$\begin{aligned} I_\xi = \int_0^1 \mathrm{d}\tilde{\xi}\tilde{\xi}_{\max}\Big[& f_-(\tilde{\xi}\tilde{\xi}_{\max})\Theta(\xi_{\max} - \tilde{\xi}\tilde{\xi}_{\max}) \\ & + f_+(2\xi_{\max} - \tilde{\xi}\tilde{\xi}_{\max})\Theta(\tilde{\xi}\tilde{\xi}_{\max} - \xi_{\max})\Big]. \end{aligned} \tag{3.49}$$

3.2.2 Phase space for final-state radiation

For FSR, the starting point for the phase space measure is again Eq. (3.8). The emitter is the 4th particle with momentum p_4. Let the momentum sum of the two outgoing partons be called $k := p_4 + p_5$. It is parametrized as

$$k = (k^0, \underline{k}\sqrt{1-c_k^2}\cos\phi_k, \underline{k}\sqrt{1-c_k^2}\sin\phi_k, \underline{k}c_k), \quad \text{with } \underline{k} := |\mathbf{k}|, \tag{3.50}$$

where $k^0 = E_4 + E_5$. Then, one can integrate over $\mathbf{k}$ instead of $\mathbf{p}_4$. Together with the parameterization Eq. (3.50), the phase space measure becomes

$$\mathrm{d}\mathbf{\Phi}_3 = \frac{1}{256\pi^5}\mathrm{d}x\ \mathrm{d}^3\mathbf{p}_3\ \mathrm{d}\underline{k}\ \mathrm{d}c_k\ \mathrm{d}\phi_k\ \mathrm{d}^3\mathbf{p}_5 \frac{\underline{k}^2}{E_3 E_4 E_5}\delta^{(4)}(p_1 + p_2 - p_3 - k), \tag{3.51}$$

where

$$\begin{aligned} E_3 &:= |\mathbf{p}_3|, \\ E_5 &:= |\mathbf{p}_5|, \\ E_4 &:= |\mathbf{k} - \mathbf{p}_5|. \end{aligned} \tag{3.52}$$

In the next step, a rotation R is performed to align k along the z-axis

$$R\,k = (k^0, 0, 0, \underline{k}). \tag{3.53}$$

To achieve this transformation, one can perform three successive rotations. The first rotates around the z-axis by the angle $-\phi$. The second rotation is around the y-axis by the angle $-\arccos c_k$. The last rotation is the inverse of the first rotation. This shifts the information of the azimuthal angle onto the incoming particles and allows an independent spherical parametrization of the final state particles in the phase space measure. Hence, the full rotation is

$$\begin{aligned} R &= R_1^{-1} R_2 R_1, \\ R_1 &= \begin{pmatrix} 1 & 0 & 0 & 0 \\ 0 & \cos(\phi_k) & \sin(\phi_k) & 0 \\ 0 & -\sin(\phi_k) & \cos(\phi_k) & 0 \\ 0 & 0 & 0 & 1 \end{pmatrix}, \\ R_2 &= \begin{pmatrix} 1 & 0 & 0 & 0 \\ 0 & c_k & 0 & -\sqrt{1-c_k^2} \\ 0 & 0 & 1 & 0 \\ 0 & \sqrt{1-c_k^2} & 0 & c_k \end{pmatrix}. \end{aligned} \tag{3.54}$$

Momenta in the rotated frame will be denoted with the upper label $^{(R)}$. The incoming momenta in the rotated frame are

$$\begin{aligned} p_1^{(R)} &= \frac{\sqrt{s}}{2}(1, -\sqrt{1-c_k^2}\cos\phi_k, -\sqrt{1-c_k^2}\sin\phi_k, c_k), \\ p_2^{(R)} &= \frac{\sqrt{s}}{2}(1, \sqrt{1-c_k^2}\cos\phi_k, \sqrt{1-c_k^2}\sin\phi_k, -c_k). \end{aligned} \tag{3.55}$$

With the variable transformations $c_k \to -c_2$ and $\phi_k \to \phi_2$, one obtains the usual spherical coordinates in the rotated frame. This allows to express all momenta in variables defined in the rotated frame, rather than the angles from the original center-of-mass frame. Further, the momentum of the radiation can be parametrized in spherical coordinated as

$$p_5^{(R)} = E_5(1, \sqrt{1-c_5^2}\cos\phi_5, \sqrt{1-c_5^2}\sin\phi_5, c_5). \tag{3.56}$$

Note that c_5 and ϕ_5 are not the FKS variables. The phase space measure $\mathbf{\Phi}_3$ in the rotated frame is

$$\begin{aligned} \mathrm{d}\mathbf{\Phi}_3 = \frac{1}{256\pi^5}\mathrm{d}x\ \mathrm{d}^3\mathbf{p}_3^{(R)}\ \mathrm{d}\underline{k}\ \mathrm{d}c_2\ \mathrm{d}\phi_2\ \mathrm{d}E_5\ \mathrm{d}\phi_5\ \mathrm{d}c_5\ \frac{\underline{k}^2 E_5}{E_3 E_4} \\ \times \delta^{(4)}\Big(p_1^{(R)} + p_2^{(R)} - p_3^{(R)} - k^{(R)}\Big). \end{aligned} \tag{3.57}$$

The 3-vector component of the delta distribution is

$$\delta^{(3)}\Big(-\mathbf{p}_3^{(R)} - \mathbf{k}^{(R)}\Big) \tag{3.58}$$

and can be easily eliminated by integrating over $\mathrm{d}^3\mathbf{p}_3^{(R)}$ yielding

$$\mathbf{p}_3^{(R)} = -\mathbf{k}^{(R)} = (0, 0, -\underline{k}) \quad \Rightarrow E_3 = \underline{k}. \tag{3.59}$$

This leads to

$$\begin{aligned} \mathrm{d}\mathbf{\Phi}_3 = \frac{1}{256\pi^5}\mathrm{d}x\ \mathrm{d}\underline{k}\ \mathrm{d}c_2\ \mathrm{d}\phi_2\ \mathrm{d}E_5\ \mathrm{d}\phi_5\ \mathrm{d}c_5\ \frac{\underline{k}E_5}{E_4} \\ \times \delta\big(\sqrt{s} - \underline{k} - E_4 - E_5\big), \\ E_4 = \sqrt{\underline{k}^2 + E_5^2 - 2\underline{k}E_5 c_5}. \end{aligned} \tag{3.60}$$

At this point, the DIS variables need to be introduced

$$\begin{aligned} Q^2 = -\big(q^{(R)}\big)^2 = -(p_1^{(R)} - p_3^{(R)})^2 = (1-c_2)\,\underline{k}\sqrt{s}, \\ y_{\mathrm{DIS}} = 1 - \frac{p_2^{(R)} p_3^{(R)}}{p_1^{(R)} p_2^{(R)}} = 1 - \frac{(1+c_2)\,\underline{k}}{\sqrt{s}}. \end{aligned} \tag{3.61}$$

Then, one can transform the integration variables

$$\begin{aligned} \underline{k} &= \frac{s(1-y_{\mathrm{DIS}}) + Q^2}{2\sqrt{s}}, \\ c_2 &= \frac{s(1-y_{\mathrm{DIS}}) - Q^2}{s(1-y_{\mathrm{DIS}}) + Q^2}, \\ \mathrm{d}\underline{k}\ \mathrm{d}c_2 &= \mathrm{d}y_{\mathrm{DIS}}\ \mathrm{d}Q^2 \frac{\sqrt{s}}{Q^2 + s(1-y_{\mathrm{DIS}})} = \mathrm{d}y_{\mathrm{DIS}}\ \mathrm{d}Q^2 \frac{1}{2\underline{k}}. \end{aligned} \tag{3.62}$$

The Q^2 integral can also be replaced by introducing $\lambda = Q^2/\left(2p_2^{(R)}q^{(R)}\right)$, which works out as

$$\mathrm{d}Q^2 = \mathrm{d}\lambda\, s\, y_{\mathrm{DIS}}. \tag{3.63}$$

The first FKS variable ξ can be introduced with

$$E_5 = \frac{\sqrt{s}}{2}\xi. \tag{3.64}$$

With all these transformations, the phase space measure becomes

$$\begin{aligned}\mathrm{d}\mathbf{\Phi}_3 = \frac{1}{1024\pi^5}\mathrm{d}x\ \mathrm{d}y_{\mathrm{DIS}}\ \mathrm{d}\lambda\ \mathrm{d}\phi_2\ \mathrm{d}\xi\ \mathrm{d}\phi_5\ \mathrm{d}c_5\ \frac{\xi s^2 y_{\mathrm{DIS}}}{2E_4} \\ \times\,\delta\left(\sqrt{s} - \frac{\sqrt{s}}{2}(\xi + 1 - y_{\mathrm{DIS}}(1-\lambda)) - E_4\right),\end{aligned} \tag{3.65}$$

where

$$2E_4 = \sqrt{s\,(2c_5\xi(y_{\mathrm{DIS}}(1-\lambda)-1) + \xi^2 + (1 - y_{\mathrm{DIS}}(1-\lambda))^2)}. \tag{3.66}$$

The last delta distribution is removed by integrating over λ. The root λ_0 of the argument of the delta distribution is

$$\lambda_0 = \frac{y_{\mathrm{DIS}}\,(\xi(1+c_5) - 2) + \xi(1-c_5)}{y_{\mathrm{DIS}}\,(\xi(1+c_5) - 2)}. \tag{3.67}$$

The additional Jacobian factor is

$$\frac{2\xi\,(1+c_5)\,(\xi-2)+4}{\sqrt{s}y_{\mathrm{DIS}}\,(\xi\,(1+c_5)-2)^2}. \tag{3.68}$$

After the λ integration, the phase space measure becomes

$$\mathrm{d}\mathbf{\Phi}_3 = \frac{1}{512\pi^5}\int \mathrm{d}x\ \mathrm{d}y_{\mathrm{DIS}}\ \mathrm{d}\phi_2\ \mathrm{d}\xi\ \mathrm{d}c_5\ \mathrm{d}\phi_5 \frac{s\xi}{2-\xi\,(c_\psi+1)}. \tag{3.69}$$

The integration variables c_5 and ϕ_5 have to be transformed into the FKS variables y and ϕ. Their definitions are

$$\begin{aligned} y &= \frac{\mathbf{p}_4\cdot\mathbf{p}_5}{E_4E_5}, \\ \phi &= \arctan2\left(\left(\frac{\hat{\mathbf{e}}_z\times\mathbf{k}}{|\hat{\mathbf{e}}_z\times\mathbf{k}|}\right)\cdot\left(\hat{\mathbf{p}}_{\mathbf{5}}\times\hat{\mathbf{k}}\right), \left(\left(\frac{\hat{\mathbf{e}}_z\times\mathbf{k}}{|\hat{\mathbf{e}}_z\times\mathbf{k}|}\right)\times\left(\hat{\mathbf{p}}_{\mathbf{5}}\times\hat{\mathbf{k}}\right)\right)\cdot\hat{\mathbf{k}}\right), \end{aligned} \tag{3.70}$$

where the second line is to be taken in the original center-of-mass frame before the rotation R. A vector with a hat is meant to be normed $\hat{\mathbf{a}} := \mathbf{a}/|\mathbf{a}|$. With these definitions one finds

$$\begin{aligned} y &= 1 - \frac{2\,(1-c_5)}{2-(2-\xi)\xi\,(1+c_5)}, \\ \phi &= (\phi_5 - \phi_2 - \pi) \mod 2\pi, \end{aligned} \tag{3.71}$$

which yields

$$\begin{aligned} \mathrm{d}c_5 &= \mathrm{d}y \frac{(2-(2-\xi)\xi\,(c_5+1))^{\,2}}{4(1-\xi)^2}, \\ \mathrm{d}\phi_r &= \mathrm{d}\phi. \end{aligned} \tag{3.72}$$

A last transformation $x = x_B/\lambda_0$ has to be done. Thereby, one has to carefully handle the integration limits in the same manner as in the ISR case

$$\mathrm{d}x = \frac{\mathrm{d}x_B}{\lambda_0}\Theta(\lambda_0 - x_B). \tag{3.73}$$

In contrast to the ISR case, the theta function cannot be eliminated by restricting the ξ integration. Consequently, one has to carry the theta function along.

Ultimately, the phase space measure becomes

$$\begin{aligned} \mathrm{d}\mathbf{\Phi}_3 &= \frac{1}{256\pi^5}\mathrm{d}x_B\;\mathrm{d}y_{\mathrm{DIS}}\;\mathrm{d}\phi_2\;\mathrm{d}\xi\;\mathrm{d}y\;\mathrm{d}\phi\;\Theta(\lambda_0 - x_B) \\ &\quad\times \frac{(1-\xi)\xi\bar{s}}{\lambda_0^2(2-\xi(1-y))(2-(2-\xi)\xi(1-y))} \\ &= \frac{1}{16\pi^3}\mathrm{d}\mathbf{\Phi}_2\;\mathrm{d}\xi\;\mathrm{d}y\;\mathrm{d}\phi\;\Theta(\lambda_0 - x_B) \\ &\quad\times \frac{(1-\xi)\xi\bar{s}}{\lambda_0^2(2-\xi(1-y))(2-(2-\xi)\xi(1-y))}. \end{aligned} \tag{3.74}$$

3.3 Generation of radiation

This section shows the implementation of the radiation generation in the `POWHEG BOX` and its modifications for DIS. The principles have been discussed in Sec. 2.5. Specifically, the choice of the upper bounding function $U(\Phi_{\mathrm{rad}}^{\alpha_r})$ and the ordering variable $k_T^{\alpha_r}(\mathbf{\Phi}_{n+1})$ is not set yet. Their choice is different for ISR and FSR, so those cases will be discussed separately.

3.3.1 Generation of initial-state radiation

In the POWHEG BOX, the upper bounding function is

$$U_{\mathrm{ISR}}(\Phi_{\mathrm{rad}}) = N\frac{\alpha_s(k_T^2)}{\xi(1-y^2)}, \tag{3.75}$$

and the ordering variable

$$k_T^2 = \frac{\bar{s}}{4(1-\xi)}\xi^2(1-y^2), \tag{3.76}$$

with $\bar{s}$ being the underlying Born center-of-mass energy squared, and

$$\alpha_s(k_T^2) = \frac{1}{b_0 \ln\left(\frac{k_T^2}{\Lambda^2}\right)}. \tag{3.77}$$

It is easy to see that k_T^2 diverges for $\xi \to 1$. For the normal POWHEG BOX and its mapping between the real phase space and the underlying Born phase space, this is not problematic, because in this mapping the upper limit of the ξ integration is strictly less than 1. However, in the mappings proposed in the previous section for DIS kinematics this does not hold true. Therefore, it is better to define a different function that is identical in the soft and collinear limit.

3.3.1.1 Generation of ISR for DIS

The choice for the ordering variable is not unique. One possible choice is very similar to the one in the POWHEG BOX

$$k_T^2 = \frac{\bar{s}\xi^2(1-y^2)}{4(1-\xi y^2)}. \tag{3.78}$$

With this definition k_T^2 would still be divergent in the simultaneous limit of $\xi \to 1$ and $y \to \pm 1$. However, this limit is not in the phase space since the maximum value of ξ is strictly less than 1 for $y \to \pm 1$. The maximum value k_T^2 inside of the real phase space is

$$\max k_T^2 = \frac{\bar{s}}{4}. \tag{3.79}$$

It it will be convenient to define the dimensionless variables

$$r := \frac{k_T^2}{\bar{s}} = \frac{\xi^2(1-y^2)}{4(1-\xi y^2)}, \tag{3.80}$$

and

$$r_{\max} := \max r = \frac{1}{4}. \tag{3.81}$$

The intermediate goal is to generate a p_T proportional to

$$\Delta^{(U)}(p_T) := \exp\left[-\int U_{\mathrm{ISR}}(\Phi_{\mathrm{rad}})\Theta(k_T - p_T)\mathrm{d}\xi\mathrm{d}y\mathrm{d}\phi\right]. \tag{3.82}$$

Then, the veto method is used to get a value p_T that is distributed proportionally to the Sudakov form factor. Therefore, the integral in Eq. (3.82) has to evaluated. One can trade the integration over y for an integral over r, which allows to eliminate the theta function by adjusting the integral limits. Therefore, one can insert

$$1 = \int_0^{1/4} \mathrm{d}r\,\delta\left(r - \frac{\xi^2(1-y^2)}{4(1-\xi y^2)}\right) \tag{3.83}$$

and eliminate the delta distribution by integrating over y. With the roots

$$y_\pm = \pm\sqrt{\frac{\xi^2 - 4r}{\xi(\xi - 4r)}}, \tag{3.84}$$

one obtains a lower limit for the ξ integration of $2\sqrt{r}$, since the square root in Eq. (3.84) has to be real. The substitution leads to

$$\begin{aligned}
-\log\Delta^{(U)}(p_T) &= N\int_{\frac{p_T^2}{\bar{s}}}^{1/4}\frac{\mathrm{d}r}{r}\int_{2\sqrt{r}}^{1}\mathrm{d}\xi\int_0^{2\pi}\mathrm{d}\phi\;\alpha_s(r\bar{s})\frac{1-y_+^2\xi}{y_+(1-\xi)\xi} \\
&= 2\pi N\int_{\frac{p_T^2}{\bar{s}}}^{1/4}\frac{\mathrm{d}r}{r}\int_{2\sqrt{r}}^{1}\mathrm{d}\xi\,\sqrt{\frac{\xi}{(\xi-4r)\,(\xi^2-4r)}} \qquad (3.85) \\
&= 8\pi N\int_{\frac{p_T^2}{\bar{s}}}^{1/4}\frac{\mathrm{d}r}{\sqrt{r}}\frac{\alpha(r\bar{s})}{\sqrt{1-2\sqrt{r}}} \\
&\quad\times\left\{K\left(2+\frac{1}{\sqrt{r}-\frac{1}{2}}\right) - F\left(\frac{\pi}{4}|2+\frac{1}{\sqrt{r}-\frac{1}{2}}\right)\right. \\
&\quad - \frac{2\sqrt{r}+1}{2\sqrt{r}}\left[\Pi\left(\frac{2}{1-2\sqrt{r}}|2+\frac{1}{\sqrt{r}-\frac{1}{2}}\right)\right. \\
&\quad \left.\left. - \Pi\left(\frac{2}{1-2\sqrt{r}};\frac{\pi}{4}|2+\frac{1}{\sqrt{r}-\frac{1}{2}}\right)\right]\right\}, \qquad (3.86)
\end{aligned}$$

where $F(\phi|m)$, $K(k) = F(\pi/2|m)$, $\Pi(n;\phi|m)$ and $\Pi(n|m)$ are elliptic integrals of first and third kind, respectively. They are defined as

$$\begin{aligned} F(\phi|m) &:= \int_0^\phi (1 - m\sin^2\theta)^{-1/2} \mathrm{d}\theta, \\ K(k) &:= F(\pi/2|m), \\ \Pi(n;\phi|m) &:= \int_0^\phi (1 - n\sin^2\theta)^{-1}(1 - m\sin^2\theta)^{-1/2}, \\ \Pi(n|m) &:= \Pi(n;\pi/2|m). \end{aligned} \tag{3.87}$$

Rather than trying to calculate the last integral of Eq. (3.86) and solve $x_r = \Delta^{(U)}(p_T)$ for p_T with a random number x_r, one can find an upper bounding function for the integrand of Eq. (3.86) and perform a second veto. Then, the integral can be calculated

$$\begin{aligned} -\log\Delta^{(U)}(p_T) &\leq -\log\tilde{\Delta}^{(U)}(p_T) \\ &= \pi N \int_{\frac{p_T^2}{\bar{s}}}^{1/4} \frac{\mathrm{d}r}{r} \frac{\log\left(\frac{4}{r}\right)}{b_0 \log\left(\frac{r\bar{s}}{\Lambda^2}\right)} \\ &= \frac{\pi N}{b_0} \left(\log\left(\frac{4\bar{s}}{\Lambda^2}\right) \log\left(\frac{\log\left(\frac{\bar{s}}{4\Lambda^2}\right)}{\log\left(\frac{p_T^2}{\Lambda^2}\right)} \right) + \log\left(\frac{4p_T^2}{\bar{s}}\right) \right). \end{aligned} \tag{3.88}$$

With a uniform random number $x_r \in (0,1)$, one can solve the equation

$$x_r = \tilde{\Delta}^{(U)}(p_T) \tag{3.89}$$

for p_T numerically and use the veto method twice to obtain a p_T value that is distributed proportional to the Sudakov form factor (Eq. (2.127)). The first veto is used with the ratio of integrands from equation Eq. (3.86) over Eq. (3.88). The second veto is done as described in section 2.5.

Once a p_T^2 is accepted, the FKS variables ξ and ϕ have to be generated. Generating ϕ is straight forward, since the integration over ϕ in $\Delta^{(U)}(p_T)$ does not depend on it. The probability density of ξ has to be proportional to the integrand of Eq. (3.85). Since this integral is difficult to handle, it is practical to use the veto method again. Therefore, the integrand is overestimated by

$$\sqrt{\frac{\xi}{(\xi - 4r)\,(\xi^2 - 4r)}} < \sqrt{\frac{1}{(2\sqrt{r} - 4r)\,(2\xi\sqrt{r} - 4r)}}. \tag{3.90}$$

Next, the integrand is normed by providing the factor $\sqrt{r}$ to have

$$\int_{2\sqrt{r}}^1 \mathrm{d}\xi\ \sqrt{r}\sqrt{\frac{1}{(2\sqrt{r} - 4r)\,(2\xi\sqrt{r} - 4r)}} = 1. \tag{3.91}$$

A randomly generated ξ' is obtained by solving

$$\int_{2\sqrt{r}}^{\xi'} \mathrm{d}\xi\ \sqrt{r}\sqrt{\frac{1}{(2\sqrt{r}-4r)\,(2\xi\sqrt{r}-4r)}} = x_\xi, \tag{3.92}$$

where x_ξ is an uniformly generated random number in the interval $(0,1)$. This leads to

$$\xi' = x_\xi^2\left(1-2\sqrt{r}\right)+2\sqrt{r}. \tag{3.93}$$

Lastly, it is checked if a new random number $\tilde{x}_\xi \in (0,1)$ fulfills

$$\tilde{x}_\xi > \frac{\sqrt{\frac{1}{(2\sqrt{r}-4r)\,(2\xi'\sqrt{r}-4r)}}}{\sqrt{\frac{\xi'}{(\xi'-4r)((\xi')^2-4r)}}}. \tag{3.94}$$

If it does, a new ξ' is generated until the inequality does not hold. Afterwards, the last FKS variable y can be obtained from Eq. (3.84) by randomly choosing either y_+ or y_-. From the FKS variables together with the prior generated Born phase space, the full $\mathbf{\Phi}_3$ phase space can be built.

This implementation for the ISR generation is implemented using the flag `rad_iupperisr = 2`, which can be set in the `powheg.input` file by adding the line `iupperisr 2`.

3.3.1.2 Alternative generation of ISR for DIS

For DIS, only the incoming parton can contribute to QCD ISR. Hence, there will only be a collinear divergence for $y \to -1$. This can be incorporated in both the upper bounding function and the ordering variable by defining them as

$$\begin{aligned} U_{\mathrm{ISR}}(\Phi_{\mathrm{rad}}) &:= N\frac{\alpha_s(k_T^2)}{\xi(1+y)}, \\ k_T^2 &:= \frac{\xi^2}{2-\xi(1-y)}\bar{s}(1+y). \end{aligned} \tag{3.95}$$

The soft collinear limit of the ordering variable is

$$k_T^2 \xrightarrow{\xi\to 0, y\to -1} \frac{\bar{s}\xi^2(1-y)}{2}. \tag{3.96}$$

This is the same limit as before. Now, a p_T^2 has to be generated using the same steps as in the other method with the only difference being the different

k_T^2 definition. Again, it is useful to define the dimensionless ordering variable

$$r := \frac{k_T^2}{\bar{s}} = \frac{\xi^2(1-y)}{2-\xi(1+y)}, \tag{3.97}$$

with

$$r_{\max} := \max r = 1. \tag{3.98}$$

This leads to

$$\begin{aligned} y &= -\frac{\xi^2 + (\xi-2)r}{\xi(\xi-r)}, \\ \mathrm{d}y &= \mathrm{d}r \frac{2(1-\xi)}{(r-\xi)^2}, \end{aligned} \tag{3.99}$$

with $\xi \in (\sqrt{r}, 1)$ to ensure $y \in (-1, 1)$. Then, the modified Sodakov form factor becomes

$$\begin{aligned} -\log \Delta^{(U)}(p_T) &= \int U_{\mathrm{ISR}}(\Phi_{\mathrm{rad}}) \Theta(k_T - p_T) \mathrm{d}\xi \mathrm{d}y \mathrm{d}\phi \\ &= 2\pi N \int_{\frac{p_T^2}{\bar{s}}}^1 \frac{\mathrm{d}r}{r} \int_{\sqrt{r}}^1 \mathrm{d}\xi \, \frac{\alpha_s(r\bar{s})}{\xi - r} \\ &= 2\pi N \int_{\frac{p_T^2}{\bar{s}}}^1 \frac{\mathrm{d}r}{r} \, \alpha_s(r\bar{s}) \log\left(\frac{1}{\sqrt{r}} + 1\right). \end{aligned} \tag{3.100}$$

Again, the last integral will be handled using the veto method by overestimating the integrand using

$$\log\left(\frac{1}{\sqrt{r}} + 1\right) \leq \frac{\log\left(\frac{4}{r}\right)}{2} \qquad \forall r \in (0, 1). \tag{3.101}$$

This leads to

$$\begin{aligned} -\log \Delta^{(U)}(p_T) &\leq -\log \tilde{\Delta}^{(U)}(p_T) \\ &= \pi N \int_{\frac{p_T^2}{\bar{s}}}^1 \frac{\mathrm{d}r}{r} \frac{\log\left(\frac{4}{r}\right)}{b_0 \log\left(\frac{r\bar{s}}{\Lambda^2}\right)} \\ &= \frac{\pi N}{b_0} \left(\log\left(\frac{4\bar{s}}{\Lambda^2}\right) \log\left(\frac{\log\left(\frac{\bar{s}}{\Lambda^2}\right)}{\log\left(\frac{p_T^2}{\Lambda^2}\right)} \right) + \log\left(\frac{p_T^2}{\bar{s}}\right) \right). \end{aligned} \tag{3.102}$$

With this result, the p_T^2 generation is carried out analogously to the previous method.

Similar as before, ξ has to be generated proportional to the integrand of Eq. (3.100). This time, no additional veto is necessary, since the integral is easy enough. Firstly, the integral is normed

$$\int_{\sqrt{r}}^{1} \mathrm{d}\xi \frac{1}{(\xi - r)\log\left(\frac{1}{\sqrt{r}} + 1\right)} = 1. \tag{3.103}$$

Then, the generated ξ' is obtained by solving

$$\int_{\sqrt{r}}^{\xi'} \mathrm{d}\xi \frac{1}{(\xi - r)\log\left(\frac{1}{\sqrt{r}} + 1\right)} = x_\xi, \tag{3.104}$$

with the uniform random number $x_\xi \in (0, 1)$. This yields

$$\xi' = \left(\sqrt{r} - r\right)\left(\frac{1}{\sqrt{r}} + 1\right)^{x_\xi} + r. \tag{3.105}$$

The FKS angle y can be obtained from Eq. (3.99) by using the generated p_T^2 and ξ'. Together with a random uniform $\phi \in (0, 2\pi)$ the full phase space with radiation can be built.

3.3.1.3 Selection of $\lambda_\pm$ branch

While building the real phase space for ISR, it turned out that the ratio $\lambda = \bar{x}/x$ can have two branches. In this context, $\bar{x}$ and x represent the momentum fractions of the parton from the incoming proton beam of the Born and real phase space, respectively. If the procedure described above generates a set of FKS variables $\{\xi, y, \phi\}$ for which both branches are possible, then the veto method has to adapted slightly.

In the last veto, it is checked whether a random number $r' \in (0, 1)$ fulfills

$$r' > \left[\frac{R_{\alpha_r}(\mathbf{\Phi}_{n+1})}{B_{f_b}(\mathbf{\Phi}_n)}\right]^{\bar{\mathbf{\Phi}}_n^{\alpha_r} = \mathbf{\Phi}_n} U(\Phi_{\mathrm{rad}}^{\alpha_r})^{-1}. \tag{3.106}$$

If both branches are possible, the real correction is

$$R_{\alpha_r}(\mathbf{\Phi}_{n+1}) = R_{\alpha_r}(\mathbf{\Phi}_{n+1}^+) + R_{\alpha_r}(\mathbf{\Phi}_{n+1}^-), \tag{3.107}$$

where $\mathbf{\Phi}_{n+1}^\pm$ is the phase space point that fulfills $\lambda_\pm = \bar{x}/x$ and $\lambda_\pm$ is given in Eq. (3.22). If an event is accepted with FKS variables $\{\xi, y, \phi\}$ that allow for both branches, then one of them has to be chosen. The probability for the positive branch, which has $\lambda_+ = \bar{x}/x$, is

$$\frac{R_{\alpha_r}(\mathbf{\Phi}_{n+1}^+)}{R_{\alpha_r}(\mathbf{\Phi}_{n+1}^+) + R_{\alpha_r}(\mathbf{\Phi}_{n+1}^-)}. \tag{3.108}$$

Consequently, the other branch is chosen with the counter probability.

3.3.2 Generation of final-state radiation

For FSR, the real contribution can have IR divergences for $\xi \to 0$ (soft limit) or $y \to 1$ (collinear limit). Therefore, the upper bounding function implemented in the `POWHEG BOX` is

$$U_{\mathrm{FSR}}(\Phi_{\mathrm{rad}}) = N \frac{\alpha_s(k_T^2)}{\xi(1-y)}, \tag{3.109}$$

and the ordering variable k_T^2 is defined as

$$k_T^2 = \frac{s}{2}\xi^2(1-y), \tag{3.110}$$

where s is the partonic center-of-mass energy of the real correction process. The mapping from the real phase space to the underlying Born phase space implemented in the `POWHEG BOX` has $s = \bar{s}$. In particular, s does not depend on the FKS variables. The mapping for the DIS modification does not have this feature. Instead in the DIS modification, one has

$$\begin{aligned} s &= \frac{\bar{s}}{\lambda_0}, \\ \lambda_0 &= 1 - \frac{\xi(1-\xi)(1-y)}{y_{\mathrm{DIS}}(2-\xi(1-y))}. \end{aligned} \tag{3.111}$$

In the soft or collinear limit $\lambda_0 \to 1$ and hence $s \to \bar{s}$. Therefore, one can modify the k_T^2 definition to

$$k_T^2 = \frac{\bar{s}}{2}\xi^2(1-y), \tag{3.112}$$

since this does not alter the soft-collinear limit. Then, one only needs to change all occurrences of s to $\bar{s}$ in the implementation, because $\bar{s}$ does not depend on the radiation.

Chapter 4

Phenomenological studies

This chapter shows the application of the POWHEG BOX implementation for DIS. Therefore, two experimental setups were simulated. To obtain the predictions for the HERA and EIC experiments, the new NLO+PS generator is interfaced with Pythia8. Pythia8 provides hadronization and beam remnant effects, which are included in the presented studies. QED shower or hadron decays are not included. This chapter in based on Ref. [1], in which the results have been published. Unless explicitly stated otherwise, all events have been generated using the ISR generation as described in Sec. 3.3.1.2.

4.1 DIS at the H1 experiment

In this section predictions obtained from the new POWHEG BOX implementation are compared to experimental data gathered from the H1 experiment at HERA in Ref. [96]. In the study, collisions of electrons or positrons with energy $E_e = 27.6$ GeV and protons with energy $E_{p,1} = 820$ GeV or $E_{p,2} = 920$ GeV were collected. This yields the center-of-mass energies $\sqrt{s_1} = 301$ GeV and $\sqrt{s_2} = 319$ GeV, respectively. For all three different collision types, the reported integrated luminosities in Ref. [96] are e^+p: $\sqrt{s_1}$, $\mathcal{L}_{\text{int}} = 30\,\text{pb}^{-1}$; e^-p: $\sqrt{s_2}$, $\mathcal{L}_{\text{int}} = 14\,\text{pb}^{-1}$; e^+p: $\sqrt{s_2}$, $\mathcal{L}_{\text{int}} = 62\,\text{pb}^{-1}$. The two different data sets for the positron-proton collisions are combined by weighing the data with their respective luminosity. Then, the combined positron data are merged with the electron data, where the two data sets are weighed by the total cross section. The PDF set NNPDF30_nnlo_as_0118_hera [97], implemented in LHAPDF v6.5.3 [98], was used. The renormalization and factorization scales μ_R and μ_F are both set equal to Q. Furthermore, only events

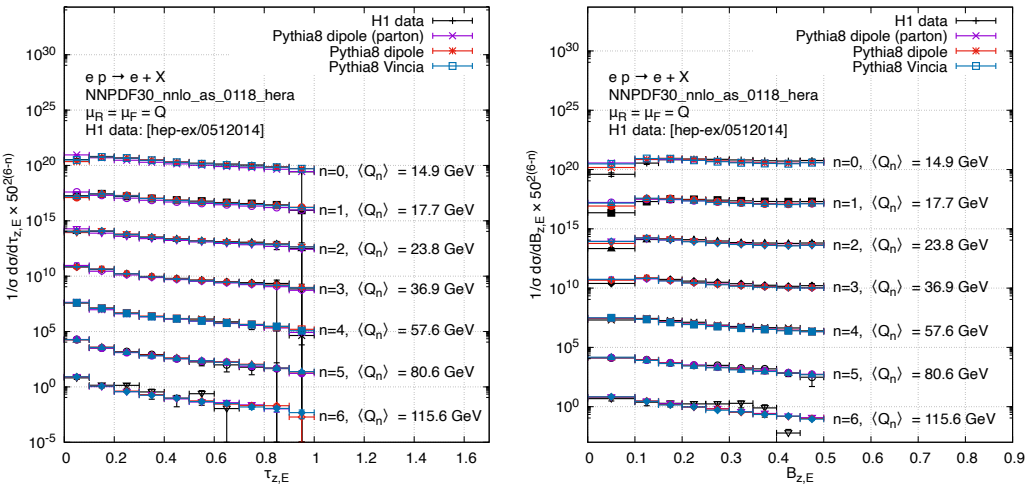

Figure 4.1: Thrust distribution (left) and broadening (right) for different bins in Q, including hadronization effects for the dipole (red), and VINCIA (blue) showers, and at the parton level (i.e. without hadronisation and beam-remnant effects) for the dipole shower (magenta), together with the H1 data of Ref. [96]. For a given Q-bin n, the average value of Q is denoted by $\langle Q_n \rangle$, and the corresponding curve is multiplied by a factor of $50^{2(6-n)}$ for better readability [1].

fulfilling

$$\begin{aligned} 14 \text{ GeV} < Q < 200 \text{ GeV}, \\ 0.1 < y_{\text{DIS}} < 0.7, \end{aligned} \tag{4.1}$$

are included in the analysis. Additionally, an event is only accepted if the energy of all particles in the current hemisphere is greater than $\epsilon_{\text{lim}} := Q/10$. This cut ensures infrared safety by removing events in which the current hemisphere contains only soft emissions. A further constriction is imposed on the longitudinal energy

$$40 \text{ GeV} < \sum_i E_i(1 - \cos\theta_i) < 70 \text{ GeV}, \tag{4.2}$$

where the sum runs over all detectable particles in the event.

Events, generated with the new `POWHEG BOX` implementation for DIS, are interfaced with `Pythia8` to obtain showered events. From these showered events, the observables jet broadening $B_{z,E}$, thrust $\tau_{z,E}$, jet mass ρ and C-parameter are calculated and filled in histograms. The definitions of these

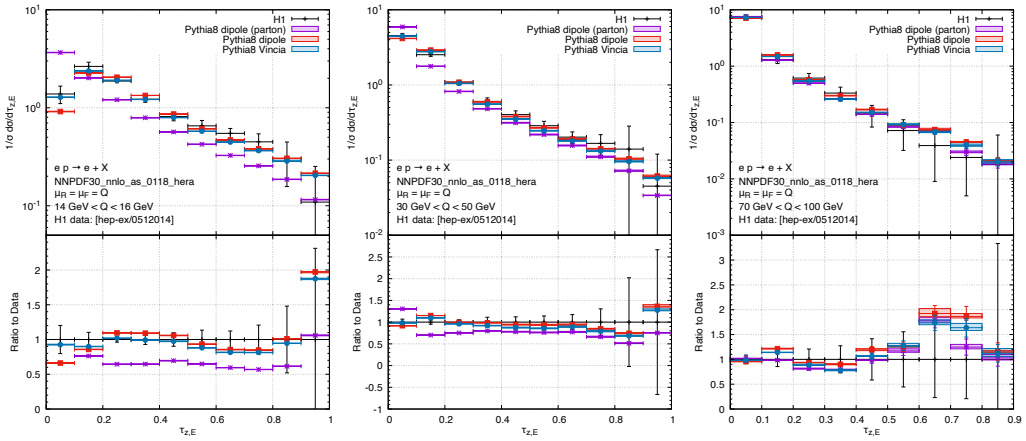

Figure 4.2: Thrust distribution including hadronization effects for the dipole (red), and VINCIA (blue) showers, and at the parton level (i.e. without hadronization and beam-remnant effects) for the dipole shower (magenta), together with the H1 data of Ref. [96], for the bins 14 GeV $< Q <$ 16 GeV (left), 30 GeV $< Q <$ 50 GeV (middle), and 70 GeV $< Q <$ 100 GeV (right). The bands represent the 7-point scale variation of μ_R and μ_F by a factor of two around the central value Q for the POWHEG results. The lower panels show the ratio of the predictions to data [1].

observables are shown in Sec. 2.6.1. For the shower algorithm, the dipole Pythia8 shower [99] and the default antenna VINCIA shower [100] are used. Both shower methods leave the DIS variables Q,x_B and y_{DIS} invariant if QED radiation is not taken into account. To illustrate the impact of hadronization effects, a third set of histograms is created with the dipole Pythia8 shower while disabling hadronization.

It is important to note that all event shapes are identical to zero for the LO DIS process. They only become greater than zero if radiation corrections are taken into account. This means, the current POWHEG BOX implementation can calculate event shape distributions only at LO accuracy which corresponds to NLO accuracy for the DIS process.

In Fig. 4.1, the thrust and jet broadening is shown for various Q-bins. In Figs. 4.2 and 4.3 the same event shape distributions are depicted for three selected Q-bins. The chosen Q-bins are the lowest bin, 14 GeV $< Q <$ 16 GeV, which is strongly dominated by the photon exchange, one Q-bin containing the Z-boson mass and an intermediate Q-bin in between the before mentioned ones. The uncertainty band for the showered results stems from the 7-point variation of μ_R and μ_F. The agreement of data with generated

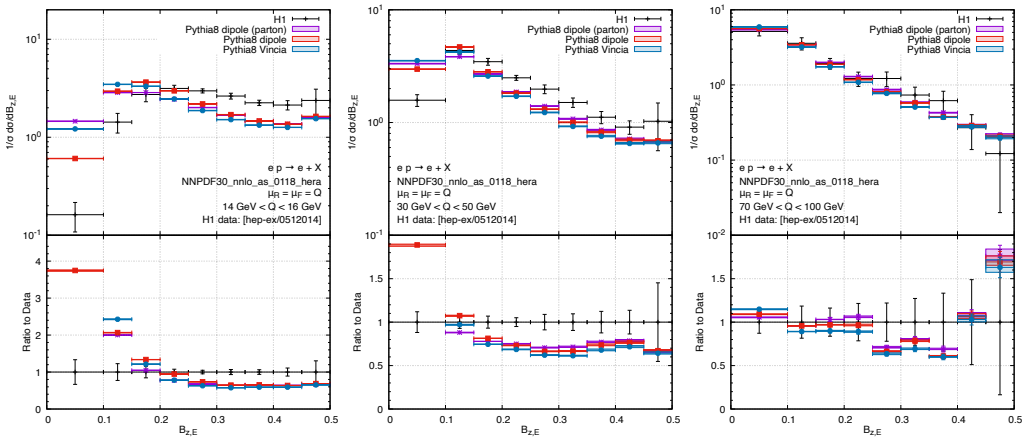

Figure 4.3: Same as Fig. 4.2, but for the broadening distribution [1].

event including hadronization effects is good for the thrust $\tau_{z,E}$. Especially for low Q values, the distribution without hadronization effects deviates from the data. For higher values of Q, these non-perturbative effects become smaller. For the jet broadening, the agreement between data and theoretical prediction is worse. However, one can observe the same trend regarding the impact of the hadronization effect that are more sizable for smaller values of Q. For both the thrust and jet broadening, the scale variation is very small for all Q values. Since all distributions are normalized, this behavior is expected.

Fig. 4.4 shows the jet mass and C-parameter for all measured Q-bins. In Figs. 4.5 and 4.6, the same Q-bins are selected as for the jet broadening and thrust before. The difference between parton shower with and without hadronization follows a similar pattern as for $\tau_{z,E}$ and $B_{z,E}$. For small Q values the prediction deviates from the data. The agreement improves with higher Q values, but one should note the large experimental uncertainty for Q values at the hard kinematic edge.

The inclusion of hadronization effects is critical to obtain sensible predictions for experimental measurements. The influence of these non-perturbative effects has also been discussed in Ref. [101] for the 1-jettiness distribution that is very similar to the thrust variable.

4.2 DIS at the EIC

This section presents predictions from the new `POWHEG BOX` implementation for the future EIC. In the previous section, the high experimental uncertain-

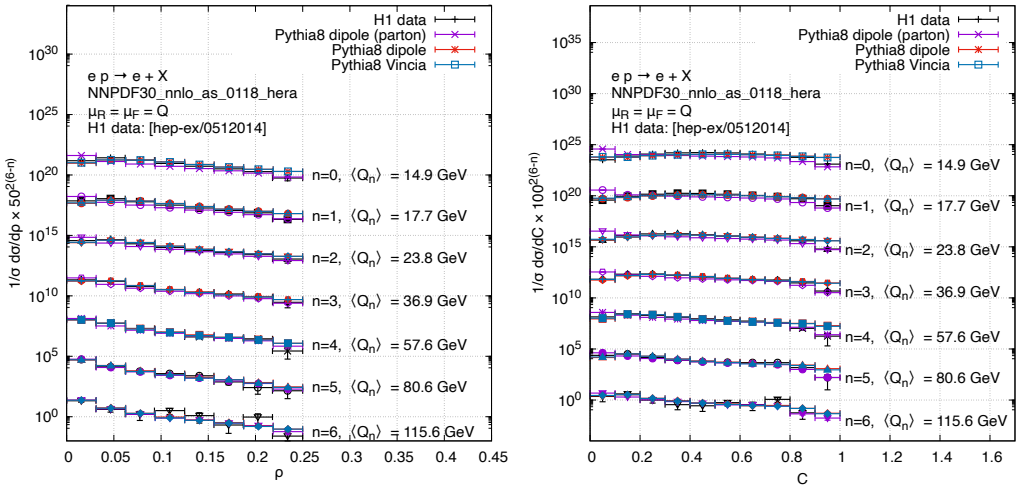

Figure 4.4: Same as Fig. 4.1, but for the squared jet mass (left) and the C-parameter (right) [1].

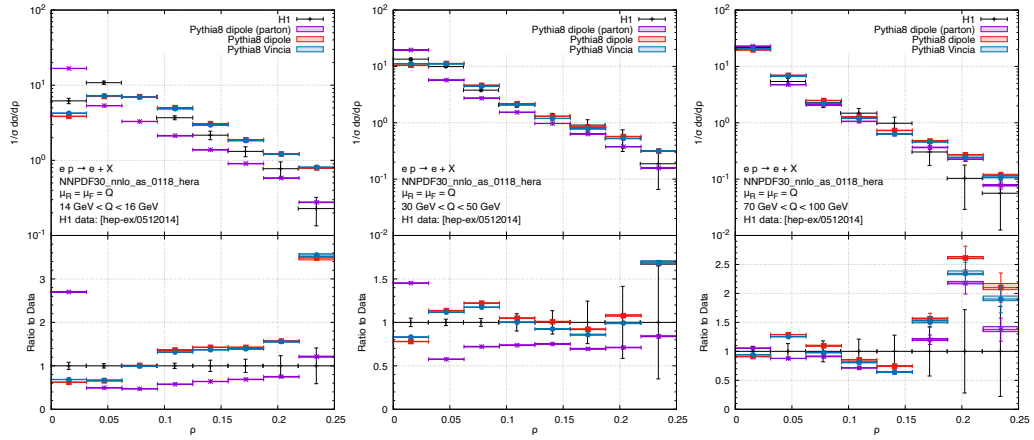

Figure 4.5: Same as Fig. 4.2, but for the squared jet mass [1].

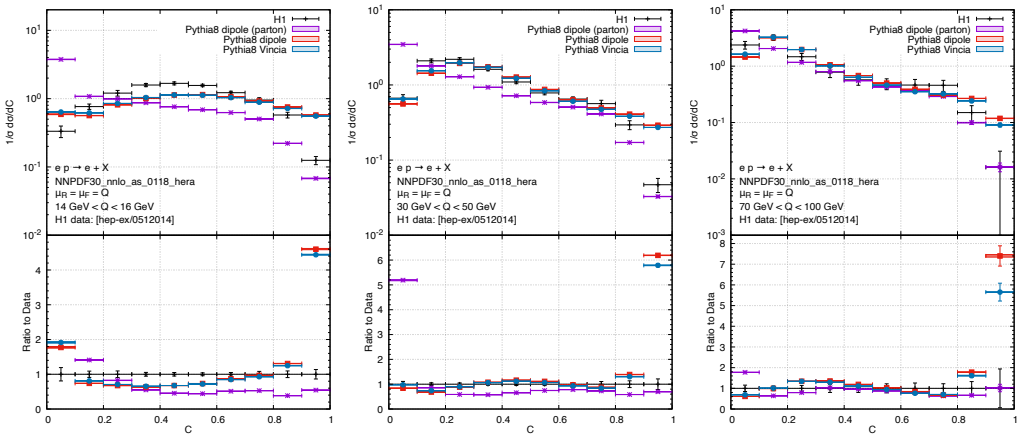

Figure 4.6: Same as Fig. 4.2, but for the C-parameter distribution [1].

ties were mentioned. With the EIC, those uncertainties will be reduced due to the much larger luminosity.

Electron proton collisions with beam energies $E_e = 18$ GeV and $E_p = 275$ GeV are considered. These values correspond to the maximal energies that are currently aimed at. Both neutral current (NC) and charged current (CC) results are shown. The generated events are restricted to

$$\begin{aligned} 25\ \text{GeV}^2 < Q^2 < 1000\ \text{GeV}^2, \\ 0.04 < y_{\text{DIS}} < 0.95, \end{aligned} \tag{4.3}$$

following Ref. [102]. For the EIC predictions the PDF set `PDF4LHC15_nlo_100_pdfas` [103] was used. This set includes constraints on the proton structure gathered at the LHC.

In contrast to the H1 data from the previous section, jet and inclusive distributions are shown here, where inclusive distributions are those in which all parton momenta are integrated out. Hence, inclusive distributions should not be modified by the parton shower, since they only depend on the lepton momenta which are not touched by the parton shower if only QCD radiation is considered. However, small deviations can be possible for low Q values, due to the reshuffling of momenta to introduce particle masses that are not present at the fixed order calculation. The jet reconstruction is done using the anti-k_T algorithm [104] for the parton momenta being in the lab frame. Thereby, the R-parameter is set to $R = 0.8$, and jets are only considered if they fulfill the restrictions on transverse momentum and pseudorapidity

$$p_T^{\text{jet}} > 5\ \text{GeV}\,, \quad |\eta^{\text{jet}}| < 3\,. \tag{4.4}$$

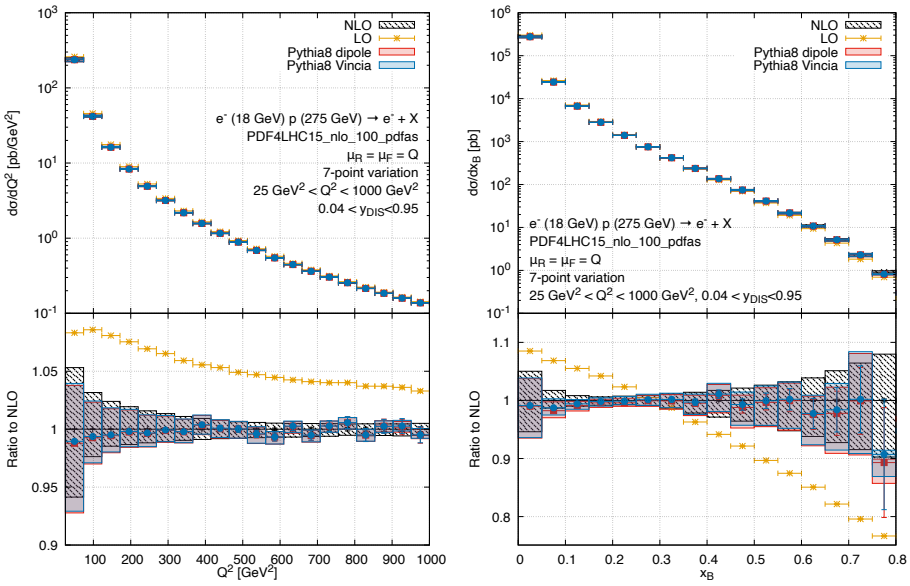

Figure 4.7: Distributions of Q^2 (left) and x_B (right) for NC DIS at the EIC with $\sqrt{s} = 140$ GeV and within the cuts of Eq. (4.3) at LO (orange), NLO (magenta), and NLO+PS results, obtained with dipole shower (red) or VINCIA (blue) `Pythia8` showers. Hadronisation and beam remnant effects are included in the NLO+PS simulations. Error bars indicate statistical uncertainties, bands are obtained by a 7-point scale variation of μ_R and μ_F by a factor of two around the central value Q. The lower panels display the ratios to the respective NLO results [1].

In Fig. 4.7, the distributions in Q^2 and x_B^2 for the NC cross section are shown. The NLO correction to the Q^2 distribution is strictly negative and becomes smaller for increasing Q^2. The NLO corrections to the x_B correction has different signs for the low and higher x_B values and becomes greater than 20 % for large values of x_B. The NLO+PS result for both the `Pythia8` dipole and VINCIA shower are almost identical. They also agree very well with the NLO result, since they do not modify the lepton momenta as stated before. For the NLO and NLO+PS results, a 7-point scale variation is performed, by varying the renormalization and factorization scales μ_R and μ_F by a factor 2 around Q.

Fig. 4.8 shows the transverse momentum and pseudo rapidity of the hardest jet fulfilling Eq. (4.4). Since the momenta are in the lab frame, the transverse momentum can be greater than zero even at LO, but it is limited by $p_T^{\text{jet}} < Q \approx 32$ GeV. At higher order, p_T^{jet} does not have this limit, since it can

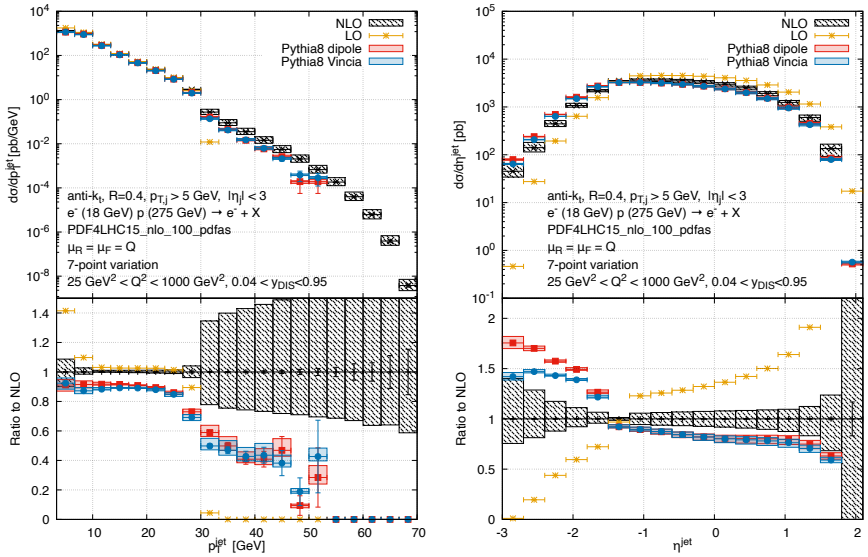

Figure 4.8: Distributions of p_T^{jet} (left) and η^{jet} (right) for NC DIS at the EIC with $\sqrt{s} = 140$ GeV and within the cuts of Eqs. (4.3)–(4.4) [1].

take the recoil of additional radiation. Beyond the threshold $p_T^{\text{jet}} > Q_{\max}$, the NLO result is only LO accurate which explains the larger scale dependence in that region. The NLO correction reduces the p_T^{jet} distribution, especially for small p_T^{jet}. The additional parton shower amplifies the effect further. Beyond the threshold, the parton shower corrections become larger and reduce the scale dependence considerably. The pseudorapidity has an asymmetric shape around zero with more weight for $\eta^{\text{jet}} < 0$. This corresponds to the proton beam direction which carries more energy than the electron beam. In addition, the NLO correction is asymmetric as well, and it becomes very large for high values of $|\eta^{\text{jet}}|$. Again, the parton shower enhances the NLO corrections further, though to a smaller extend. Similar to the transverse momentum distribution, the parton shower corrections are especially large in the regions where the NLO result has a large scale dependence. The two different showers agree very well except in the region $\eta^{\text{jet}} < 1.8$. In general, the differences between the fixed order and NLO+PS results are greater than their 7-point scale variation.

Fig. 4.9 compares the two options for ISR generation described in Secs. 3.3.1.1 and 3.3.1.2. In the p_T^{jet} distribution below the threshold $p_T^{\text{jet}} < Q_{\max}$, the two different options agree very well with each other. In the region with low p_T^{jet}, the numerical difference between the different ordering variables and upper bounding variables becomes small since in the soft-collinear limit p_T^{jet}

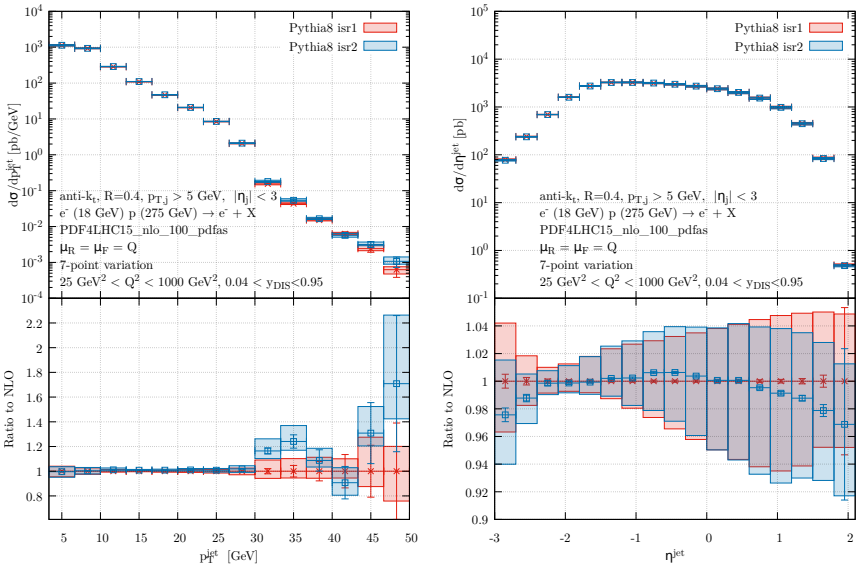

Figure 4.9: Distributions of p_T^{jet} (left) and η^{jet} (right) for NC DIS at the EIC with $\sqrt{s} = 140$ GeV and within the cuts of Eqs. (4.3)–(4.4). For the red line, ISR is generated as described in Sec. 3.3.1.2, while for the blue line, the ordering variable and upper bounding function are as described in Sec. 3.3.1.1. The error bars are due to statistical uncertainties, while the shaded areas stem from the 7-point variation.

approaches 0. Hence, it is expected that the two different options agree for low p_T^{jet}. Above the threshold, the difference becomes larger, and the behavior is similar to the difference of the two shower algorithms in Fig. 4.8. The η^{jet} distributions for the two ISR methods agree within the uncertainties. They deviate for large values of $|\eta^{\text{jet}}|$ similar to the different shower algorithms, albeit to a much lesser extent.

The Q^2 and x_B distributions of the CC are depicted in Fig. 4.10. While in the NC channel both the photon and the Z-boson can be the exchange particle carrying Q^2, in the CC channel the incoming lepton interacts only weakly via the W-boson with the proton constituents. Therefore, the cross section in the CC channel is roughly three orders of magnitude smaller, and the Q^2 distribution does not rise as quickly with decreasing Q^2, due to the missing massless exchange particle. However, the NLO correction, which is entirely due to QCD effects, does not affect the leptons either way. Therefore, the relative NLO and parton shower corrections are identical between the NC and CC channel in shape and numerical values for the inclusive distributions.

Fig. 4.11 shows the transverse momentum and pseudorapidity distribu-

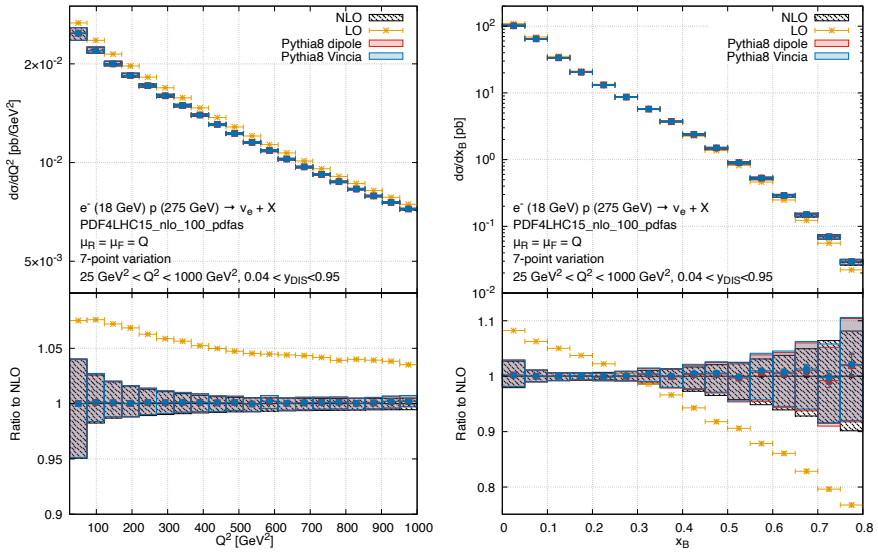

Figure 4.10: Same as Fig. 4.7, but for the charged current channel [1].

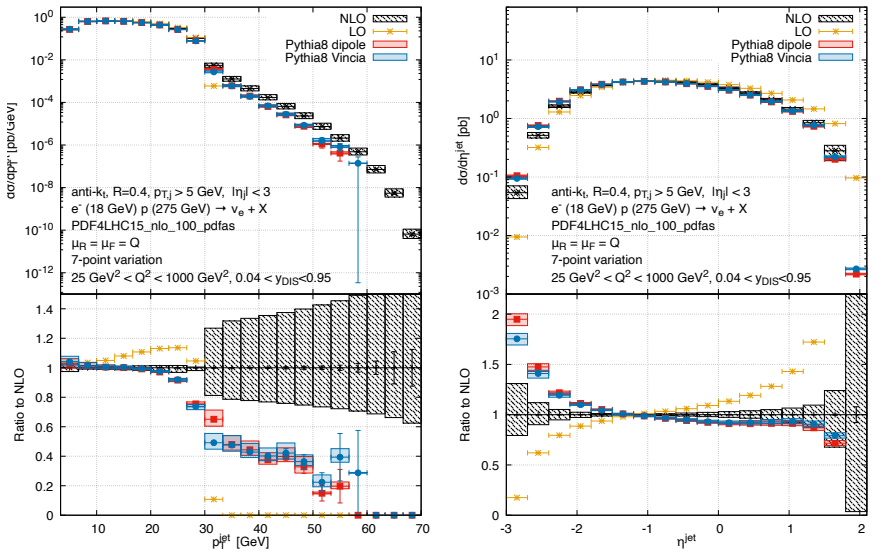

Figure 4.11: Same as Fig. 4.8, but for the charged current channel [1].

tions for the CC channel. In contrast to the NC channel, the NLO corrections are very small for low values of p_T^{jet}, but they become increasingly negative in the intermediate region before the threshold. Additionally, the parton shower effect is also very small below the threshold $p_T^{\text{jet}} < Q_{\max}$ and becomes comparable to the parton shower correction in the NC channel near the threshold and beyond. The correction to the pseudorapidity distributions is similar between NC and CC channels. A notable difference is that the NLO and NLO+PS corrections are more weighted towards higher values of $|\eta^{\text{jet}}|$ compared to the NC channel.

Chapter 5

Summary and outlook

In this work, a new event generator is presented that is based on the POWHEG BOX RES [105] enabling the generation of events for the DIS process at NLO accuracy in QCD and their matching to a parton shower. The theoretical foundation for any calculation in the field of high energy physics is QFT. In the first part of this thesis, some basic concepts of QFT are summarized. Additionally, a brief overview of the SM is given to form the basis needed to calculate the DIS cross section. In the next sections, an outline for the general strategy to obtain high precision results within the SM is shown. The difficulties and tools to perform NLO calculations, the concept of parton showers and their interfacing with NLO calculations are discussed. The next section presents the DIS process and its special kinematic features. The Breit frame is a particularly useful frame for processes like DIS that can be reduced to a subprocess in which one of the incoming particles scatters off of a virtual boson emitted by the other incoming particle.

Chapter 3 explains the changes to the POWHEG BOXthat are necessary to account for lepton-hadron collisions. In particular, the FKS momentum mappings had do be adapted. The mapping between Born and real momentum configurations for ISR, as it is implemented in the original version of the POWHEG BOX RES, modifies both incoming particle momenta. This is only sensible if both particles are understood as constituents of a hadron. For FSR this problem does not occur, since the mapping implemented in the POWHEG BOX conserves momenta of incoming particles in this case. However, neither the ISR nor the FSR mapping preserves the DIS variables Q^2, y_{DIS} and x_B. An alternative mapping for both cases is presented that does conserve the DIS variables and the incoming lepton momentum. This allows for efficient phenomenological studies in which constraints on the DIS variables are imposed. These changes to the momentum mappings led to a necessary modification of the ordering variable in the ISR generation.

In chapter 4, two phenomenological studies are presented. The first study compares experimental data from the H1 experiment at HERA with the generated events obtained with the new implementation interfaced with the parton shower program `Pythia8` [45]. The compared event shapes vanish at LO DIS. Hence, calculating DIS with two partons in the final state will only yield LO accuracy for those event shape variables. In order to improve the accuracy by an order, one would have to implement DIS with two partons in the final state as already as Born process. Then, the FKS momentum mappings would need to be adjusted to handle the extra final state particle. In their current state, they map from a two-particle final state to a three-particle final state. It would be worthwhile to generalize the momentum mappings to n particles in the final state at Born level and $n + 1$ particles for the real correction.

The second study in chapter 4 shows theoretical predictions for the future EIC. It was found that NLO corrections are sizable and impact the shape of the Q^2 and x_B dependence as well as the the transverse momentum and pseudorapidity distributions of the hardest jet.

Apart from the already mentioned generalization of the FKS momentum mappings, it could prove useful to do these mappings in the Breit frame rather than in the center-of-mass frame. This would affect far more elements of the `POWHEG BOX` than the current modification. For example, the counter terms governing the IR divergence would need to be rederived in the new frame of reference. Further, the FSR mapping would also encounter the problem of two different branches similar to the ISR mapping.

A new family of parton showers designed for DIS and similar processes was published in Ref. [106]. These showers achieve next-to leading logarithm (NLL) accuracy rather than leading logarithm (LL) as in the parton showers used in this thesis. It would be interesting to interface the new family of parton shower to the new presented DIS event generator.

In summary, the newly developed implementation of DIS for the `POWHEG BOX` is the first fully dedicated event generator to this process. It is a useful tool to obtain theory predictions for the future EIC, and it provides a starting point for more processes that share a similar kinematic structure.

Appendix A

Installation

First the POWHEG BOX RES has to be installed. It can be downloaded via svn using the command[1]

```
$ svn checkout [--revision n] --username anonymous --password \
anonymous svn://powhegbox.mib.infn.it/trunk/POWHEG-BOX-RES
```

The argument [-revision n] is optional and specifies a particular revision of the code. The extension for DIS works with revision 4036. After the download is complete, change the directory to the downloaded POWHEG BOX RES.

```
$ cd POWHEG-BOX-RES
```

From here, download the DIS process

```
$ svn co --username anonymous --password anonymous \
svn://powhegbox.mib.infn.it/trunk/User-Processes-RES/DIS
```

If the DIS directory is not placed as a subdirectory in the POWHEG BOX RES installation, the Makefile has to be adjusted accordingly by modifying the line

```
POWHEGPATH=$(PWD)/..
```

to the actual path. The process depends on LHAPDF [98], FastJet [107] and Pythia8 [44, 45].

The compilation of the code requires gfortran and g++. In particular, the code was not tested with the Intel® Fortran Compiler. The POWHEG executable is created by running the command make, and the Pythia8 interface is created with the command make main-PYTHIA8-lhef. By modifying the variable ANALYSIS, the analysis Fortran file can be selected.

[1] A POWHEG BOX guide can be found at https://powhegbox.mib.infn.it/

To run the code, the user has to create a run directory. The run directory has to contain the `powheg.input` file, a file with distinct positive integer numbers named `pwgseeds.dat` and the file `main31.cmnd`. The file `powheg.input` contains the `POWHEG BOX` input parameters, while `main31.cmnd` contains the settings for the `Pythia8` shower. In the subdirectory `parallel-runs`, one can find example versions for all the files together with a script `run-parallel.sh` that will execute the code in parallel. The script will run eight processes in parallel, and it will execute the grid optimization twice. These settings can be adjusted by modifying the according variables. In any case, the executable `pwhg_main` has to be called from the run directory. During the fourth stage, the code will produce the event files named `pwgevents-<N>.lhe`, with `<N>` being the seed number if run in parallel, or `pwgevent.lhe` if the code is run serial. To run the shower, `main-PYTHIA8-lhef` has to be called from the directory containing the event files. The program automatically looks for the file `pwgevent.lhe`. If this file is not present, the filename has to be entered. The created histograms will be saved as top files named `pwgPOWHEG+PYTHIA8-output-<N>-W<M>.top`, where `<N>` is the seed number and `<M>` is the weight number if multiple weights are specified.

Appendix B

Input files

B.1 Runs for H1 data

The events used for the data in Sec. 4.1 where generated in three runs. The `powheg.input` files are almost identical, hence for the last two files only the difference to the first file is shown.

- Positron-proton run with $\sqrt{s} = 319$ GeV:

```
numevts 200000       ! number of events to be generated
ih1 -11              ! incoming positron
ih2  1               ! hadron 2 (1 for protons)
ebeam1 27.6d0        ! energy of beam 1 (lepton)
ebeam2 920d0  ! energy of beam 2 (hadron)
Qmin 10d0
Qmax 250d0
xmin 0d0
xmax 1d0
ymin 0d0
ymax 1d0

q2suppr 200d0

! To be set only if using LHA pdfs
lhans1   275200
lhans2   275200    ! pdf set for hadron 2 (LHA numbering)

alphas_from_pdf 1
```

```
renscfact  1d0      ! (default 1d0) ren scale factor:
! muren  = muref * renscfact
facscfact  1d0      ! (default 1d0) fac scale factor:
! mufact = muref * facscfact

! Parameters to allow or not the use of stored data
use-old-grid    1    ! If 1 use old grid if
! file pwggrids.dat is present (<> 1 regenerate)
use-old-ubound  1    ! If 1 use norm of upper bounding
! function stored in pwgubound.dat, if present;
! <> 1 regenerate

ncall1 500000         ! No. calls for the construction
! of the importance sampling grid
itmx1 1               ! No. iterations for grid
ncall2 10000000       ! No. calls for the computation
! of the upper bounding
! envelope for the generation of radiation
itmx2 1              ! No. iterations for the above
foldcsi 1            ! No. folds on csi integration
foldy   1            ! No. folds on  y  integration
foldphi 1            ! No. folds on phi integration

nubound 100000       ! No. calls to set up the
! upper bounding norms for radiation.
! This is performed using only the Born cross section
iupperisr 1

fastbtlbound 1
storemintupb 1
ubexcess_correct 1
storeinfo_rwgt 1   ! store info to allow for reweighting
hdamp 0
bornzerodamp  1

! OPTIONAL PARAMETERS

withnegweights 1     ! (default 0).
! If 1 use negative weights.
flg_jacsing 1
```

```
testplots  1        ! do NLO and PWHG distributions

xupbound 2d0        ! increase upper bound for
! radiation generation

iseed    12          ! Start the random number
! generator with seed iseed
manyseeds 1         ! Used to perform multiple
! runs with different random
! seeds in the same directory.
! If set to 1, the program asks for an integer j;
! The file pwgseeds.dat at line j is read, and the
! integer at line j is used to initialize the random
! sequence for the generation of the event.
! The event file is called pwgevents-'j'.lhe

doublefsr 0
! Default 0; if 1 use new mechanism to generate regions
! such that the emitted harder than the
! emitter in FSR is suppressed. If doublefsr=0 this is
! only the case for emitted gluons (old behaviour). If
! 1 it is also applied to emitted quarks.
! If set, it strongly reduces spikes on showered output.


runningscales 1

channel_type 4 ! full NC = 4; CC = 3;
vtype 3 ! 1: photon exchange only, 2: Z exchange only,
! 3: photon+Z exchange
smartsig 1
nores 1

parallelstage 1
xgriditeration 1

flg_dis_isr    1
flg_dis_fsr    1
flg_dis 1
btlscalereal 1
btlscalect 1
```

```
softtest 0
colltest 0

novirtual 0

py8QED 0
py8mpi 1
py8had 2
py8shower 1



#######################################
### Multiple weights (scale vars) #####
#######################################
rwl_file '-' ! If set to '-' read the xml reweighting info
! from this same file. Otherwise, it specifies the xml
! file with weight information
<initrwgt>
<weight id='1'>default</weight>
<weight id='2' > renscfact=2d0 facscfact=2d0 </weight>
<weight id='3' > renscfact=0.5d0 facscfact=0.5d0 </weight>
<weight id='4' > renscfact=1d0 facscfact=2d0 </weight>
<weight id='5' > renscfact=1d0 facscfact=0.5d0 </weight>
<weight id='6' > renscfact=2d0 facscfact=1d0 </weight>
<weight id='7' > renscfact=0.5d0 facscfact=1d0 </weight>
</initrwgt>
rwl_group_events 10  ! It keeps 10 events in memory,
!  reprocessing them together for reweighting
lhapdf6maxsets 10     ! Maximum number of lhapdf6 sets
! that it can keep in memory
```

- Positron-proton run with $\sqrt{s} = 301$ GeV:

```
(...)
ebeam2 820d0  ! energy of beam 2 (hadron)
(...)
```

- Electron-proton run with $\sqrt{s} = 319$ GeV:

```
(...)
ih1  11              ! incoming electron
(...)
```

B.2 Runs for EIC data

The NC data for Figs. 4.7 and 4.8 in Sec. 4.2 were obtained with the `powheg.input` file:

```
numevts 200000       ! number of events to be generated
ih1  11              ! incoming electron
ih2  1               ! hadron 2 (1 for protons)
ebeam1 18d0        ! energy of beam 1 (lepton)
ebeam2 275d0  ! energy of beam 2 (hadron)
Qmin 5d0
Qmax 32d0
xmin 0d0
xmax 1d0
ymin 0.04d0
ymax 0.95d0

! To be set only if using LHA pdfs
lhans1   90200
lhans2   90200    ! pdf set for hadron 2 (LHA numbering)

alphas_from_pdf 1

renscfact  1d0      ! (default 1d0) ren scale factor:
! muren  = muref * renscfact
facscfact  1d0      ! (default 1d0) fac scale factor:
! mufact = muref * facscfact

! Parameters to allow or not the use of stored data
use-old-grid    1    ! If 1 use old grid if
! file pwggrids.dat is present (<> 1 regenerate)
use-old-ubound  1    ! If 1 use norm of upper bounding
! function stored in pwgubound.dat, if present; <> 1 regenerate
```

```
ncall1 500000         ! No. calls for the construction
! of the importance sampling grid
itmx1 1               ! No. iterations for grid
ncall2 10000000       ! No. calls for the computation
! of the upper bounding
! envelope for the generation of radiation
itmx2 1              ! No. iterations for the above
foldcsi 1            ! No. folds on csi integration
foldy   1            ! No. folds on  y  integration
foldphi 1            ! No. folds on phi integration

nubound 100000       ! No. calls to set up the
! upper bounding norms for radiation.
! This is performed using only the Born cross section (fast)
iupperisr 1

fastbtlbound 1
storemintupb 1
ubexcess_correct 1
storeinfo_rwgt 1   ! store info to allow for reweighting
hdamp 0
bornzerodamp  1

! OPTIONAL PARAMETERS

withnegweights 1     ! (default 0). If 1 use negative weights.
flg_jacsing 1
testplots  1        ! do NLO and PWHG distributions

xupbound 2d0        ! increase upper bound for
! radiation generation

iseed    12          ! Start the random number
! generator with seed iseed
manyseeds 1         ! Used to perform multiple
! runs with different random
! seeds in the same directory.
! If set to 1, the program asks for an integer j;
! The file pwgseeds.dat at line j is read, and the
! integer at line j is used to initialize the random
```

```
! sequence for the generation of the event.
! The event file is called pwgevents-'j'.lhe

doublefsr 0
! Default 0; if 1 use new mechanism to generate regions
! such that the emitted harder than the
! emitter in FSR is suppressed. If doublefsr=0 this is
! only the case for emitted gluons (old behaviour). If
! 1 it is also applied to emitted quarks.
! If set, it strongly reduces spikes on showered output.


runningscales 1

channel_type 4 ! full NC = 4; CC = 3;
vtype 3 ! 1: photon exchange only, 2: Z exchange only,
! 3: photon+Z exchange
smartsig 1
nores 1

parallelstage 1
xgriditeration 1

flg_dis_isr    1
flg_dis_fsr    1
flg_dis 1
btlscalereal 1
btlscalect 1

softtest 0
colltest 0

novirtual 0

py8QED 0
py8mpi 1
py8had 2
py8shower 1
```

```
#######################################
### Multiple weights (scale vars) #####
#######################################
rwl_file '-' ! If set to '-' read the xml reweighting info
! from this same file. Otherwise, it specifies the xml
! file with weight information
<initrwgt>
<weight id='1'>default</weight>
<weight id='2' > renscfact=2d0 facscfact=2d0 </weight>
<weight id='3' > renscfact=0.5d0 facscfact=0.5d0 </weight>
<weight id='4' > renscfact=1d0 facscfact=2d0 </weight>
<weight id='5' > renscfact=1d0 facscfact=0.5d0 </weight>
<weight id='6' > renscfact=2d0 facscfact=1d0 </weight>
<weight id='7' > renscfact=0.5d0 facscfact=1d0 </weight>
</initrwgt>
rwl_group_events 10  ! It keeps 10 events in memory,
!  reprocessing them together for reweighting
lhapdf6maxsets 10     ! Maximum number of lhapdf6 sets
! that it can keep in memory
```

The input file to obtain the CC data of Figs. 4.10 and 4.11 differs only in one line compared to the one from the NC data.

```
(...)
channel_type 3 ! full NC = 4; CC = 3;
(...)
```

The comparison of the two ISR generation methods was conducted by two separate runs, each covering a different Q range, for both ISR methods. This resulted in a total of four runs.

- ISR method 1 with high Q:

```
numevts 100000     ! number of events to be generated
ih1  11             ! electron
ih2  1              ! proton
ebeam1 18d0         ! energy of beam 1 (electron)
ebeam2 275d0        ! energy of beam 2 (proton)
```

```
Qmin 20d0
Qmax 32d0
xmin 0d0
xmax 1d0
ymin 0.04d0
ymax 0.95d0

! To be set only if using LHA pdfs
lhans1  90200
lhans2  90200      ! pdf set for hadron 2 (LHA numbering)

alphas_from_pdf 1

renscfact  1d0      ! (default 1d0) ren scale factor:
! muren  = muref * renscfact
facscfact  1d0      ! (default 1d0) fac scale factor:
! mufact = muref * facscfact

! Parameters to allow or not the use of stored data
use-old-grid    1    ! If 1 use old grid
use-old-ubound  1    ! If 1 use norm of upper
! bounding function stored in pwgubound.dat, if present

ncall1 100000        ! No. calls for the construction
! of the importance sampling grid
itmx1 1              ! No. iterations for grid
ncall2 300000        ! No. calls for the computation
! of the upper bounding
! envelope for the generation of radiation
itmx2 1              ! No. iterations for the above
foldcsi 1            ! No. folds on csi integration
foldy   1            ! No. folds on  y  integration
foldphi 1            ! No. folds on phi integration

nubound 100000       ! No. calls to set up the upper
! bounding norms for radiation.
! This is performed using only the Born cross section
iupperfsr 1
iupperisr 1

fastbtlbound 1
```

```
storemintupb 1
ubexcess_correct 1
storeinfo_rwgt 1   ! store info to allow for reweighting
hdamp 0
bornzerodamp  1

! OPTIONAL PARAMETERS

withnegweights 1     ! If 1 use negative weights.
flg_jacsing 1
testplots  1        ! do NLO and PWHG distributions
withdamp 0
withsubtr 1

xupbound 2d0        ! increase upper bound
! for radiation generation

manyseeds 1         ! Used to perform multiple
! runs with different random
! seeds in the same directory.
! If set to 1, the program asks for an integer j;
! The file pwgseeds.dat at line j is read, and the
! integer at line j is used to initialize the random
! sequence for the generation of the event.
! The event file is called pwgevents-'j'.lhe

runningscales 1

channel_type 4 ! full NC = 4; CC = 3;
vtype 3 ! 1: photon exchange only,
! 2: Z exchange only, 3: photon+Z exchange
smartsig 1
nores 1

parallelstage 1
xgriditeration 1


flg_dis_isr    1
flg_dis_fsr    1
flg_dis 1
```

```
btlscalereal 1
btlscalect 1

softtest 0
colltest 0

#######################################
### Multiple weights (scale vars) #####
#######################################
rwl_file '-' ! If set to '-' read the xml reweighting
! info from this same file. Otherwise, it specifies
! the xml file with weight information
<initrwgt>
<weight id='1'>default</weight>
<weight id='2' > renscfact=2d0 facscfact=2d0 </weight>
<weight id='3' > renscfact=0.5d0 facscfact=0.5d0 </weight>
<weight id='4' > renscfact=1d0 facscfact=2d0 </weight>
<weight id='5' > renscfact=1d0 facscfact=0.5d0 </weight>
<weight id='6' > renscfact=2d0 facscfact=1d0 </weight>
<weight id='7' > renscfact=0.5d0 facscfact=1d0 </weight>
</initrwgt>
!rwl_group_events 10  ! It keeps 10 events in memory,
! reprocessing them together for reweighting
lhapdf6maxsets 10     ! Maximum number of lhapdf6 sets
! that it can keep in memory

py8QED 0
py8mpi 1
py8had 2
py8shower 1
```

- ISR method 1 with low Q:

```
(...)
Qmin 5d0
Qmax 20d0
(...)
iupperisr 1
(...)
```

- ISR method 2 with high Q:

```
(...)
Qmin 20d0
Qmax 32d0
(...)
iupperisr 2
(...)
```

- ISR method 2 with low Q:

```
(...)
Qmin 5d0
Qmax 20d0
(...)
iupperisr 2
(...)
```

Bibliography

[1] A. Banfi, S. Ferrario Ravasio, B. Jäger, A. Karlberg, F. Reichenbach and G. Zanderighi, *A POWHEG generator for deep inelastic scattering*, *JHEP* **02** (2024) 023 [arXiv:2309.02127].

[2] S. Chatrchyan, V. Khachatryan, A. Sirunyan, A. Tumasyan, W. Adam, E. Aguilo et al., *Observation of a new boson at a mass of 125 gev with the cms experiment at the lhc*, *Physics Letters B* **716** (2012) 30.

[3] G. Aad, T. Abajyan, B. Abbott, J. Abdallah, S. Abdel Khalek, A. Abdelalim et al., *Observation of a new particle in the search for the standard model higgs boson with the atlas detector at the lhc*, *Physics Letters B* **716** (2012) 1.

[4] P. Higgs, *Broken symmetries, massless particles and gauge fields*, *Physics Letters* **12** (1964) 132.

[5] P. W. Higgs, *Broken symmetries and the masses of gauge bosons*, *Phys. Rev. Lett.* **13** (1964) 508.

[6] G. S. Guralnik, C. R. Hagen and T. W. B. Kibble, *Global conservation laws and massless particles*, *Phys. Rev. Lett.* **13** (1964) 585.

[7] P. W. Higgs, *Spontaneous symmetry breakdown without massless bosons*, *Phys. Rev.* **145** (1966) 1156.

[8] T. W. B. Kibble, *Symmetry breaking in non-abelian gauge theories*, *Phys. Rev.* **155** (1967) 1554.

[9] F. Englert and R. Brout, *Broken symmetry and the mass of gauge vector mesons*, *Phys. Rev. Lett.* **13** (1964) 321.

[10] H1, ZEUS collaboration, F. D. Aaron et al., *Combined Measurement and QCD Analysis of the Inclusive e+- p Scattering Cross Sections at HERA*, *JHEP* **01** (2010) 109 [arXiv:0911.0884].

[11] H1, ZEUS collaboration, H. Abramowicz et al., *Combination and QCD Analysis of Charm Production Cross Section Measurements in Deep-Inelastic ep Scattering at HERA*, *Eur. Phys. J. C* **73** (2013) 2311 [arXiv:1211.1182].

[12] H1, ZEUS collaboration, H. Abramowicz et al., *Combination of measurements of inclusive deep inelastic $e^{\pm}p$ scattering cross sections and QCD analysis of HERA data*, *Eur. Phys. J. C* **75** (2015) 580 [arXiv:1506.06042].

[13] H1, ZEUS collaboration, H. Abramowicz et al., *Combination and QCD analysis of charm and beauty production cross-section measurements in deep inelastic ep scattering at HERA*, *Eur. Phys. J. C* **78** (2018) 473 [arXiv:1804.01019].

[14] H1 collaboration, T. Ahmed et al., *Hard scattering in gamma p interactions*, *Phys. Lett. B* **297** (1992) 205.

[15] ZEUS collaboration, M. Derrick et al., *Measurement of total and partial photon proton cross-sections at 180-GeV center-of-mass energy*, *Z. Phys. C* **63** (1994) 391.

[16] H1 collaboration, C. Adloff et al., *Inclusive D0 and D*+- production in deep inelastic e p scattering at HERA*, *Z. Phys. C* **72** (1996) 593 [arXiv:hep-ex/9607012].

[17] ZEUS collaboration, J. Breitweg et al., *Comparison of ZEUS data with standard model predictions for $e^+p \to e^+X$ scattering at high x and Q^2*, *Z. Phys. C* **74** (1997) 207 [arXiv:hep-ex/9702015].

[18] H1 collaboration, C. Adloff et al., *Measurement of open beauty production at HERA*, *Phys. Lett. B* **467** (1999) 156 [arXiv:hep-ex/9909029].

[19] H1 collaboration, C. Adloff et al., *Deep inelastic inclusive e p scattering at low x and a determination of alpha(s)*, *Eur. Phys. J. C* **21** (2001) 33 [arXiv:hep-ex/0012053].

[20] ZEUS collaboration, S. Chekanov et al., *Inclusive jet cross-sections in the Breit frame in neutral current deep inelastic scattering at HERA and determination of alpha(s)*, *Phys. Lett. B* **547** (2002) 164 [arXiv:hep-ex/0208037].

[21] ZEUS collaboration, S. Chekanov et al., *Measurement of D*+- production in deep inelastic e+- p scattering at HERA*, *Phys. Rev. D* **69** (2004) 012004 [arXiv:hep-ex/0308068].

[22] ZEUS collaboration, S. Chekanov et al., *An NLO QCD analysis of inclusive cross-section and jet-production data from the zeus experiment*, *Eur. Phys. J. C* **42** (2005) 1 [arXiv:hep-ph/0503274].

[23] F. Aaron, A. Aktas, C. Alexa, V. Andreev, B. Antunovic, S. Aplin et al., *Charged particle production in high q2 deep-inelastic scattering at hera*, *Physics Letters B* **654** (2007) 148.

[24] H1 collaboration, F. D. Aaron et al., *Measurement of the Inclusive ep Scattering Cross Section at Low Q^2 and x at HERA*, *Eur. Phys. J. C* **63** (2009) 625 [arXiv:0904.0929].

[25] T.-J. Hou, J. Gao, T. J. Hobbs, K. Xie, S. Dulat, M. Guzzi et al., *New cteq global analysis of quantum chromodynamics with high-precision data from the lhc*, *Phys. Rev. D* **103** (2021) 014013.

[26] S. Bailey, T. Cridge, L. A. Harland-Lang, A. D. Martin and R. S. Thorne, *Parton distributions from LHC, HERA, tevatron and fixed target data: MSHT20 PDFs*, *The European Physical Journal C* **81** (2021) .

[27] R. D. Ball, S. Carrazza, J. Cruz-Martinez, L. D. Debbio, S. Forte, T. Giani et al., *The path to proton structure at 1% accuracy*, *The European Physical Journal C* **82** (2022) .

[28] PDF4LHC Working Group collaboration, R. D. Ball et al., *The PDF4LHC21 combination of global PDF fits for the LHC Run III*, *J. Phys. G* **49** (2022) 080501 [arXiv:2203.05506].

[29] M. Seidel, *Luminosity upgrade of hera*, in *Proceedings of the 1999 Particle Accelerator Conference (Cat. No.99CH36366)*, vol. 1, pp. 34–36 vol.1, 1999, DOI.

[30] R. Abdul Khalek et al., *Science Requirements and Detector Concepts for the Electron-Ion Collider: EIC Yellow Report*, *Nucl. Phys. A* **1026** (2022) 122447 [arXiv:2103.05419].

[31] O. Brüning, A. Seryi and S. Verdú-Andrés, *Electron-Hadron Colliders: EIC, LHeC and FCC-eh*, *Front. in Phys.* **10** (2022) 886473.

[32] R. Abdul Khalek et al., *Snowmass 2021 White Paper: Electron Ion Collider for High Energy Physics*, in *2022 Snowmass Summer Study*, 3, 2022, arXiv:2203.13199.

[33] G. Heinrich, *Collider Physics at the Precision Frontier*, *Phys. Rept.* **922** (2021) 1 [arXiv:2009.00516].

[34] F. Gross et al., *50 Years of Quantum Chromodynamics*, arXiv:2212.11107.

[35] J. Currie, T. Gehrmann, E. W. N. Glover, A. Huss, J. Niehues and A. Vogt, *N^3LO corrections to jet production in deep inelastic scattering using the Projection-to-Born method*, *JHEP* **05** (2018) 209 [arXiv:1803.09973].

[36] T. Gehrmann, A. Huss, J. Niehues, A. Vogt and D. M. Walker, *Jet production in charged-current deep-inelastic scattering to third order in QCD*, *Phys. Lett. B* **792** (2019) 182 [arXiv:1812.06104].

[37] P. Nason, *A New method for combining NLO QCD with shower Monte Carlo algorithms*, *JHEP* **11** (2004) 040 [arXiv:hep-ph/0409146].

[38] S. Frixione, P. Nason and C. Oleari, *Matching NLO QCD computations with Parton Shower simulations: the POWHEG method*, *JHEP* **11** (2007) 070 [arXiv:0709.2092].

[39] S. Frixione and B. R. Webber, *Matching NLO QCD computations and parton shower simulations*, *JHEP* **06** (2002) 029 [arXiv:hep-ph/0204244].

[40] M. Bahr et al., *Herwig++ Physics and Manual*, *Eur. Phys. J. C* **58** (2008) 639 [arXiv:0803.0883].

[41] J. Bellm et al., *Herwig 7.2 release note*, *Eur. Phys. J. C* **80** (2020) 452 [arXiv:1912.06509].

[42] T. Gleisberg, S. Hoeche, F. Krauss, M. Schonherr, S. Schumann, F. Siegert et al., *Event generation with SHERPA 1.1*, *JHEP* **02** (2009) 007 [arXiv:0811.4622].

[43] Sherpa collaboration, E. Bothmann et al., *Event Generation with Sherpa 2.2*, *SciPost Phys.* **7** (2019) 034 [arXiv:1905.09127].

[44] T. Sjöstrand, S. Ask, J. R. Christiansen, R. Corke, N. Desai, P. Ilten et al., *An introduction to PYTHIA 8.2*, *Comput. Phys. Commun.* **191** (2015) 159 [arXiv:1410.3012].

[45] C. Bierlich et al., *A comprehensive guide to the physics and usage of PYTHIA 8.3*, arXiv:2203.11601.

[46] A. S. Wightman, *Quantum field theory in terms of vacuum expectation values*, *Phys. Rev.* **101** (1956) 860.

[47] R. Haag, *On quantum field theories*, *Kong. Dan. Vid. Sel. Mat. Fys. Med.* **29N12** (1955) 1.

[48] H. Lehmann, K. Symanzik and W. Zimmermann, *On the formulation of quantized field theories*, *Nuovo Cim.* **1** (1955) 205.

[49] R. Haag and B. Schroer, *Postulates of Quantum Field Theory*, *Journal of Mathematical Physics* **3** (2004) 248.

[50] M. Gell-Mann and F. Low, *Bound states in quantum field theory*, *Phys. Rev.* **84** (1951) 350.

[51] G. C. Wick, *The evaluation of the collision matrix*, *Phys. Rev.* **80** (1950) 268.

[52] R. P. Feynman, *Space-time approach to quantum electrodynamics*, *Phys. Rev.* **76** (1949) 769.

[53] H. Weyl, *Electron and Gravitation. 1. (In German)*, *Z. Phys.* **56** (1929) 330.

[54] P. A. M. Dirac, *The quantum theory of the electron*, *Proc. Roy. Soc. Lond. A* **117** (1928) 610.

[55] W. Heisenberg and W. Pauli, *On Quantum Field Theory. (In German)*, *Z. Phys.* **56** (1929) 1.

[56] L. D. Faddeev and V. N. Popov, *Feynman Diagrams for the Yang-Mills Field*, *Phys. Lett. B* **25** (1967) 29.

[57] C. N. Yang and R. L. Mills, *Conservation of isotopic spin and isotopic gauge invariance*, *Phys. Rev.* **96** (1954) 191.

[58] S. L. Glashow, *Partial-symmetries of weak interactions*, *Nuclear Physics* **22** (1961) 579.

[59] S. Weinberg, *A model of leptons*, *Phys. Rev. Lett.* **19** (1967) 1264.

[60] A. Salam, *Weak and Electromagnetic Interactions*, *Conf. Proc. C* **680519** (1968) 367.

[61] G. M. Shore, *Symmetry restoration and the background field method in gauge theories*, *Annals of Physics* **137** (1981) 262.

[62] M. B. Einhorn and J. Wudka, *Screening of heavy-higgs-boson radiative effects*, *Phys. Rev. D* **39** (1989) 2758.

[63] A. Denner, G. Weiglein and S. Dittmaier, *Gauge invariance of green functions: background-field method versus pinch technique*, *Physics Letters B* **333** (1994) 420.

[64] A. Denner, G. Weiglein and S. Dittmaier, *Application of the background-field method to the electroweak standard model*, *Nuclear Physics B* **440** (1995) 95.

[65] A. Helset, M. Paraskevas and M. Trott, *Gauge fixing the standard model effective field theory*, *Physical Review Letters* **120** (2018) .

[66] J. C. Collins, D. E. Soper and G. Sterman, *Factorization of hard processes in qcd*, 2004.

[67] K. G. Wilson and J. B. Kogut, *The Renormalization group and the epsilon expansion*, *Phys. Rept.* **12** (1974) 75.

[68] J. C. Collins, *Renormalization: An Introduction to Renormalization, The Renormalization Group, and the Operator Product Expansion*, vol. 26 of *Cambridge Monographs on Mathematical Physics*. Cambridge University Press, Cambridge, 1986.

[69] R. P. Feynman, *Space - time approach to quantum electrodynamics*, *Phys. Rev.* **76** (1949) 769.

[70] G. C. Wick, *Properties of bethe-salpeter wave functions*, *Phys. Rev.* **96** (1954) 1124.

[71] G. 't Hooft and M. J. G. Veltman, *Scalar One Loop Integrals*, *Nucl. Phys. B* **153** (1979) 365.

[72] G. Passarino and M. J. G. Veltman, *One Loop Corrections for e+ e- Annihilation Into mu+ mu- in the Weinberg Model*, *Nucl. Phys. B* **160** (1979) 151.

[73] A. Denner, *Techniques for the calculation of electroweak radiative corrections at the one-loop level and results for w-physics at lep200*, 2007.

[74] M. E. Peskin and D. V. Schroeder, *An Introduction to quantum field theory*. Addison-Wesley, Reading, USA, 1995.

[75] S. Weinberg, *The Quantum theory of fields. Vol. 1: Foundations*. Cambridge University Press, 6, 2005, 10.1017/CBO9781139644167.

[76] F. Bloch and A. Nordsieck, *Note on the Radiation Field of the electron*, *Phys. Rev.* **52** (1937) 54.

[77] H. Hannesdottir and M. D. Schwartz, *Finite s matrix*, *Phys. Rev. D* **107** (2023) L021701.

[78] T. D. Lee and M. Nauenberg, *Degenerate systems and mass singularities*, *Phys. Rev.* **133** (1964) B1549.

[79] T. Kinoshita, *Mass Singularities of Feynman Amplitudes*, *Journal of Mathematical Physics* **3** (2004) 650.

[80] G. Altarelli and G. Parisi, *Asymptotic Freedom in Parton Language*, *Nucl. Phys. B* **126** (1977) 298.

[81] W. T. Giele, E. W. N. Glover and D. A. Kosower, *Next-to-leading order calculations in jet physics*, in *27th Rencontres de Moriond: QCD and High-energy Hadronic Interactions*, pp. 95–102, 1992.

[82] S. Frixione, Z. Kunszt and A. Signer, *Three jet cross-sections to next-to-leading order*, *Nucl. Phys. B* **467** (1996) 399 [arXiv:hep-ph/9512328].

[83] S. Frixione, *A general approach to jet cross sections in QCD*, *Nuclear Physics B* **507** (1997) 295.

[84] R. K. Ellis, W. J. Stirling and B. R. Webber, *QCD and collider physics*, vol. 8. Cambridge University Press, 2, 2011, 10.1017/CBO9780511628788.

[85] T. Sjöstrand, *A model for initial state parton showers*, *Physics Letters B* **157** (1985) 321.

[86] T. D. Gottschalk, *Backwards evolved initial state parton showers*, *Nuclear Physics B* **277** (1986) 700.

[87] G. Marchesini and B. Webber, *Simulation of qcd jets including soft gluon interference*, *Nuclear Physics B* **238** (1984) 1.

[88] A. Buckley, J. Butterworth, S. Gieseke, D. Grellscheid, S. Höche, H. Hoeth et al., *General-purpose event generators for lhc physics*, *Physics Reports* **504** (2011) 145.

[89] T. Sjöstrand, *Status and developments of event generators*, *PoS* **LHCP2016** (2016) 007 [arXiv:1608.06425].

[90] R. Devenish and A. Cooper-Sarkar, *Deep inelastic scattering*. 2004, 10.1093/acprof:oso/9780198506713.001.0001.

[91] T. Hahn, *Generating feynman diagrams and amplitudes with FeynArts 3*, *Computer Physics Communications* **140** (2001) 418.

[92] R. Mertig, M. Böhm and A. Denner, *Feyn calc - computer-algebraic calculation of feynman amplitudes*, *Computer Physics Communications* **64** (1991) 345.

[93] V. Shtabovenko, R. Mertig and F. Orellana, *New developments in FeynCalc 9.0*, *Computer Physics Communications* **207** (2016) 432.

[94] V. Shtabovenko, R. Mertig and F. Orellana, *FeynCalc 9.3: New features and improvements*, *Computer Physics Communications* **256** (2020) 107478.

[95] S. Alioli, P. Nason, C. Oleari and E. Re, *A general framework for implementing NLO calculations in shower Monte Carlo programs: the POWHEG BOX*, *JHEP* **06** (2010) 043 [arXiv:1002.2581].

[96] H1 collaboration, A. Aktas et al., *Measurement of event shape variables in deep-inelastic scattering at HERA*, *Eur. Phys. J. C* **46** (2006) 343 [arXiv:hep-ex/0512014].

[97] NNPDF collaboration, R. D. Ball et al., *Parton distributions for the LHC Run II*, *JHEP* **04** (2015) 040 [arXiv:1410.8849].

[98] A. Buckley, J. Ferrando, S. Lloyd, K. Nordström, B. Page, M. Rüfenacht et al., *LHAPDF6: parton density access in the LHC precision era*, *Eur. Phys. J. C* **75** (2015) 132 [arXiv:1412.7420].

[99] B. Cabouat and T. Sjöstrand, *Some Dipole Shower Studies*, *Eur. Phys. J. C* **78** (2018) 226 [arXiv:1710.00391].

[100] H. Brooks, C. T. Preuss and P. Skands, *Sector Showers for Hadron Collisions*, *JHEP* **07** (2020) 032 [arXiv:2003.00702].

[101] M. Knobbe, D. Reichelt and S. Schumann, *(N)NLO+NLL' accurate predictions for plain and groomed 1-jettiness in neutral current DIS*, arXiv:2306.17736.

[102] I. Borsa, D. de Florian and I. Pedron, *NNLO jet production in neutral and charged current polarized deep inelastic scattering*, *Phys. Rev. D* **107** (2023) 054027 [arXiv:2212.06625].

[103] J. Butterworth et al., *PDF4LHC recommendations for LHC Run II*, *J. Phys. G* **43** (2016) 023001 [arXiv:1510.03865].

[104] M. Cacciari, G. P. Salam and G. Soyez, *The anti-k_t jet clustering algorithm*, *JHEP* **04** (2008) 063 [arXiv:0802.1189].

[105] T. Ježo and P. Nason, *On the Treatment of Resonances in Next-to-Leading Order Calculations Matched to a Parton Shower*, *JHEP* **12** (2015) 065 [arXiv:1509.09071].

[106] M. van Beekveld and S. Ferrario Ravasio, *Next-to-leading-logarithmic PanScales showers for Deep Inelastic Scattering and Vector Boson Fusion*, arXiv:2305.08645.

[107] M. Cacciari, G. P. Salam and G. Soyez, *FastJet user manual*, *The European Physical Journal C* **72** (2012) .

Acknowledgments

This work was made possible by the support of the German Research Foundation (DFG) through the Research Unit FOR 2926 and the state of Baden-Württemberg through bwHPC and the DFG through grant no. INST 39/963-1 FUGG. Additionally, I thank thank the University Oxford and the Rudolf Peierls Center for Theoretical Physics for the hospitality during my visit. I also thank the Theory Department at CERN for the invitation and hospitality.

I am grateful for the opportunity given by my supervisor, Pr. Dr. Barbara Jäger, to join her research group and compose my PhD thesis. I am thankful for the support and encouragement throughout the last years.

I want to thank Alexander Karlberg, Silvia Ferrario Ravasio, Giulia Zanderighi and Andra Banfi for the collaboration that led to the publication of [1]. I am especially grateful for the many helpful discussions with Alexander Karlberg and Silvia Ferrario Ravasio that really accelerated the project.

Thanks to my colleagues at the Institute for Theoretical Physics, including Santiago Lopez Portillo Chavez, Robin Feser, Felix Kunzelmann, Martin Vollmann, Simon Reinhardt, Johannes Scheller, Gabriele Coniglio, Maurizio Abele, and many others, I had a wonderful time in Tübingen. I am grateful for the numerous discussions about physics and everything else, as well as for the friendships both inside and outside the institute.

I would like to give special thanks to my partner, Lea Seibert, for her constant emotional support and for proofreading this work. Ich möchte auch meinen Eltern und meinem Bruder für die jahrelange Unterstüzung danken, die diese Arbeit erst ermöglicht haben.